

Squark and Gaugino Hadroproduction and Decays in Non-Minimal Flavour Violating Supersymmetry

Giuseppe Bozzi

Institut für Theoretische Physik, Universität Karlsruhe, Postfach 6980, D-76128 Karlsruhe, Germany

Benjamin Fuks, Björn Herrmann, and Michael Klasen*

Laboratoire de Physique Subatomique et de Cosmologie,

Université Joseph Fourier/CNRS-IN2P3, 53 Avenue des Martyrs, F-38026 Grenoble, France

(Dated: October 29, 2018)

We present an extensive analysis of squark and gaugino hadroproduction and decays in non-minimal flavour violating supersymmetry. We employ the so-called super-CKM basis to define the possible misalignment of quark and squark rotations, and we use generalized (possibly complex) charges to define the mutual couplings of (s)quarks and gauge bosons/gauginos. The cross sections for all squark-(anti)-squark/gaugino pair and squark-gaugino associated production processes as well as their decay widths are then given in compact analytic form. For four different constrained supersymmetry breaking models with non-minimal flavour violation in the second/third generation squark sector only, we establish the parameter space regions allowed/favoured by low-energy, electroweak precision, and cosmological constraints and display the chirality and flavour decomposition of all up- and down-type squark mass eigenstates. Finally, we compute numerically the dependence of a representative sample of production cross sections at the LHC on the off-diagonal mass matrix elements in the experimentally allowed/favoured ranges.

I. INTRODUCTION

Weak scale supersymmetry (SUSY) remains a both theoretically and phenomenologically attractive extension of the Standard Model (SM) of particle physics [1, 2]. Apart from linking bosons with fermions and unifying internal and external (space-time) symmetries, SUSY allows for a stabilization of the gap between the Planck and the electroweak scale and for gauge coupling unification at high energies. It appears naturally in string theories, includes gravity, and contains a stable lightest SUSY particle (LSP) as a dark matter candidate. Spin partners of the SM particles have not yet been observed, and in order to remain a viable solution to the hierarchy problem, SUSY must be broken at low energy via soft mass terms in the Lagrangian. As a consequence, the SUSY particles must be massive in comparison to their SM counterparts, and the Tevatron and the LHC will perform a conclusive search covering a wide range of masses up to the TeV scale.

If SUSY particles exist, they should also appear in virtual particle loops and affect low-energy and electroweak precision observables. In particular, flavour-changing neutral currents (FCNC), which appear only at the one-loop level even in the SM, put severe constraints on new physics contributions appearing at the same perturbative order. Extended technicolour and many composite models have thus been ruled out, while the Minimal Supersymmetric Standard Model (MSSM) has passed these crucial tests. This is largely due to the assumption of constrained Minimal Flavour Violation (cMFV) [3, 4] or Minimal Flavour Violation (MFV) [5, 6, 7], where heavy SUSY particles may appear in the loops, but flavour changes are either neglected or completely dictated by the structure of the Yukawa couplings and thus the CKM-matrix [8, 9].

The squark mass matrices M_Q^2 , M_U^2 , and M_D^2 are usually expressed in the super-CKM flavour basis [10]. In MFV SUSY scenarios, their flavour violating non-diagonal entries Δ_{ij} , where $i, j = L, R$ refer to the helicity of the (SM partner of the) squark, stem from the trilinear Yukawa couplings of the fermion and Higgs supermultiplets and the resulting different renormalizations of the quark and squark mass matrices, which induce additional flavour violation at the weak scale through renormalization group running [11, 12, 13, 14], while in cMFV scenarios, these flavour violating off-diagonal entries are simply neglected at both the SUSY-breaking and the weak scale.

When SUSY is embedded in larger structures such as grand unified theories (GUTs), new sources of flavour violation can appear [15]. For example, local gauge symmetry allows for R -parity violating terms in the SUSY Lagrangian, but these terms are today severely constrained by proton decay and collider searches. In non-minimal flavour violating (NMFV) SUSY, additional sources of flavour violation are included in the mass matrices at the weak scale, and

*klasen@lpsc.in2p3.fr

their flavour violating off-diagonal terms cannot be simply deduced from the CKM matrix alone. NMFV is then conveniently parameterized in the super-CKM basis by considering them as free parameters. The scaling of these entries with the SUSY-breaking scale M_{SUSY} implies a hierarchy $\Delta_{\text{LL}} \gg \Delta_{\text{LR,RL}} \gg \Delta_{\text{RR}}$ [15].

Squark mixing is expected to be largest for the second and third generations due to the large Yukawa couplings involved [16]. In addition, stringent experimental constraints for the first generation are imposed by precise measurements of $K^0 - \bar{K}^0$ mixing and first evidence of $D^0 - \bar{D}^0$ mixing [17, 18, 19]. Furthermore, direct searches of flavour violation depend on the possibility of flavour tagging, established experimentally only for heavy flavours. We therefore consider here only flavour mixings of second- and third-generation squarks.

The direct search for SUSY particles constitutes a major physics goal of present (Tevatron) and future (LHC) hadron colliders. SUSY particle hadroproduction and decay has therefore been studied in detail theoretically. Next-to-leading order (NLO) SUSY-QCD calculations exist for the production of squarks and gluinos [20], sleptons [21], and gauginos [22] as well as for their associated production [23]. The production of top [24] and bottom [25] squarks with large helicity mixing has received particular attention. Recently, both QCD one-loop and electroweak tree-level contributions have been calculated for non-diagonal, diagonal and mixed top and bottom squark pair production [26]. However, flavour violation has never been considered in the context of collider searches apart from the CKM-matrix appearing in the electroweak stop-sbottom production channel [26].

It is the aim of this paper to investigate for the first time the possible effects of non-minimal flavour violation at hadron colliders. To this end, we re-calculate all squark and gaugino production and decay helicity amplitudes, keeping at the same time the CKM-matrix and the quark masses to account for non-diagonal charged-current gaugino and Higgsino Yukawa interactions, and generalizing the two-dimensional helicity mixing matrices, often assumed to be real, to generally complex six-dimensional helicity and generational mixing matrices. We keep the notation compact by presenting all analytical expressions in terms of generalized couplings. In order to obtain numerical predictions for hadron colliders, we have implemented all our results in a flexible computer program. In our phenomenological analysis of NMFV squark and gaugino production, we concentrate on the LHC due to its larger centre-of-mass energy and luminosity. We pay particular attention to the interesting interplay of parton density functions (PDFs), which are dominated by light quarks, strong gluino contributions, which are generally larger than electroweak contributions and need not be flavour-diagonal, and the appearance of third-generation squarks in the final state, which are easily identified experimentally and generally lighter than first- and second-generation squarks.

After reviewing the MSSM with NMFV and setting up our notation in Sec. II, we define in Sec. III generalized couplings of quarks, squarks, gauge bosons, and gauginos. We then use these couplings to present our analytical calculations in concise form. In particular, we have computed partonic cross sections for NMFV squark-antisquark and squark-squark pair production, squark and gaugino associated and gaugino pair production as well as NMFV two-body decay widths of all squarks and gauginos. Section IV is devoted to a precise numerical analysis of the experimentally allowed NMFV SUSY parameter space, an investigation of the corresponding helicity and flavour decomposition of the up- and down-type squarks, and the definition of four collider-friendly benchmark points. These points are then investigated in detail in Sec. V so as to determine the possible sensitivity of the LHC experiments on the allowed NMFV parameter regions in the above-mentioned production channels. Our conclusions are presented in Sec. VI.

II. NON-MINIMAL FLAVOUR VIOLATION IN THE MSSM

Within the SM, the only source of flavour violation arises through the rotation of the up-type (down-type) quark interaction eigenstates $u'_{L,R}$ ($d'_{L,R}$) to the basis of physical mass eigenstates $u_{L,R}$ ($d_{L,R}$), such that

$$d_{L,R} = V_{L,R}^d d'_{L,R} \quad \text{and} \quad u_{L,R} = V_{L,R}^u u'_{L,R}. \quad (1)$$

The four bi-unitary matrices $V_{L,R}^{u,d}$ diagonalize the quark Yukawa matrices and render the charged-current interactions proportional to the unitary CKM-matrix [8, 9]

$$V = V_L^u V_L^{d\dagger} = \begin{pmatrix} V_{ud} & V_{us} & V_{ub} \\ V_{cd} & V_{cs} & V_{cb} \\ V_{td} & V_{ts} & V_{tb} \end{pmatrix}. \quad (2)$$

In the super-CKM basis [10], the squark interaction eigenstates undergo the same rotations at high energy scale as their quark counterparts, so that their charged-current interactions are also proportional to the SM CKM-matrix. However, different renormalizations of quarks and squarks introduce a mismatch of quark and squark field rotations

at low energies, so that the squark mass matrices effectively become non-diagonal [11, 12, 13, 14]. NMFV is then conveniently parameterized by non-diagonal entries $\Delta_{ij}^{qq'}$ with $i, j = L, R$ in the squared squark mass matrices

$$M_u^2 = \left(\begin{array}{ccc|ccc} M_{\tilde{L}_u}^2 & \Delta_{LL}^{uc} & \Delta_{LL}^{ut} & m_u X_u & \Delta_{LR}^{uc} & \Delta_{LR}^{ut} \\ \Delta_{LL}^{cu} & M_{\tilde{L}_c}^2 & \Delta_{LL}^{ct} & \Delta_{RL}^{cu} & m_c X_c & \Delta_{LR}^{ct} \\ \Delta_{LL}^{tu} & \Delta_{LL}^{tc} & M_{\tilde{L}_t}^2 & \Delta_{RL}^{tu} & \Delta_{RL}^{tc} & m_t X_t \\ \hline m_u X_u & \Delta_{RL}^{uc} & \Delta_{RL}^{ut} & M_{\tilde{R}_u}^2 & \Delta_{RR}^{uc} & \Delta_{RR}^{ut} \\ \Delta_{LR}^{cu} & m_c X_c & \Delta_{RL}^{ct} & \Delta_{RR}^{cu} & M_{\tilde{R}_c}^2 & \Delta_{RR}^{ct} \\ \Delta_{LR}^{tu} & \Delta_{LR}^{tc} & m_t X_t & \Delta_{RR}^{tu} & \Delta_{RR}^{tc} & M_{\tilde{R}_t}^2 \end{array} \right) \quad (3)$$

and

$$M_d^2 = \left(\begin{array}{ccc|ccc} M_{\tilde{L}_d}^2 & \Delta_{LL}^{ds} & \Delta_{LL}^{db} & m_d X_d & \Delta_{LR}^{ds} & \Delta_{LR}^{db} \\ \Delta_{LL}^{sd} & M_{\tilde{L}_s}^2 & \Delta_{LL}^{sb} & \Delta_{RL}^{sd} & m_s X_s & \Delta_{LR}^{sb} \\ \Delta_{LL}^{bd} & \Delta_{LL}^{bs} & M_{\tilde{L}_b}^2 & \Delta_{RL}^{bd} & \Delta_{RL}^{bs} & m_b X_b \\ \hline m_d X_d & \Delta_{RL}^{ds} & \Delta_{RL}^{db} & M_{\tilde{R}_d}^2 & \Delta_{RR}^{ds} & \Delta_{RR}^{db} \\ \Delta_{LR}^{sd} & m_s X_s & \Delta_{RL}^{sb} & \Delta_{RR}^{sd} & M_{\tilde{R}_s}^2 & \Delta_{RR}^{sb} \\ \Delta_{LR}^{bd} & \Delta_{LR}^{bs} & m_b X_b & \Delta_{RR}^{bd} & \Delta_{RR}^{bs} & M_{\tilde{R}_b}^2 \end{array} \right), \quad (4)$$

where the diagonal elements are given by

$$M_{\tilde{L}_q}^2 = M_{\tilde{Q}_q}^2 + m_q^2 + \cos 2\beta M_Z^2 (T_q^3 - e_q s_W^2), \quad (5)$$

$$M_{\tilde{R}_q}^2 = M_{\tilde{U}_q}^2 + m_q^2 + \cos 2\beta M_Z^2 e_q s_W^2 \quad \text{for up - type squarks}, \quad (6)$$

$$M_{\tilde{R}_q}^2 = M_{\tilde{D}_q}^2 + m_q^2 + \cos 2\beta M_Z^2 e_q s_W^2 \quad \text{for down - type squarks}, \quad (7)$$

while the well-known squark helicity mixing is generated by the elements

$$X_q = A_q - \mu \begin{cases} \cot \beta & \text{for up - type squarks,} \\ \tan \beta & \text{for down - type squarks.} \end{cases} \quad (8)$$

Here, m_q , T_q^3 , and e_q denote the mass, weak isospin quantum number, and electric charge of the quark q . m_Z is the Z -boson mass, and s_W (c_W) is the sine (cosine) of the electroweak mixing angle θ_W . The soft SUSY-breaking mass terms are $M_{\tilde{Q}_q}^2$ and $M_{\tilde{U}_q, \tilde{D}_q}^2$ for the left- and right-handed squarks. A_q and μ are the trilinear coupling and off-diagonal Higgs mass parameter, respectively, and $\tan \beta = v_u/v_d$ is the ratio of vacuum expectation values of the two Higgs doublets. The scaling of the flavour violating entries $\Delta_{ij}^{qq'}$ with the SUSY-breaking scale M_{SUSY} implies a hierarchy $\Delta_{LL}^{qq'} \gg \Delta_{LR, RL}^{qq'} \gg \Delta_{RR}^{qq'}$ among them [15]. They are usually normalized to the diagonal entries [18], so that

$$\Delta_{ij}^{qq'} = \lambda_{ij}^{qq'} M_{\tilde{q}_i} M_{\tilde{q}_{j'}}. \quad (9)$$

Note also that $SU(2)$ gauge invariance relates the (numerically largest) $\Delta_{LL}^{qq'}$ of up- and down-type quarks through the CKM-matrix, implying that a large difference between them is not allowed.

The diagonalization of the mass matrices M_u^2 and M_d^2 requires the introduction of two additional 6×6 matrices R^u and R^d with

$$\text{diag}(m_{\tilde{u}_1}^2, \dots, m_{\tilde{u}_6}^2) = R^u M_u^2 R^{u\dagger} \quad \text{and} \quad \text{diag}(m_{\tilde{d}_1}^2, \dots, m_{\tilde{d}_6}^2) = R^d M_d^2 R^{d\dagger}. \quad (10)$$

By convention, the masses are ordered according to $m_{\tilde{q}_1} < \dots < m_{\tilde{q}_6}$. The physical mass eigenstates are given by

$$\begin{pmatrix} \tilde{u}_1 \\ \tilde{u}_2 \\ \tilde{u}_3 \\ \tilde{u}_4 \\ \tilde{u}_5 \\ \tilde{u}_6 \end{pmatrix} = R^u \begin{pmatrix} \tilde{u}_L \\ \tilde{c}_L \\ \tilde{t}_L \\ \tilde{u}_R \\ \tilde{c}_R \\ \tilde{t}_R \end{pmatrix} \quad \text{and} \quad \begin{pmatrix} \tilde{d}_1 \\ \tilde{d}_2 \\ \tilde{d}_3 \\ \tilde{d}_4 \\ \tilde{d}_5 \\ \tilde{d}_6 \end{pmatrix} = R^d \begin{pmatrix} \tilde{d}_L \\ \tilde{s}_L \\ \tilde{b}_L \\ \tilde{d}_R \\ \tilde{s}_R \\ \tilde{b}_R \end{pmatrix}. \quad (11)$$

In the limit of vanishing off-diagonal parameters $\Delta_{ij}^{qq'}$, the matrices R^q become flavour-diagonal, leaving only the well-known helicity mixing already present in cMFV.

III. ANALYTICAL RESULTS FOR PRODUCTION CROSS SECTIONS AND DECAY WIDTHS

In this section, we introduce concise definitions of generalized strong and electroweak couplings in NMFV SUSY and compute analytically the corresponding partonic cross sections for squark and gaugino production as well as their decay widths. The cross sections of the production processes

$$a_{h_a}(p_a) b_{h_b}(p_b) \rightarrow \begin{cases} \tilde{q}_i^{(*)}(p_1) \tilde{q}_j^{(*)}(p_2), \\ \tilde{\chi}_j^\pm(p_1) \tilde{q}_i^{(*)}(p_2), \\ \tilde{\chi}_i^{\pm(0)}(p_1) \tilde{\chi}_j^{\pm(0)}(p_2) \end{cases} \quad (12)$$

are presented for definite helicities $h_{a,b}$ of the initial partons $a, b = q, \bar{q}, g$ and expressed in terms of the squark, chargino, neutralino, and gluino masses $m_{\tilde{q}_k}$, $m_{\tilde{\chi}_k^\pm}$, $m_{\tilde{\chi}_k^0}$, and $m_{\tilde{g}}$, the conventional Mandelstam variables,

$$s = (p_a + p_b)^2, \quad t = (p_a - p_1)^2, \quad \text{and} \quad u = (p_a - p_2)^2, \quad (13)$$

and the masses of the neutral and charged electroweak gauge bosons m_Z and m_W . Propagators appear as mass-subtracted Mandelstam variables,

$$\begin{aligned} s_w &= s - m_W^2, & s_z &= s - m_Z^2, \\ t_{\tilde{\chi}_k^0} &= t - m_{\tilde{\chi}_k^0}^2, & u_{\tilde{\chi}_k^0} &= u - m_{\tilde{\chi}_k^0}^2, \\ t_{\tilde{\chi}_j^\pm} &= t - m_{\tilde{\chi}_j^\pm}^2, & u_{\tilde{\chi}_j^\pm} &= u - m_{\tilde{\chi}_j^\pm}^2, \\ t_{\tilde{g}} &= t - m_{\tilde{g}}^2, & u_{\tilde{g}} &= u - m_{\tilde{g}}^2, \\ t_{\tilde{q}_i} &= t - m_{\tilde{q}_i}^2, & u_{\tilde{q}_i} &= u - m_{\tilde{q}_i}^2. \end{aligned} \quad (14)$$

Unpolarized cross sections, averaged over initial spins, can easily be derived from the expression

$$d\hat{\sigma} = \frac{d\hat{\sigma}_{1,1} + d\hat{\sigma}_{1,-1} + d\hat{\sigma}_{-1,1} + d\hat{\sigma}_{-1,-1}}{4}, \quad (15)$$

while single- and double-polarized cross sections, including the same average factor for initial spins, are given by

$$d\Delta\hat{\sigma}_L = \frac{d\hat{\sigma}_{1,1} + d\hat{\sigma}_{1,-1} - d\hat{\sigma}_{-1,1} - d\hat{\sigma}_{-1,-1}}{4} \quad \text{and} \quad d\Delta\hat{\sigma}_{LL} = \frac{d\hat{\sigma}_{1,1} - d\hat{\sigma}_{1,-1} - d\hat{\sigma}_{-1,1} + d\hat{\sigma}_{-1,-1}}{4}, \quad (16)$$

so that the single- and double-spin asymmetries become

$$A_L = \frac{d\Delta\hat{\sigma}_L}{d\hat{\sigma}} \quad \text{and} \quad A_{LL} = \frac{d\Delta\hat{\sigma}_{LL}}{d\hat{\sigma}}. \quad (17)$$

A. Generalized Strong and Electroweak Couplings in NMFV SUSY

Considering the strong interaction first, it is well known that the interaction of quarks, squarks, and gluinos, whose coupling is normally just given by $g_s = \sqrt{4\pi\alpha_s}$, can in general lead to flavour violation in the left- and right-handed sectors through non-diagonal entries in the matrices R^q ,

$$\{L_{\tilde{q}_j q_k \tilde{g}}, R_{\tilde{q}_j q_k \tilde{g}}\} = \{R_{jk}^q, -R_{j(k+3)}^q\}. \quad (18)$$

Of course, the involved quark and squark both have to be up- or down-type, since the gluino is electrically neutral.

For the electroweak interaction, we define the square of the weak coupling constant $g_W^2 = e^2/\sin^2\theta_W$ in terms of the electromagnetic fine structure constant $\alpha = e^2/(4\pi)$ and the squared sine of the electroweak mixing angle $x_W = \sin^2\theta_W = s_W^2 = 1 - \cos^2\theta_W = 1 - c_W^2$. Following the standard notation, the $W^\pm - \tilde{\chi}_i^0 - \tilde{\chi}_j^\pm$, $Z - \tilde{\chi}_i^+ - \tilde{\chi}_j^-$, and $Z - \tilde{\chi}_i^0 - \tilde{\chi}_j^0$ interaction vertices are proportional to [2]

$$\begin{aligned} O_{ij}^L &= -\frac{1}{\sqrt{2}}N_{i4}V_{j2}^* + N_{i2}V_{j1}^* & \text{and} & & O_{ij}^R &= \frac{1}{\sqrt{2}}N_{i3}^*U_{j2} + N_{i2}^*U_{j1}, \\ O_{ij}'^L &= -V_{i1}V_{j1}^* - \frac{1}{2}V_{i2}V_{j2}^* + \delta_{ij}x_W & \text{and} & & O_{ij}'^R &= -U_{i1}^*U_{j1} - \frac{1}{2}U_{i2}^*U_{j2} + \delta_{ij}x_W, \\ O_{ij}''^L &= -\frac{1}{2}N_{i3}N_{j3}^* + \frac{1}{2}N_{i4}N_{j4}^* & \text{and} & & O_{ij}''^R &= \frac{1}{2}N_{i3}^*N_{j3} - \frac{1}{2}N_{i4}^*N_{j4}. \end{aligned} \quad (19)$$

In NMFV, the coupling strengths of left- and right-handed (s)quarks to the electroweak gauge bosons are given by

$$\begin{aligned}
\{L_{qq'Z}, R_{qq'Z}\} &= (2T_q^3 - 2e_q x_W) \times \delta_{qq'}, \\
\{L_{\bar{q}_i \bar{q}_j Z}, R_{\bar{q}_i \bar{q}_j Z}\} &= (2T_{\bar{q}}^3 - 2e_{\bar{q}} x_W) \times \sum_{k=1}^3 \{R_{ik}^u R_{jk}^{u*}, R_{i(3+k)}^u R_{j(3+k)}^{u*}\}, \\
\{L_{qq'W}, R_{qq'W}\} &= \{\sqrt{2}c_W V_{qq'}, 0\}, \\
\{L_{\bar{u}_i \bar{d}_j W}, R_{\bar{u}_i \bar{d}_j W}\} &= \sum_{k,l=1}^3 \{\sqrt{2}c_W V_{u_k d_l} R_{ik}^u R_{jl}^{d*}, 0\},
\end{aligned} \tag{20}$$

where the weak isospin quantum numbers are $T_{\{q,\bar{q}\}}^3 = \pm 1/2$ for left-handed and $T_{\{q,\bar{q}\}}^3 = 0$ for right-handed up- and down-type (s)quarks, their fractional electromagnetic charges are denoted by $e_{\{q,\bar{q}\}}$, and V_{kl} are the elements of the CKM-matrix defined in Eq. (2). To simplify the notation, we have introduced flavour indices in the latter, $d_1 = d$, $d_2 = s$, $d_3 = b$, $u_1 = u$, $u_2 = c$, and $u_3 = t$.

The SUSY counterparts of these vertices correspond to the quark-squark-gaugino couplings,

$$\begin{aligned}
L_{\bar{d}_j d_k \tilde{\chi}_i^0} &= \left[(e_q - T_q^3) s_W N_{i1} + T_q^3 c_W N_{i2} \right] R_{jk}^{d*} + \frac{m_{d_k} c_W N_{i3} R_{j(k+3)}^{d*}}{2 m_W \cos \beta}, \\
-R_{\bar{d}_j d_k \tilde{\chi}_i^0} &= e_q s_W N_{i1} R_{j(k+3)}^d - \frac{m_{d_k} c_W N_{i3} R_{jk}^d}{2 m_W \cos \beta}, \\
L_{\bar{u}_j u_k \tilde{\chi}_i^0} &= \left[(e_q - T_q^3) s_W N_{i1} + T_q^3 c_W N_{i2} \right] R_{jk}^{u*} + \frac{m_{u_k} c_W N_{i4} R_{j(k+3)}^{u*}}{2 m_W \sin \beta}, \\
-R_{\bar{u}_j u_k \tilde{\chi}_i^0} &= e_q s_W N_{i1} R_{j(k+3)}^u - \frac{m_{u_k} c_W N_{i4} R_{jk}^u}{2 m_W \sin \beta}, \\
L_{\bar{d}_j u_l \tilde{\chi}_i^\pm} &= \sum_{k=1}^3 \left[U_{i1} R_{jk}^{d*} - \frac{m_{d_k} U_{i2} R_{j(k+3)}^{d*}}{\sqrt{2} m_W \cos \beta} \right] V_{u_l d_k}, \\
-R_{\bar{d}_j u_l \tilde{\chi}_i^\pm} &= \sum_{k=1}^3 \frac{m_{u_l} V_{i2} V_{u_l d_k}^* R_{jk}^d}{\sqrt{2} m_W \sin \beta}, \\
L_{\bar{u}_j d_l \tilde{\chi}_i^\pm} &= \sum_{k=1}^3 \left[V_{i1}^* R_{jk}^u - \frac{m_{u_k} V_{i2}^* R_{j(k+3)}^u}{\sqrt{2} m_W \sin \beta} \right] V_{u_k d_l}, \\
-R_{\bar{u}_j d_l \tilde{\chi}_i^\pm} &= \sum_{k=1}^3 \frac{m_{d_l} U_{i2}^* V_{u_k d_l} R_{jk}^{u*}}{\sqrt{2} m_W \cos \beta},
\end{aligned} \tag{21}$$

where the matrices N , U and V relate to the gaugino/Higgsino mixing (see App. A). All other couplings vanish due to (electromagnetic) charge conservation (e.g. $L_{\bar{u}_j u_l \tilde{\chi}_i^\pm}$). These general expressions can be simplified by neglecting the Yukawa couplings except for the one of the top quark, whose mass is not small compared to m_W . For the sake of simplicity, we use the generic notation

$$\{\mathcal{C}_{abc}^1, \mathcal{C}_{abc}^2\} = \{L_{abc}, R_{abc}\} \tag{22}$$

in the following.

B. Squark-Antisquark Pair Production

The production of charged squark-antisquark pairs

$$q(h_a, p_a) \bar{q}'(h_b, p_b) \rightarrow \tilde{u}_i(p_1) \tilde{d}_j^*(p_2), \tag{23}$$

where $i, j = 1, \dots, 6$ label up- and down-type squark mass eigenstates, $h_{a,b}$ helicities, and $p_{a,b,1,2}$ four-momenta, proceeds from an equally charged quark-antiquark initial state through the tree-level Feynman diagrams shown in Fig. 1. The corresponding cross section can be written in a compact way as

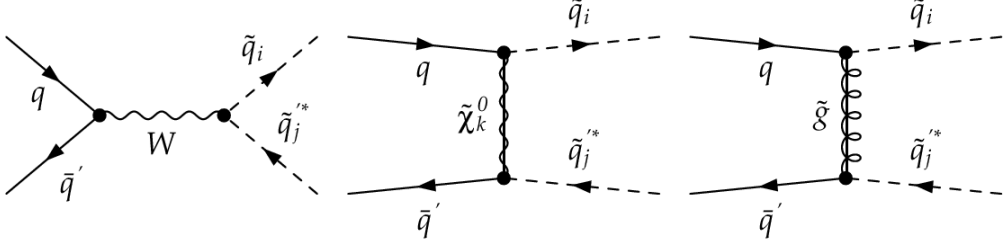


FIG. 1: Tree-level Feynman diagrams for the production of charged squark-antisquark pairs in quark-antiquark collisions.

$$\begin{aligned}
\frac{d\hat{\sigma}_{h_a, h_b}^{q\bar{q}'}}{dt} &= (1 - h_a)(1 + h_b) \left[\frac{\mathcal{W}}{s_w^2} + \left(\sum_{k,l=1,\dots,4} \frac{\mathcal{N}_{11}^{kl}}{t_{\tilde{\chi}_k^0} t_{\tilde{\chi}_l^0}} \right) + \frac{\mathcal{G}_{11}}{t_g^2} + \left(\sum_{k=1,\dots,4} \frac{[\mathcal{N}\mathcal{W}]^k}{t_{\tilde{\chi}_k^0} s_w} \right) + \frac{[\mathcal{G}\mathcal{W}]}{t_g s_w} \right] \\
&+ (1 - h_a)(1 - h_b) \left[\left(\sum_{k,l=1,\dots,4} \frac{\mathcal{N}_{12}^{kl}}{t_{\tilde{\chi}_k^0} t_{\tilde{\chi}_l^0}} \right) + \frac{\mathcal{G}_{12}}{t_g^2} \right] + (1 + h_a)(1 + h_b) \left[\left(\sum_{k,l=1,\dots,4} \frac{\mathcal{N}_{21}^{kl}}{t_{\tilde{\chi}_k^0} t_{\tilde{\chi}_l^0}} \right) + \frac{\mathcal{G}_{21}}{t_g^2} \right] \\
&+ (1 + h_a)(1 - h_b) \left[\left(\sum_{k,l=1,\dots,4} \frac{\mathcal{N}_{22}^{kl}}{t_{\tilde{\chi}_k^0} t_{\tilde{\chi}_l^0}} \right) + \frac{\mathcal{G}_{22}}{t_g^2} \right] \quad (24)
\end{aligned}$$

thanks to the form factors

$$\begin{aligned}
\mathcal{W} &= \frac{\pi \alpha^2}{16 x_W^2 (1 - x_W)^2 s^2} \left| L_{qq'W}^* L_{\tilde{u}_i \tilde{d}_j W} \right|^2 \left(ut - m_{\tilde{u}_i}^2 m_{\tilde{d}_j}^2 \right), \\
\mathcal{N}_{mn}^{kl} &= \frac{\pi \alpha^2}{x_W^2 (1 - x_W)^2 s^2} \mathcal{C}_{\tilde{d}_j q' \tilde{\chi}_k^0}^n \mathcal{C}_{\tilde{u}_i q \tilde{\chi}_l^0}^{m*} \mathcal{C}_{\tilde{d}_j q' \tilde{\chi}_l^0}^{n*} \mathcal{C}_{\tilde{u}_i q \tilde{\chi}_k^0}^m \left[\left(ut - m_{\tilde{u}_i}^2 m_{\tilde{d}_j}^2 \right) \delta_{mn} + \left(m_{\tilde{\chi}_k^0} m_{\tilde{\chi}_l^0} s \right) (1 - \delta_{mn}) \right], \\
\mathcal{G}_{mn} &= \frac{2\pi \alpha_s^2}{9 s^2} \left| \mathcal{C}_{\tilde{d}_j q' \tilde{g}}^{n*} \mathcal{C}_{\tilde{u}_i q \tilde{g}}^m \right|^2 \left[\left(ut - m_{\tilde{u}_i}^2 m_{\tilde{d}_j}^2 \right) \delta_{mn} + \left(m_{\tilde{g}}^2 s \right) (1 - \delta_{mn}) \right], \\
[\mathcal{N}\mathcal{W}]^k &= \frac{\pi \alpha^2}{6 x_W^2 (1 - x_W)^2 s^2} \text{Re} \left[L_{qq'W}^* L_{\tilde{u}_i \tilde{d}_j W} L_{\tilde{u}_i q \tilde{\chi}_k^0} L_{\tilde{d}_j q' \tilde{\chi}_k^0}^* \right] \left(ut - m_{\tilde{u}_i}^2 m_{\tilde{d}_j}^2 \right), \\
[\mathcal{G}\mathcal{W}] &= \frac{4\pi \alpha_s \alpha}{18 x_W (1 - x_W) s^2} \text{Re} \left[L_{\tilde{u}_i q \tilde{g}}^* L_{\tilde{d}_j q' \tilde{g}} L_{qq'W}^* L_{\tilde{u}_i \tilde{d}_j W} \right] \left(ut - m_{\tilde{u}_i}^2 m_{\tilde{d}_j}^2 \right), \quad (25)
\end{aligned}$$

which combine coupling constants and Dirac traces of the squared and interference diagrams. In cMFV, superpartners of heavy flavours can only be produced through the purely left-handed s -channel W -exchange, since the t -channel diagrams are suppressed by the small bottom and negligible top quark densities in the proton, and one recovers the result in Ref. [26]. In NMFV, t -channel exchanges can, however, contribute to heavy-flavour final state production from light-flavour initial states and even become dominant, due to the strong gluino coupling.

Neutral squark-antisquark pair production proceeds either from equally neutral quark-antiquark initial states

$$q(h_a, p_a) \bar{q}'(h_b, p_b) \rightarrow \tilde{q}_i(p_1) \tilde{q}_j^*(p_2), \quad (26)$$

through the five different gauge-boson/gaugino exchanges shown in Fig. 2 (top) or from gluon-gluon initial states

$$g(h_a, p_a) g(h_b, p_b) \rightarrow \tilde{q}_i(p_1) \tilde{q}_i^*(p_2) \quad (27)$$

through the purely strong couplings shown in Fig. 2 (bottom). The differential cross section for quark-antiquark

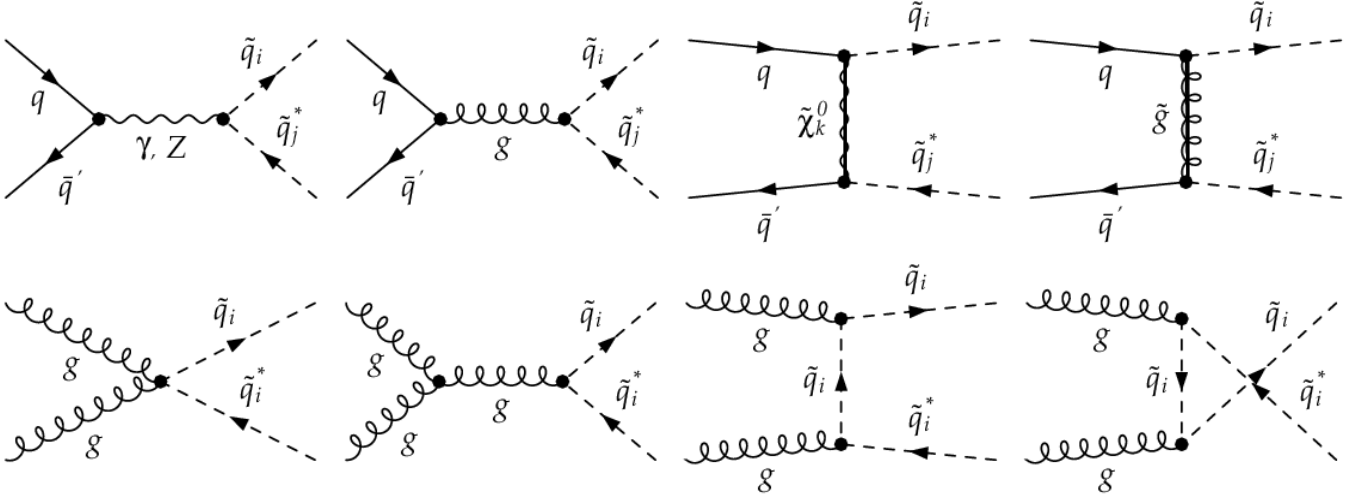


FIG. 2: Tree-level Feynman diagrams for the production of neutral squark-antisquark pairs in quark-antiquark (top) and gluon-gluon collisions (bottom).

scattering

$$\begin{aligned}
\frac{d\hat{\sigma}_{h_a, h_b}^{q\bar{q}'}}{dt} &= (1-h_a)(1+h_b) \left[\frac{\mathcal{Y}}{s^2} + \frac{\mathcal{Z}_1}{s_z^2} + \frac{\mathcal{G}}{s^2} + \frac{\tilde{\mathcal{G}}_{11}}{t_{\tilde{g}}^2} + \frac{[\mathcal{Y}\mathcal{Z}]_1}{s s_z} + \frac{[\tilde{\mathcal{G}}\mathcal{Y}]_1}{t_{\tilde{g}} s} + \frac{[\tilde{\mathcal{G}}\mathcal{Z}]_1}{t_{\tilde{g}} s_z} + \frac{[\tilde{\mathcal{G}}\mathcal{G}]_1}{t_{\tilde{g}} s} \right. \\
&\quad \left. + \sum_{k,l=1,\dots,4} \left(\frac{\mathcal{N}_{11}^{kl}}{t_{\tilde{\chi}_k^0} t_{\tilde{\chi}_l^0}} \right) + \sum_{k=1,\dots,4} \left(\frac{[\mathcal{N}\mathcal{Y}]_1^k}{t_{\tilde{\chi}_k^0} s} + \frac{[\mathcal{N}\mathcal{Z}]_1^k}{t_{\tilde{\chi}_k^0} s_z} + \frac{[\mathcal{N}\mathcal{G}]_1^k}{t_{\tilde{\chi}_k^0} s} \right) \right] \\
&\quad + (1+h_a)(1-h_b) \left[\frac{\mathcal{Y}}{s^2} + \frac{\mathcal{Z}_2}{s_z^2} + \frac{\mathcal{G}}{s^2} + \frac{\tilde{\mathcal{G}}_{22}}{t_{\tilde{g}}^2} + \frac{[\mathcal{Y}\mathcal{Z}]_2}{s s_z} + \frac{[\tilde{\mathcal{G}}\mathcal{Y}]_2}{t_{\tilde{g}} s} + \frac{[\tilde{\mathcal{G}}\mathcal{Z}]_2}{t_{\tilde{g}} s_z} + \frac{[\tilde{\mathcal{G}}\mathcal{G}]_2}{t_{\tilde{g}} s} \right. \\
&\quad \left. + \sum_{k,l=1,\dots,4} \left(\frac{\mathcal{N}_{22}^{kl}}{t_{\tilde{\chi}_k^0} t_{\tilde{\chi}_l^0}} \right) + \sum_{k=1,\dots,4} \left(\frac{[\mathcal{N}\mathcal{Y}]_2^k}{t_{\tilde{\chi}_k^0} s} + \frac{[\mathcal{N}\mathcal{Z}]_2^k}{t_{\tilde{\chi}_k^0} s_z} + \frac{[\mathcal{N}\mathcal{G}]_2^k}{t_{\tilde{\chi}_k^0} s} \right) \right] \\
&\quad + (1-h_a)(1-h_b) \left[\frac{\tilde{\mathcal{G}}_{12}}{t_{\tilde{g}}^2} + \sum_{k,l=1,\dots,4} \left(\frac{\mathcal{N}_{12}^{kl}}{t_{\tilde{\chi}_k^0} t_{\tilde{\chi}_l^0}} \right) \right] + (1+h_a)(1+h_b) \left[\frac{\tilde{\mathcal{G}}_{21}}{t_{\tilde{g}}^2} + \sum_{k,l=1,\dots,4} \left(\frac{\mathcal{N}_{21}^{kl}}{t_{\tilde{\chi}_k^0} t_{\tilde{\chi}_l^0}} \right) \right] \quad (28)
\end{aligned}$$

involves many different form factors,

$$\begin{aligned}
\mathcal{Y} &= \frac{\pi \alpha^2 e_q^2 e_{\tilde{q}}^2 \delta_{ij} \delta_{qq'}}{s^2} \left(ut - m_{\tilde{q}_i}^2 m_{\tilde{q}'_j}^2 \right), \\
\mathcal{Z}_m &= \frac{\pi \alpha^2}{16 s^2 x_W^2 (1-x_W)^2} |L_{\tilde{q}_i \tilde{q}_j Z} + R_{\tilde{q}_i \tilde{q}_j Z}|^2 (C_{qq'Z}^m)^2 \left(ut - m_{\tilde{q}_i}^2 m_{\tilde{q}'_j}^2 \right), \\
\mathcal{G} &= \frac{2 \pi \alpha_s^2 \delta_{ij} \delta_{qq'}}{9 s^2} \left(ut - m_{\tilde{q}_i}^2 m_{\tilde{q}'_j}^2 \right), \\
\mathcal{N}_{mn}^{kl} &= \frac{\pi \alpha^2}{x_W^2 (1-x_W)^2 s^2} C_{\tilde{q}_i q \tilde{\chi}_k^0}^{m*} C_{\tilde{q}_i q \tilde{\chi}_l^0}^m C_{\tilde{q}_j q' \tilde{\chi}_k^0}^n C_{\tilde{q}_j q' \tilde{\chi}_l^0}^{n*} \left[\left(ut - m_{\tilde{q}_i}^2 m_{\tilde{q}'_j}^2 \right) \delta_{mn} + \left(m_{\tilde{\chi}_k^0} m_{\tilde{\chi}_l^0} s \right) (1 - \delta_{mn}) \right], \\
\tilde{\mathcal{G}}_{mn} &= \frac{2 \pi \alpha_s^2}{9 s^2} \left| C_{\tilde{q}_i q \tilde{g}}^m C_{\tilde{q}_j q' \tilde{g}}^{n*} \right|^2 \left[\left(ut - m_{\tilde{q}_i}^2 m_{\tilde{q}'_j}^2 \right) \delta_{mn} + \left(m_{\tilde{g}}^2 s \right) (1 - \delta_{mn}) \right], \\
[\mathcal{Y}\mathcal{Z}]_m &= \frac{\pi \alpha^2 e_q e_{\tilde{q}} \delta_{ij} \delta_{qq'}}{2 s^2 x_W (1-x_W)} \text{Re} \left[L_{\tilde{q}_i \tilde{q}_j Z} + R_{\tilde{q}_i \tilde{q}_j Z} \right] C_{qq'Z}^m \left(ut - m_{\tilde{q}_i}^2 m_{\tilde{q}'_j}^2 \right), \\
[\mathcal{N}\mathcal{Y}]_m^k &= \frac{2 \pi \alpha^2 e_q e_{\tilde{q}} \delta_{ij} \delta_{qq'}}{3 x_W (1-x_W) s^2} \text{Re} \left[C_{\tilde{q}_i q \tilde{\chi}_k^0}^m C_{\tilde{q}_j q' \tilde{\chi}_k^0}^{m*} \right] \left(ut - m_{\tilde{q}_i}^2 m_{\tilde{q}'_j}^2 \right),
\end{aligned}$$

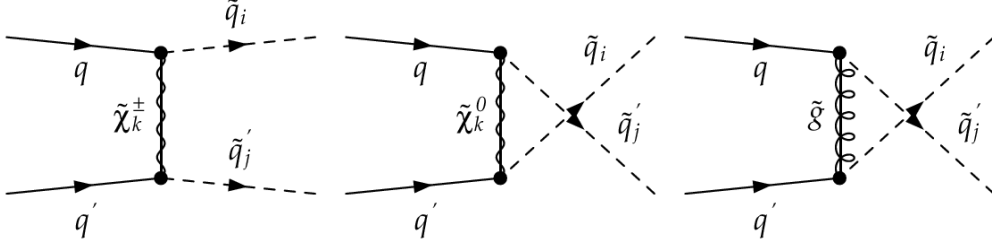


FIG. 3: Tree-level Feynman diagrams for the production of one down-type squark (\tilde{q}_i) and one up-type squark (\tilde{q}'_j) in the collision of an up-type quark (q) and a down-type quark (q').

$$\begin{aligned}
[\mathcal{N}\mathcal{Z}]_m^k &= \frac{\pi \alpha^2}{6 x_W^2 (1 - x_W)^2 s^2} \text{Re} \left[C_{\tilde{q}_i q \tilde{\chi}_k^+}^m C_{\tilde{q}_j q' \tilde{\chi}_k^0}^{m*} (L_{\tilde{q}_i \tilde{q}_j Z} + R_{\tilde{q}_i \tilde{q}_j Z}) \right] C_{q q' Z}^m \left(u t - m_{\tilde{q}_i}^2 m_{\tilde{q}_j}^2 \right), \\
[\mathcal{N}\mathcal{G}]_m^k &= \frac{8 \pi \alpha \alpha_s \delta_{ij} \delta_{qq'}}{9 x_W (1 - x_W) s^2} \text{Re} \left[C_{\tilde{q}_i q \tilde{\chi}_k^0}^m C_{\tilde{q}_j q' \tilde{\chi}_k^0}^{m*} \right] \left(u t - m_{\tilde{q}_i}^2 m_{\tilde{q}_j}^2 \right), \\
[\tilde{\mathcal{G}}\mathcal{G}]_m &= -\frac{4 \pi \alpha_s^2 \delta_{ij} \delta_{qq'}}{27 s^2} \text{Re} \left[C_{\tilde{q}_i q \tilde{g}}^{m*} C_{\tilde{q}_j q' \tilde{g}}^m \right] \left(u t - m_{\tilde{q}_i}^2 m_{\tilde{q}_j}^2 \right), \\
[\tilde{\mathcal{G}}\mathcal{Y}]_m &= \frac{8 \pi \alpha \alpha_s e_q e_{\tilde{q}} \delta_{ij} \delta_{qq'}}{9 s^2} \text{Re} \left[C_{\tilde{q}_i q \tilde{g}}^{m*} C_{\tilde{q}_j q' \tilde{g}}^m \right] \left(u t - m_{\tilde{q}_i}^2 m_{\tilde{q}_j}^2 \right), \\
[\tilde{\mathcal{G}}\mathcal{Z}]_m &= \frac{2 \pi \alpha \alpha_s}{9 x_W (1 - x_W) s^2} \text{Re} \left[C_{\tilde{q}_i q \tilde{g}}^{m*} C_{\tilde{q}_j q' \tilde{g}}^m (L_{\tilde{q}_i \tilde{q}_j Z} + R_{\tilde{q}_i \tilde{q}_j Z}) \right] C_{q q' Z}^m \left(u t - m_{\tilde{q}_i}^2 m_{\tilde{q}_j}^2 \right), \tag{29}
\end{aligned}$$

since only very few interferences (those between strong and electroweak channels of the same propagator type) are eliminated due to colour conservation. On the other hand, the gluon-initiated cross section

$$\frac{d\hat{\sigma}_{h_a, h_b}^{gg}}{dt} = \frac{\pi \alpha_s^2}{128 s^2} \left[24 \left(1 - 2 \frac{t_{\tilde{q}_i} u_{\tilde{q}_i}}{s^2} \right) - \frac{8}{3} \right] \left[(1 - h_a h_b) - 2 \frac{s m_{\tilde{q}_i}^2}{t_{\tilde{q}_i} u_{\tilde{q}_i}} \left((1 - h_a h_b) - \frac{s m_{\tilde{q}_i}^2}{t_{\tilde{q}_i} u_{\tilde{q}_i}} \right) \right] \tag{30}$$

involves only the strong coupling constant and is thus quite compact. In the case of cMFV, but diagonal or non-diagonal squark helicity, our results agree with those in Ref. [26]. Diagonal production of identical squark-antisquark mass eigenstates is, of course, dominated by the strong quark-antiquark and gluon-gluon channels. Their relative importance depends on the partonic luminosity and thus on the type and energy of the hadron collider under consideration. Non-diagonal production of squarks of different helicity or flavour involves only electroweak and gluino-mediated quark-antiquark scattering, and the relative importance of these processes depends largely on the gluino mass.

C. Squark Pair Production

While squark-antisquark pairs are readily produced in $p\bar{p}$ collisions, e.g. at the Tevatron, from valence quarks and antiquarks, pp colliders have a larger quark-quark luminosity and will thus more easily lead to squark pair production. The production of one down-type and one up-type squark

$$q(h_a, p_a) q'(h_b, p_b) \rightarrow \tilde{d}_i(p_1) \tilde{u}_j(p_2), \tag{31}$$

in the collision of an up-type quark q and a down-type quark q' proceeds through the t -channel chargino or u -channel neutralino and gluino exchanges shown in Fig. 3. The corresponding cross section

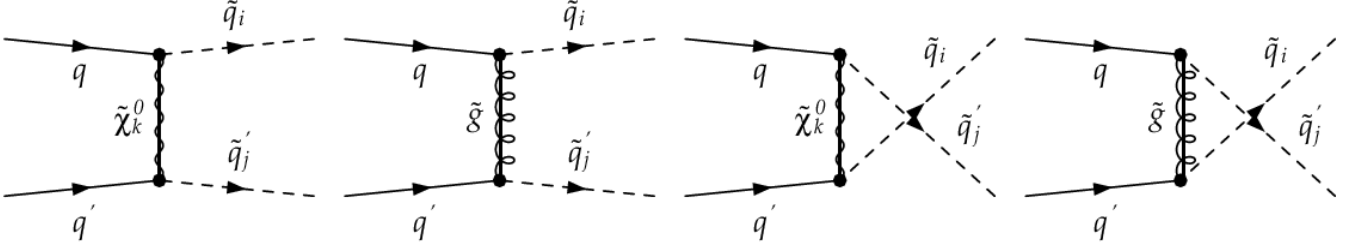


FIG. 4: Tree-level Feynman diagrams for the production of two up-type or down-type squarks.

$$\begin{aligned}
\frac{d\hat{\sigma}_{h_a, h_b}^{qq'}}{dt} &= (1-h_a)(1-h_b) \left[\left(\sum_{\substack{k=1,2 \\ l=1,2}} \frac{\mathcal{C}_{11}^{kl}}{t_{\tilde{\chi}_k} t_{\tilde{\chi}_l}} \right) + \left(\sum_{\substack{k=1,\dots,4 \\ l=1,\dots,4}} \frac{\mathcal{N}_{11}^{kl}}{u_{\tilde{\chi}_k^0} u_{\tilde{\chi}_l^0}} \right) + \frac{\mathcal{G}_{11}}{u_{\tilde{g}}^2} + \left(\sum_{\substack{k=1,2 \\ l=1,\dots,4}} \frac{[\mathcal{CN}]_{11}^{kl}}{t_{\tilde{\chi}_k} u_{\tilde{\chi}_l^0}} \right) + \left(\sum_{k=1,2} \frac{[\mathcal{CG}]_{11}^k}{t_{\tilde{\chi}_k} u_{\tilde{g}}} \right) \right] \\
&+ (1+h_a)(1+h_b) \left[\left(\sum_{\substack{k=1,2 \\ l=1,2}} \frac{\mathcal{C}_{22}^{kl}}{t_{\tilde{\chi}_k} t_{\tilde{\chi}_l}} \right) + \left(\sum_{\substack{k=1,\dots,4 \\ l=1,\dots,4}} \frac{\mathcal{N}_{22}^{kl}}{u_{\tilde{\chi}_k^0} u_{\tilde{\chi}_l^0}} \right) + \frac{\mathcal{G}_{22}}{u_{\tilde{g}}^2} + \left(\sum_{\substack{k=1,2 \\ l=1,\dots,4}} \frac{[\mathcal{CN}]_{22}^{kl}}{t_{\tilde{\chi}_k} u_{\tilde{\chi}_l^0}} \right) + \left(\sum_{k=1,2} \frac{[\mathcal{CG}]_{22}^k}{t_{\tilde{\chi}_k} u_{\tilde{g}}} \right) \right] \\
&+ (1-h_a)(1+h_b) \left[\left(\sum_{\substack{k=1,2 \\ l=1,2}} \frac{\mathcal{C}_{12}^{kl}}{t_{\tilde{\chi}_k} t_{\tilde{\chi}_l}} \right) + \left(\sum_{\substack{k=1,\dots,4 \\ l=1,\dots,4}} \frac{\mathcal{N}_{12}^{kl}}{u_{\tilde{\chi}_k^0} u_{\tilde{\chi}_l^0}} \right) + \frac{\mathcal{G}_{12}}{u_{\tilde{g}}^2} + \left(\sum_{\substack{k=1,2 \\ l=1,\dots,4}} \frac{[\mathcal{CN}]_{12}^{kl}}{t_{\tilde{\chi}_k} u_{\tilde{\chi}_l^0}} \right) + \left(\sum_{k=1,2} \frac{[\mathcal{CG}]_{12}^k}{t_{\tilde{\chi}_k} u_{\tilde{g}}} \right) \right] \\
&+ (1+h_a)(1-h_b) \left[\left(\sum_{\substack{k=1,2 \\ l=1,2}} \frac{\mathcal{C}_{21}^{kl}}{t_{\tilde{\chi}_k} t_{\tilde{\chi}_l}} \right) + \left(\sum_{\substack{k=1,\dots,4 \\ l=1,\dots,4}} \frac{\mathcal{N}_{21}^{kl}}{u_{\tilde{\chi}_k^0} u_{\tilde{\chi}_l^0}} \right) + \frac{\mathcal{G}_{21}}{u_{\tilde{g}}^2} + \left(\sum_{\substack{k=1,2 \\ l=1,\dots,4}} \frac{[\mathcal{CN}]_{21}^{kl}}{t_{\tilde{\chi}_k} u_{\tilde{\chi}_l^0}} \right) + \left(\sum_{k=1,2} \frac{[\mathcal{CG}]_{21}^k}{t_{\tilde{\chi}_k} u_{\tilde{g}}} \right) \right] \quad (32)
\end{aligned}$$

involves the form factors

$$\begin{aligned}
\mathcal{C}_{mn}^{kl} &= \frac{\pi \alpha^2}{4 x_W^2 s^2} \mathcal{C}_{\tilde{u}_j q' \tilde{\chi}_k^\pm}^n \mathcal{C}_{\tilde{d}_i q \tilde{\chi}_k^\pm}^{m*} \mathcal{C}_{\tilde{u}_j q' \tilde{\chi}_l^\pm}^{n*} \mathcal{C}_{\tilde{d}_i q \tilde{\chi}_l^\pm}^m \left[\left(u t - m_{\tilde{d}_i}^2 m_{\tilde{u}_j}^2 \right) (1 - \delta_{mn}) + m_{\tilde{\chi}_k^\pm} m_{\tilde{\chi}_l^\pm} s \delta_{mn} \right], \\
\mathcal{N}_{mn}^{kl} &= \frac{\pi \alpha^2}{x_W^2 (1-x_W)^2 s^2} \mathcal{C}_{\tilde{u}_j q \tilde{\chi}_k^0}^{m*} \mathcal{C}_{\tilde{d}_i q' \tilde{\chi}_k^0}^{n*} \mathcal{C}_{\tilde{u}_j q \tilde{\chi}_l^0}^m \mathcal{C}_{\tilde{d}_i q' \tilde{\chi}_l^0}^n \left[\left(u t - m_{\tilde{d}_i}^2 m_{\tilde{u}_j}^2 \right) (1 - \delta_{mn}) + m_{\tilde{\chi}_k^0} m_{\tilde{\chi}_l^0} s \delta_{mn} \right], \\
\mathcal{G}_{mn} &= \frac{2 \pi \alpha_s^2}{9 s^2} \left| \mathcal{C}_{\tilde{u}_j q \tilde{g}}^m \mathcal{C}_{\tilde{d}_i q' \tilde{g}}^n \right|^2 \left[\left(u t - m_{\tilde{d}_i}^2 m_{\tilde{u}_j}^2 \right) (1 - \delta_{mn}) + m_{\tilde{g}}^2 s \delta_{mn} \right], \\
[\mathcal{CN}]_{mn}^{kl} &= \frac{\pi \alpha^2}{3 x_W^2 (1-x_W) s^2} \text{Re} \left[\mathcal{C}_{\tilde{u}_j q' \tilde{\chi}_k^\pm}^n \mathcal{C}_{\tilde{d}_i q \tilde{\chi}_k^\pm}^{m*} \mathcal{C}_{\tilde{u}_j q \tilde{\chi}_l^0}^m \mathcal{C}_{\tilde{d}_i q' \tilde{\chi}_l^0}^n \right] \left[\left(u t - m_{\tilde{d}_i}^2 m_{\tilde{u}_j}^2 \right) (\delta_{mn} - 1) + m_{\tilde{\chi}_k^\pm} m_{\tilde{\chi}_l^0} s \delta_{mn} \right], \\
[\mathcal{CG}]_{mn}^k &= \frac{4 \pi \alpha \alpha_s}{9 s^2 x_W} \text{Re} \left[\mathcal{C}_{\tilde{u}_j q' \tilde{\chi}_k^\pm}^n \mathcal{C}_{\tilde{d}_i q \tilde{\chi}_k^\pm}^{m*} \mathcal{C}_{\tilde{u}_j q \tilde{g}}^m \mathcal{C}_{\tilde{d}_i q' \tilde{g}}^n \right] \left[\left(u t - m_{\tilde{d}_i}^2 m_{\tilde{u}_j}^2 \right) (\delta_{mn} - 1) + m_{\tilde{\chi}_k^\pm} m_{\tilde{g}} s \delta_{mn} \right], \quad (33)
\end{aligned}$$

where the neutralino-gluino interference term is absent due to colour conservation. The cross section for the charge-conjugate production of antisquarks from antiquarks can be obtained from the equations above by replacing $h_{a,b} \rightarrow -h_{a,b}$. Heavy-flavour final states are completely absent in cMFV due to the negligible top quark and small bottom quark densities in the proton and can thus only be obtained in NMFV.

The Feynman diagrams for pair production of two up- or down-type squarks

$$q(h_a, p_a) q'(h_b, p_b) \rightarrow \tilde{q}_i(p_1) \tilde{q}_j(p_2) \quad (34)$$

are shown in Fig. 4. In NMFV, neutralino and gluino exchanges can lead to identical squark flavours for different

quark initial states, so that both t - and u -channels contribute and may interfere. The cross section

$$\begin{aligned}
\frac{d\hat{\sigma}_{h_a, h_b}^{qq'}}{dt} &= (1 - h_a)(1 - h_b) \left[\left(\sum_{\substack{k=1, \dots, 4 \\ l=1, \dots, 4}} \frac{[\mathcal{NT}]_{11}^{kl}}{t_{\tilde{\chi}_k^0} t_{\tilde{\chi}_l^0}} + \frac{[\mathcal{NU}]_{11}^{kl}}{u_{\tilde{\chi}_k^0} u_{\tilde{\chi}_l^0}} + \frac{[\mathcal{NTU}]_{11}^{kl}}{t_{\tilde{\chi}_k^0} u_{\tilde{\chi}_l^0}} \right) + \frac{[\mathcal{GT}]_{11}}{t_{\tilde{g}}^2} + \frac{[\mathcal{GU}]_{11}}{u_{\tilde{g}}^2} + \frac{[\mathcal{GTU}]_{11}}{u_{\tilde{g}} t_{\tilde{g}}} \right. \\
&+ \left. \left(\sum_{k=1, \dots, 4} \frac{[\mathcal{NGA}]_{11}^k}{t_{\tilde{\chi}_k^0} u_{\tilde{g}}} + \frac{[\mathcal{NGB}]_{11}^k}{u_{\tilde{\chi}_k^0} t_{\tilde{g}}} \right) \right] \frac{1}{1 + \delta_{ij}} \\
&+ (1 + h_a)(1 + h_b) \left[\left(\sum_{\substack{k=1, \dots, 4 \\ l=1, \dots, 4}} \frac{[\mathcal{NT}]_{22}^{kl}}{t_{\tilde{\chi}_k^0} t_{\tilde{\chi}_l^0}} + \frac{[\mathcal{NU}]_{22}^{kl}}{u_{\tilde{\chi}_k^0} u_{\tilde{\chi}_l^0}} + \frac{[\mathcal{NTU}]_{22}^{kl}}{t_{\tilde{\chi}_k^0} u_{\tilde{\chi}_l^0}} \right) + \frac{[\mathcal{GT}]_{22}}{t_{\tilde{g}}^2} + \frac{[\mathcal{GU}]_{22}}{u_{\tilde{g}}^2} + \frac{[\mathcal{GTU}]_{22}}{u_{\tilde{g}} t_{\tilde{g}}} \right. \\
&+ \left. \left(\sum_{k=1, \dots, 4} \frac{[\mathcal{NGA}]_{22}^k}{t_{\tilde{\chi}_k^0} u_{\tilde{g}}} + \frac{[\mathcal{NGB}]_{22}^k}{u_{\tilde{\chi}_k^0} t_{\tilde{g}}} \right) \right] \frac{1}{1 + \delta_{ij}} \\
&+ (1 - h_a)(1 + h_b) \left[\left(\sum_{\substack{k=1, \dots, 4 \\ l=1, \dots, 4}} \frac{[\mathcal{NT}]_{12}^{kl}}{t_{\tilde{\chi}_k^0} t_{\tilde{\chi}_l^0}} + \frac{[\mathcal{NU}]_{12}^{kl}}{u_{\tilde{\chi}_k^0} u_{\tilde{\chi}_l^0}} + \frac{[\mathcal{NTU}]_{12}^{kl}}{t_{\tilde{\chi}_k^0} u_{\tilde{\chi}_l^0}} \right) + \frac{[\mathcal{GT}]_{12}}{t_{\tilde{g}}^2} + \frac{[\mathcal{GU}]_{12}}{u_{\tilde{g}}^2} + \frac{[\mathcal{GTU}]_{12}}{u_{\tilde{g}} t_{\tilde{g}}} \right. \\
&+ \left. \left(\sum_{k=1, \dots, 4} \frac{[\mathcal{NGA}]_{12}^k}{t_{\tilde{\chi}_k^0} u_{\tilde{g}}} + \frac{[\mathcal{NGB}]_{12}^k}{u_{\tilde{\chi}_k^0} t_{\tilde{g}}} \right) \right] \frac{1}{1 + \delta_{ij}} \\
&+ (1 + h_a)(1 - h_b) \left[\left(\sum_{\substack{k=1, \dots, 4 \\ l=1, \dots, 4}} \frac{[\mathcal{NT}]_{21}^{kl}}{t_{\tilde{\chi}_k^0} t_{\tilde{\chi}_l^0}} + \frac{[\mathcal{NU}]_{21}^{kl}}{u_{\tilde{\chi}_k^0} u_{\tilde{\chi}_l^0}} + \frac{[\mathcal{NTU}]_{21}^{kl}}{t_{\tilde{\chi}_k^0} u_{\tilde{\chi}_l^0}} \right) + \frac{[\mathcal{GT}]_{21}}{t_{\tilde{g}}^2} + \frac{[\mathcal{GU}]_{21}}{u_{\tilde{g}}^2} + \frac{[\mathcal{GTU}]_{21}}{u_{\tilde{g}} t_{\tilde{g}}} \right. \\
&+ \left. \left(\sum_{k=1, \dots, 4} \frac{[\mathcal{NGA}]_{21}^k}{t_{\tilde{\chi}_k^0} u_{\tilde{g}}} + \frac{[\mathcal{NGB}]_{21}^k}{u_{\tilde{\chi}_k^0} t_{\tilde{g}}} \right) \right] \frac{1}{1 + \delta_{ij}} \tag{35}
\end{aligned}$$

depends therefore on the form factors

$$\begin{aligned}
[\mathcal{NT}]_{mn}^{kl} &= \frac{\pi \alpha^2}{x_W^2 (1 - x_W)^2 s^2} \mathcal{C}_{\tilde{q}_i q' \tilde{\chi}_k^0}^{n*} \mathcal{C}_{\tilde{q}_i q \tilde{\chi}_k^0}^{m*} \mathcal{C}_{\tilde{q}_j q' \tilde{\chi}_l^0}^n \mathcal{C}_{\tilde{q}_i q \tilde{\chi}_l^0}^m \left[(ut - m_{\tilde{q}_i}^2 m_{\tilde{q}_j}^2) (1 - \delta_{mn}) + m_{\tilde{\chi}_k^0} m_{\tilde{\chi}_l^0} s \delta_{mn} \right], \\
[\mathcal{NU}]_{mn}^{kl} &= \frac{\pi \alpha^2}{x_W^2 (1 - x_W)^2 s^2} \mathcal{C}_{\tilde{q}_i q' \tilde{\chi}_k^0}^{n*} \mathcal{C}_{\tilde{q}_j q \tilde{\chi}_k^0}^{m*} \mathcal{C}_{\tilde{q}_i q' \tilde{\chi}_l^0}^n \mathcal{C}_{\tilde{q}_j q \tilde{\chi}_l^0}^m \left[(ut - m_{\tilde{q}_i}^2 m_{\tilde{q}_j}^2) (1 - \delta_{mn}) + m_{\tilde{\chi}_k^0} m_{\tilde{\chi}_l^0} s \delta_{mn} \right], \\
[\mathcal{NTU}]_{mn}^{kl} &= \frac{2 \pi \alpha^2}{3 x_W^2 (1 - x_W)^2 s^2} \text{Re} \left[\mathcal{C}_{\tilde{q}_i q \tilde{\chi}_k^0}^{m*} \mathcal{C}_{\tilde{q}_j q' \tilde{\chi}_k^0}^{n*} \mathcal{C}_{\tilde{q}_i q' \tilde{\chi}_l^0}^n \mathcal{C}_{\tilde{q}_j q \tilde{\chi}_l^0}^m \right] \left[(ut - m_{\tilde{q}_i}^2 m_{\tilde{q}_j}^2) (1 - \delta_{mn}) + m_{\tilde{\chi}_k^0} m_{\tilde{\chi}_l^0} s \delta_{mn} \right], \\
[\mathcal{GT}]_{mn} &= \frac{2 \pi \alpha_s^2}{9 s^2} \left| \mathcal{C}_{\tilde{q}_j q' \tilde{g}}^n \mathcal{C}_{\tilde{q}_i q \tilde{g}}^m \right|^2 \left[(ut - m_{\tilde{q}_i}^2 m_{\tilde{q}_j}^2) (1 - \delta_{mn}) + m_{\tilde{g}}^2 s \delta_{mn} \right], \\
[\mathcal{GU}]_{mn} &= \frac{2 \pi \alpha_s^2}{9 s^2} \left| \mathcal{C}_{\tilde{q}_i q' \tilde{g}}^m \mathcal{C}_{\tilde{q}_j q \tilde{g}}^n \right|^2 \left[(ut - m_{\tilde{q}_i}^2 m_{\tilde{q}_j}^2) (1 - \delta_{mn}) + m_{\tilde{g}}^2 s \delta_{mn} \right], \\
[\mathcal{GTU}]_{mn} &= \frac{-4 \pi \alpha_s^2}{27 s^2} \text{Re} \left[\mathcal{C}_{\tilde{q}_i q \tilde{g}}^m \mathcal{C}_{\tilde{q}_j q' \tilde{g}}^n \mathcal{C}_{\tilde{q}_i q' \tilde{g}}^{m*} \mathcal{C}_{\tilde{q}_j q \tilde{g}}^{n*} \right] \left[(ut - m_{\tilde{q}_i}^2 m_{\tilde{q}_j}^2) (1 - \delta_{mn}) + m_{\tilde{g}}^2 s \delta_{mn} \right], \\
[\mathcal{NGA}]_{mn}^k &= \frac{8 \pi \alpha \alpha_s}{9 s^2 x_W (1 - x_W)} \text{Re} \left[\mathcal{C}_{\tilde{q}_i q' \tilde{\chi}_k^0}^{n*} \mathcal{C}_{\tilde{q}_i q \tilde{\chi}_k^0}^{m*} \mathcal{C}_{\tilde{q}_i q' \tilde{g}}^{m*} \mathcal{C}_{\tilde{q}_j q \tilde{g}}^{n*} \right] \left[(ut - m_{\tilde{q}_i}^2 m_{\tilde{q}_j}^2) (1 - \delta_{mn}) + m_{\tilde{\chi}_k^0} m_{\tilde{g}} s \delta_{mn} \right], \\
[\mathcal{NGB}]_{mn}^k &= \frac{8 \pi \alpha \alpha_s}{9 s^2 x_W (1 - x_W)} \text{Re} \left[\mathcal{C}_{\tilde{q}_i q' \tilde{\chi}_k^0}^{n*} \mathcal{C}_{\tilde{q}_j q \tilde{\chi}_k^0}^{m*} \mathcal{C}_{\tilde{q}_j q' \tilde{g}}^{n*} \mathcal{C}_{\tilde{q}_i q \tilde{g}}^{m*} \right] \left[(ut - m_{\tilde{q}_i}^2 m_{\tilde{q}_j}^2) (1 - \delta_{mn}) + m_{\tilde{\chi}_k^0} m_{\tilde{g}} s \delta_{mn} \right]. \tag{36}
\end{aligned}$$

Gluginos will dominate over neutralino exchanges due to their strong coupling, and the two will only interfere in the mixed t - and u -channels due to colour conservation. At the LHC, up-type squark pair production should dominate over mixed up-/down-type squark production and down-type squark pair production, since the proton contains two valence up-quarks and only one valence down-quark. As before, the charge-conjugate production of antisquark pairs

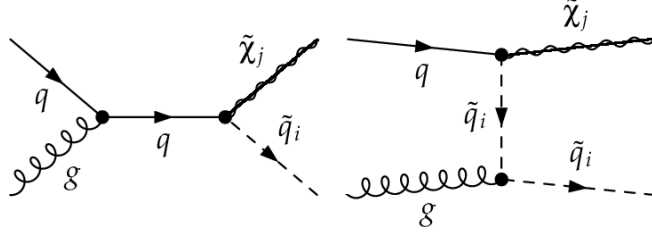


FIG. 5: Tree-level Feynman diagrams for the associated production of squarks and gauginos.

is obtained by making the replacement $h_{a,b} \rightarrow -h_{a,b}$. If we neglect electroweak contributions as well as squark flavour and helicity mixing and sum over left- and right-handed squark states, our results agree with those of Ref. [27].

D. Associated Production of Squarks and Gauginos

The associated production of squarks and neutralinos or charginos

$$q(h_a, p_a) g(h_b, p_b) \rightarrow \tilde{\chi}_j(p_1) \tilde{q}_i(p_2) \quad (37)$$

is a semi-weak process that originates from quark-gluon initial states and has both an s -channel quark and a t -channel squark contribution. They involve both a quark-squark-gaugino vertex that can in general be flavour violating. The corresponding Feynman diagrams can be seen in Fig. 5. The squark-gaugino cross section

$$\begin{aligned} \frac{d\hat{\sigma}_{h_a, h_b}^{qg}}{dt} &= \frac{\pi \alpha \alpha_s}{n_{\tilde{\chi}} s^2} \left\{ \frac{-u_{\tilde{\chi}_j}}{s} \left[(1-h_a)(1-h_b) |L_{\tilde{q}_i q \tilde{\chi}_j}|^2 + (1+h_a)(1+h_b) |R_{\tilde{q}_i q \tilde{\chi}_j}|^2 \right] \right. \\ &+ \frac{t_{\tilde{\chi}_j} (t + m_{\tilde{q}_i}^2)}{t_{\tilde{q}_i}^2} \left[(1-h_a) |L_{\tilde{q}_i q \tilde{\chi}_j}|^2 + (1+h_a) |R_{\tilde{q}_i q \tilde{\chi}_j}|^2 \right] \\ &+ \frac{2(u t - m_{\tilde{q}_i}^2 m_{\tilde{\chi}_j}^2)}{s t_{\tilde{q}_i}} \left[(1-h_a)(1-h_b) |L_{\tilde{q}_i q \tilde{\chi}_j}|^2 + (1+h_a)(1+h_b) |R_{\tilde{q}_i q \tilde{\chi}_j}|^2 \right] \\ &\left. + \frac{t_{\tilde{\chi}_j} (t_{\tilde{\chi}_j} - u_{\tilde{q}_i})}{s t_{\tilde{q}_i}} \left[(1-h_a) |L_{\tilde{q}_i q \tilde{\chi}_j}|^2 + (1+h_a) |R_{\tilde{q}_i q \tilde{\chi}_j}|^2 \right] \right\}, \quad (38) \end{aligned}$$

where $n_{\tilde{\chi}} = 6x_W(1-x_W)$ for neutralinos and $n_{\tilde{\chi}} = 12x_W$ for charginos, is sufficiently compact to be written without the definition of form factors. Note that the t -channel diagram involves the coupling of the gluon to scalars and does thus not depend on its helicity h_b . The cross section of the charge-conjugate process can be obtained by taking $h_a \rightarrow -h_a$. Third-generation squarks can only be produced in NMFV, preferably through a light (valence) quark in the s -channel. For non-mixing squarks and gauginos, we agree again with the results of Ref. [27].

E. Gaugino Pair Production

Finally, we consider the purely electroweak production of gaugino pairs

$$q(h_a, p_a) \bar{q}(h_b, p_b) \rightarrow \tilde{\chi}_i(p_1) \tilde{\chi}_j(p_2) \quad (39)$$

from quark-antiquark initial states, where flavour violation can occur via the quark-squark-gaugino vertices in the t - and u -channels (see Fig. 6). However, if it were not for different parton density weights, summation over complete squark multiplet exchanges would make these channels insensitive to the exchanged squark flavour. Furthermore there are no final state squarks that could be experimentally tagged. The cross section can be expressed generically as

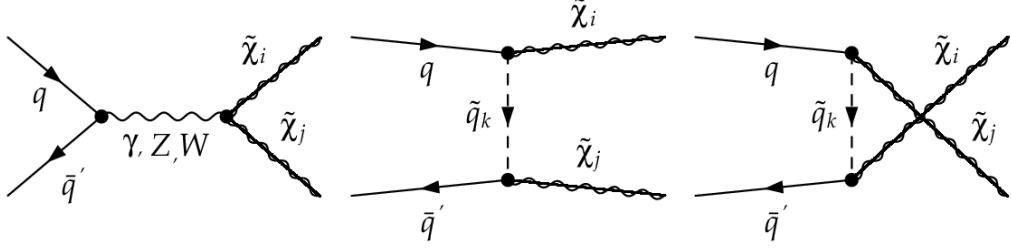


FIG. 6: Tree-level Feynman diagrams for the production of gaugino pairs.

$$\begin{aligned}
\frac{d\hat{\sigma}_{h_a, h_b}^{q\bar{q}'}}{dt} &= \frac{\pi\alpha^2}{3s^2}(1-h_a)(1+h_b) \left[|Q_{LL}^u|^2 u_{\tilde{\chi}_i} u_{\tilde{\chi}_j} + |Q_{LL}^t|^2 t_{\tilde{\chi}_i} t_{\tilde{\chi}_j} + 2\text{Re}[Q_{LL}^{u*} Q_{LL}^t] m_{\tilde{\chi}_i} m_{\tilde{\chi}_j} s \right] \\
&+ \frac{\pi\alpha^2}{3s^2}(1+h_a)(1-h_b) \left[|Q_{RR}^u|^2 u_{\tilde{\chi}_i} u_{\tilde{\chi}_j} + |Q_{RR}^t|^2 t_{\tilde{\chi}_i} t_{\tilde{\chi}_j} + 2\text{Re}[Q_{RR}^{u*} Q_{RR}^t] m_{\tilde{\chi}_i} m_{\tilde{\chi}_j} s \right] \\
&+ \frac{\pi\alpha^2}{3s^2}(1+h_a)(1+h_b) \left[|Q_{RL}^u|^2 u_{\tilde{\chi}_i} u_{\tilde{\chi}_j} + |Q_{RL}^t|^2 t_{\tilde{\chi}_i} t_{\tilde{\chi}_j} + \text{Re}[Q_{RL}^{u*} Q_{RL}^t] (ut - m_{\tilde{\chi}_i}^2 m_{\tilde{\chi}_j}^2) \right] \\
&+ \frac{\pi\alpha^2}{3s^2}(1-h_a)(1-h_b) \left[|Q_{LR}^u|^2 u_{\tilde{\chi}_i} u_{\tilde{\chi}_j} + |Q_{LR}^t|^2 t_{\tilde{\chi}_i} t_{\tilde{\chi}_j} + \text{Re}[Q_{LR}^{u*} Q_{LR}^t] (ut - m_{\tilde{\chi}_i}^2 m_{\tilde{\chi}_j}^2) \right], \quad (40)
\end{aligned}$$

i.e. in terms of generalized charges. For $\tilde{\chi}_i^- \tilde{\chi}_j^+$ -production, these charges are given by

$$\begin{aligned}
Q_{LL}^{u-+} &= \left(\frac{e_q \delta_{ij} \delta_{qq'}}{s} - \frac{L_{qq'Z} O_{ij}^{\prime R*}}{2x_W(1-x_W)s_z} + \sum_{k=1}^6 \frac{L_{\tilde{d}_k q' \tilde{\chi}_i^\pm} L_{\tilde{d}_k q \tilde{\chi}_j^\pm}^*}{2x_W u_{\tilde{d}_k}} \right), \\
Q_{LL}^{t-+} &= \left(\frac{e_q \delta_{ij} \delta_{qq'}}{s} - \frac{L_{qq'Z} O_{ij}^{\prime L*}}{2x_W(1-x_W)s_z} - \sum_{k=1}^6 \frac{L_{\tilde{u}_k q' \tilde{\chi}_j^\pm} L_{\tilde{u}_k q \tilde{\chi}_i^\pm}^*}{2x_W t_{\tilde{u}_k}} \right), \\
Q_{RR}^{u-+} &= \left(\frac{e_q \delta_{ij} \delta_{qq'}}{s} - \frac{R_{qq'Z} O_{ij}^{\prime L*}}{2x_W(1-x_W)s_z} + \sum_{k=1}^6 \frac{R_{\tilde{d}_k q' \tilde{\chi}_i^\pm} R_{\tilde{d}_k q \tilde{\chi}_j^\pm}^*}{2x_W u_{\tilde{d}_k}} \right), \\
Q_{RR}^{t-+} &= \left(\frac{e_q \delta_{ij} \delta_{qq'}}{s} - \frac{R_{qq'Z} O_{ij}^{\prime R*}}{2x_W(1-x_W)s_z} - \sum_{k=1}^6 \frac{R_{\tilde{u}_k q' \tilde{\chi}_j^\pm}^* R_{\tilde{u}_k q \tilde{\chi}_i^\pm}}{2x_W t_{\tilde{u}_k}} \right), \\
Q_{LR}^{u-+} &= \sum_{k=1}^6 \frac{R_{\tilde{d}_k q' \tilde{\chi}_i^\pm} L_{\tilde{d}_k q \tilde{\chi}_j^\pm}^*}{2x_W u_{\tilde{d}_k}}, \\
Q_{LR}^{t-+} &= \sum_{k=1}^6 \frac{R_{\tilde{u}_k q' \tilde{\chi}_j^\pm}^* L_{\tilde{u}_k q \tilde{\chi}_i^\pm}}{2x_W t_{\tilde{u}_k}}, \\
Q_{RL}^{u-+} &= \sum_{k=1}^6 \frac{L_{\tilde{d}_k q' \tilde{\chi}_i^\pm} R_{\tilde{d}_k q \tilde{\chi}_j^\pm}^*}{2x_W u_{\tilde{d}_k}}, \\
Q_{RL}^{t-+} &= \sum_{k=1}^6 \frac{L_{\tilde{u}_k q' \tilde{\chi}_j^\pm}^* R_{\tilde{u}_k q \tilde{\chi}_i^\pm}}{2x_W t_{\tilde{u}_k}}. \quad (41)
\end{aligned}$$

Note that there is no interference between t - and u -channel diagrams due to (electromagnetic) charge conservation. The cross section for chargino-pair production in e^+e^- -collisions can be deduced by setting $e_q \rightarrow e_l = -1$, $L_{qq'Z} \rightarrow L_{eeZ} = (2T_l^3 - 2e_l x_W)$ and $R_{qq'Z} \rightarrow R_{eeZ} = -2e_l x_W$. Neglecting all Yukawa couplings, we can then reproduce the calculations of Ref. [28].

The charges of the chargino-neutralino associated production are given by

$$\begin{aligned}
Q_{LL}^{u+0} &= \frac{1}{\sqrt{2(1-x_W)}x_W} \left[\frac{O_{ji}^{L*}L_{qq'W}^*}{\sqrt{2}s_w} + \sum_{k=1}^6 \frac{L_{\tilde{u}_k q' \tilde{\chi}_i^\pm}^* L_{\tilde{u}_k q \tilde{\chi}_j^0}^*}{u_{\tilde{u}_k}} \right], \\
Q_{LL}^{t+0} &= \frac{1}{\sqrt{2(1-x_W)}x_W} \left[\frac{O_{ji}^{R*}L_{qq'W}^*}{\sqrt{2}s_w} - \sum_{k=1}^6 \frac{L_{\tilde{d}_k q \tilde{\chi}_i^\pm}^* L_{\tilde{d}_k q' \tilde{\chi}_j^0}^*}{t_{\tilde{d}_k}} \right], \\
Q_{RR}^{u+0} &= \frac{1}{\sqrt{2(1-x_W)}x_W} \sum_{k=1}^6 \frac{R_{\tilde{u}_k q' \tilde{\chi}_i^\pm}^* R_{\tilde{u}_k q \tilde{\chi}_j^0}^*}{u_{\tilde{u}_k}}, \\
Q_{RR}^{t+0} &= \frac{-1}{\sqrt{2(1-x_W)}x_W} \sum_{k=1}^6 \frac{R_{\tilde{d}_k q \tilde{\chi}_i^\pm}^* R_{\tilde{d}_k q' \tilde{\chi}_j^0}^*}{t_{\tilde{d}_k}}, \\
Q_{LR}^{u+0} &= \frac{1}{\sqrt{2(1-x_W)}x_W} \sum_{k=1}^6 \frac{R_{\tilde{u}_k q' \tilde{\chi}_i^\pm}^* L_{\tilde{u}_k q \tilde{\chi}_j^0}^*}{u_{\tilde{u}_k}}, \\
Q_{LR}^{t+0} &= \frac{1}{\sqrt{2(1-x_W)}x_W} \sum_{k=1}^6 \frac{L_{\tilde{d}_k q \tilde{\chi}_i^\pm}^* R_{\tilde{d}_k q' \tilde{\chi}_j^0}^*}{t_{\tilde{d}_k}}, \\
Q_{RL}^{u+0} &= \frac{1}{\sqrt{2(1-x_W)}x_W} \sum_{k=1}^6 \frac{L_{\tilde{u}_k q' \tilde{\chi}_i^\pm}^* R_{\tilde{u}_k q \tilde{\chi}_j^0}^*}{u_{\tilde{u}_k}}, \\
Q_{RL}^{t+0} &= \frac{1}{\sqrt{2(1-x_W)}x_W} \sum_{k=1}^6 \frac{R_{\tilde{d}_k q \tilde{\chi}_i^\pm}^* L_{\tilde{d}_k q' \tilde{\chi}_j^0}^*}{t_{\tilde{d}_k}}. \tag{42}
\end{aligned}$$

The charge-conjugate process is again obtained by making the replacement $h_{a,b} \rightarrow -h_{a,b}$ in Eq. (40). In the case of non-mixing squarks with neglected Yukawa couplings, we agree with the results of Ref. [22], provided we correct a sign in their Eq. (2) as described in Ref. [29].

Finally, the charges for the neutralino pair production are given by

$$\begin{aligned}
Q_{LL}^{u00} &= \frac{1}{x_W(1-x_W)\sqrt{1+\delta_{ij}}} \left[\frac{L_{qq'Z}O_{ij}''L}{2s_z} + \sum_{k=1}^6 \frac{L_{\tilde{Q}_k q' \tilde{\chi}_i^0} L_{\tilde{Q}_k q \tilde{\chi}_j^0}^*}{u_{\tilde{Q}_k}} \right], \\
Q_{LL}^{t00} &= \frac{1}{x_W(1-x_W)\sqrt{1+\delta_{ij}}} \left[\frac{L_{qq'Z}O_{ij}''R}{2s_z} - \sum_{k=1}^6 \frac{L_{\tilde{Q}_k q \tilde{\chi}_i^0}^* L_{\tilde{Q}_k q' \tilde{\chi}_j^0}}{t_{\tilde{Q}_k}} \right], \\
Q_{RR}^{u00} &= \frac{1}{x_W(1-x_W)\sqrt{1+\delta_{ij}}} \left[\frac{R_{qq'Z}O_{ij}''R}{2s_z} + \sum_{k=1}^6 \frac{R_{\tilde{Q}_k q' \tilde{\chi}_i^0} R_{\tilde{Q}_k q \tilde{\chi}_j^0}^*}{u_{\tilde{Q}_k}} \right], \\
Q_{RR}^{t00} &= \frac{1}{x_W(1-x_W)\sqrt{1+\delta_{ij}}} \left[\frac{R_{qq'Z}O_{ij}''L}{2s_z} - \sum_{k=1}^6 \frac{R_{\tilde{Q}_k q \tilde{\chi}_i^0}^* R_{\tilde{Q}_k q' \tilde{\chi}_j^0}}{t_{\tilde{Q}_k}} \right], \\
Q_{LR}^{u00} &= \frac{1}{x_W(1-x_W)\sqrt{1+\delta_{ij}}} \sum_{k=1}^6 \frac{R_{\tilde{Q}_k q' \tilde{\chi}_i^0} L_{\tilde{Q}_k q \tilde{\chi}_j^0}^*}{u_{\tilde{Q}_k}}, \\
Q_{LR}^{t00} &= \frac{1}{x_W(1-x_W)\sqrt{1+\delta_{ij}}} \sum_{k=1}^6 \frac{L_{\tilde{Q}_k q \tilde{\chi}_i^0}^* R_{\tilde{Q}_k q' \tilde{\chi}_j^0}}{t_{\tilde{Q}_k}}, \\
Q_{RL}^{u00} &= \frac{1}{x_W(1-x_W)\sqrt{1+\delta_{ij}}} \sum_{k=1}^6 \frac{L_{\tilde{Q}_k q' \tilde{\chi}_i^0} R_{\tilde{Q}_k q \tilde{\chi}_j^0}^*}{u_{\tilde{Q}_k}}, \\
Q_{RL}^{t00} &= \frac{1}{x_W(1-x_W)\sqrt{1+\delta_{ij}}} \sum_{k=1}^6 \frac{R_{\tilde{Q}_k q \tilde{\chi}_i^0}^* L_{\tilde{Q}_k q' \tilde{\chi}_j^0}}{t_{\tilde{Q}_k}}, \tag{43}
\end{aligned}$$

which agrees with the results of Ref. [30] in the case of non-mixing squarks.

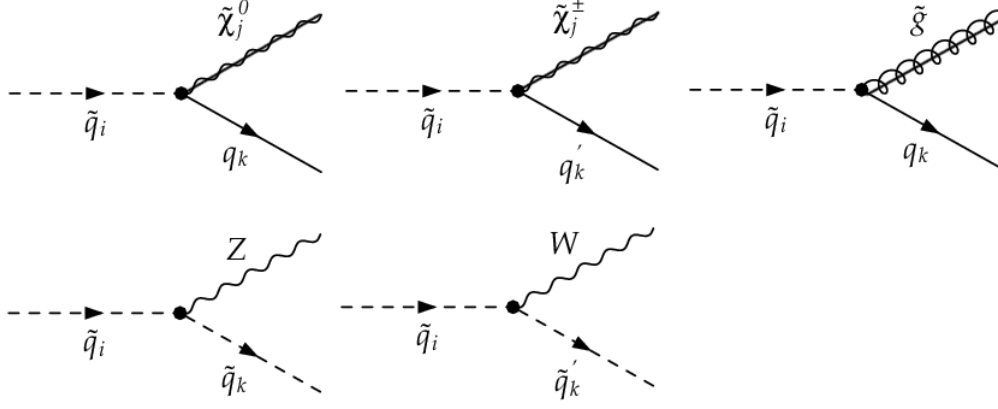


FIG. 7: Tree-level Feynman diagrams for squark decays into gauginos and quarks (top) and into electroweak gauge bosons and lighter squarks (bottom).

F. Squark Decays

We turn now from SUSY particle production to decay processes and show in Fig. 7 the possible decays of squarks into gauginos and quarks (top) as well as into electroweak gauge bosons and lighter squarks (bottom). Both processes can in general induce flavour violation. The decay widths of the former are given by

$$\begin{aligned} \Gamma_{\tilde{q}_i \rightarrow \tilde{\chi}_j^0 q_k} &= \frac{\alpha}{2 m_{\tilde{q}_i}^3 x_W (1 - x_W)} \left(\left(m_{\tilde{q}_i}^2 - m_{\tilde{\chi}_j^0}^2 - m_{q_k}^2 \right) \left(|L_{\tilde{q}_i q_k \tilde{\chi}_j^0}|^2 + |R_{\tilde{q}_i q_k \tilde{\chi}_j^0}|^2 \right) \right. \\ &\quad \left. - 4 m_{\tilde{\chi}_j^0} m_{q_k} \operatorname{Re} \left[L_{\tilde{q}_i q_k \tilde{\chi}_j^0} R_{\tilde{q}_i q_k \tilde{\chi}_j^0}^* \right] \right) \lambda^{1/2}(m_{\tilde{q}_i}^2, m_{\tilde{\chi}_j^0}^2, m_{q_k}^2), \end{aligned} \quad (44)$$

$$\begin{aligned} \Gamma_{\tilde{q}_i \rightarrow \tilde{\chi}_j^\pm q'_k} &= \frac{\alpha}{4 m_{\tilde{q}_i}^3 x_W} \left(\left(m_{\tilde{q}_i}^2 - m_{\tilde{\chi}_j^\pm}^2 - m_{q'_k}^2 \right) \left(|L_{\tilde{q}_i q'_k \tilde{\chi}_j^\pm}|^2 + |R_{\tilde{q}_i q'_k \tilde{\chi}_j^\pm}|^2 \right) \right. \\ &\quad \left. - 4 m_{\tilde{\chi}_j^\pm} m_{q'_k} \operatorname{Re} \left[L_{\tilde{q}_i q'_k \tilde{\chi}_j^\pm} R_{\tilde{q}_i q'_k \tilde{\chi}_j^\pm}^* \right] \right) \lambda^{1/2}(m_{\tilde{q}_i}^2, m_{\tilde{\chi}_j^\pm}^2, m_{q'_k}^2), \end{aligned} \quad (45)$$

$$\begin{aligned} \Gamma_{\tilde{q}_i \rightarrow \tilde{g} q_k} &= \frac{2 \alpha_s}{3 m_{\tilde{q}_i}^3 x_W} \left(\left(m_{\tilde{q}_i}^2 - m_{\tilde{g}}^2 - m_{q_k}^2 \right) \left(|L_{\tilde{q}_i q_k \tilde{g}}|^2 + |R_{\tilde{q}_i q_k \tilde{g}}|^2 \right) - 4 m_{\tilde{g}} m_{q_k} \operatorname{Re} \left[L_{\tilde{q}_i q_k \tilde{g}} R_{\tilde{q}_i q_k \tilde{g}}^* \right] \right) \\ &\quad \times \lambda^{1/2}(m_{\tilde{q}_i}^2, m_{\tilde{g}}^2, m_{q_k}^2), \end{aligned} \quad (46)$$

while those of the latter are given by

$$\Gamma_{\tilde{q}_i \rightarrow Z \tilde{q}_k} = \frac{\alpha}{16 m_{\tilde{q}_i}^3 m_Z^2 x_W (1 - x_W)} |L_{\tilde{q}_i \tilde{q}_k Z} + R_{\tilde{q}_i \tilde{q}_k Z}|^2 \lambda^{3/2}(m_{\tilde{q}_i}^2, m_Z^2, m_{\tilde{q}_k}^2), \quad (47)$$

$$\Gamma_{\tilde{q}_i \rightarrow W^\pm \tilde{q}'_k} = \frac{\alpha}{16 m_{\tilde{q}_i}^3 m_W^2 x_W (1 - x_W)} |L_{\tilde{q}_i \tilde{q}'_k W}|^2 \lambda^{3/2}(m_{\tilde{q}_i}^2, m_W^2, m_{\tilde{q}'_k}^2). \quad (48)$$

The usual Källén function is

$$\lambda(x, y, z) = x^2 + y^2 + z^2 - 2(xy + yz + zx). \quad (49)$$

In cMFV, our results agree with those of Ref. [31].

G. Gluino Decays

Heavy gluinos can decay strongly into squarks and quarks as shown in Fig. 8. The corresponding decay width

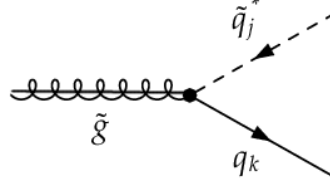


FIG. 8: Tree-level Feynman diagram for gluino decays into squarks and quarks.

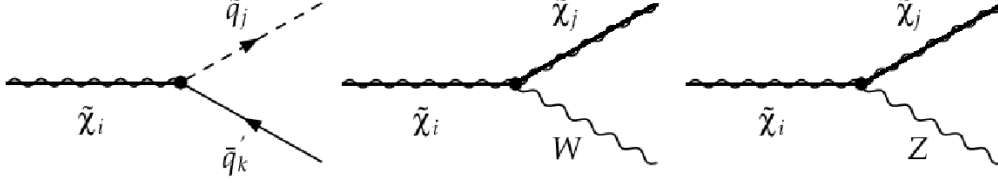


FIG. 9: Tree-level Feynman diagrams for gaugino decays into squarks and quarks (left) and into lighter gauginos and electroweak gauge bosons (centre and right).

$$\begin{aligned} \Gamma_{\tilde{g} \rightarrow \tilde{q}_j^* q_k} &= \frac{\alpha_s}{8 m_{\tilde{g}}^3} \left(\left(m_{\tilde{g}}^2 - m_{\tilde{q}_j}^2 + m_{q_k}^2 \right) \left(|L_{\tilde{q}_j q_k \tilde{g}}|^2 + |R_{\tilde{q}_j q_k \tilde{g}}|^2 \right) + 4 m_{\tilde{g}} m_{q_k} \operatorname{Re} \left[L_{\tilde{q}_j q_k \tilde{g}} R_{\tilde{q}_j q_k \tilde{g}}^* \right] \right) \\ &\times \lambda^{1/2}(m_{\tilde{g}}^2, m_{\tilde{q}_j}^2, m_{q_k}^2) \end{aligned} \quad (50)$$

can in general also induce flavour violation. In cMFV, our result agrees again with the one of Ref. [31].

H. Gaugino Decays

Heavier gauginos can decay into squarks and quarks as shown in Fig. 9 (left) or into lighter gauginos and electroweak gauge bosons (Fig. 9 centre and right). The analytical decay widths are

$$\begin{aligned} \Gamma_{\tilde{\chi}_i^\pm \rightarrow \tilde{q}_j \tilde{q}'_k} &= \frac{3\alpha}{8 m_{\tilde{\chi}_i^\pm}^3 x_W} \left(\left(m_{\tilde{\chi}_i^\pm}^2 - m_{\tilde{q}_j}^2 + m_{\tilde{q}'_k}^2 \right) \left(|L_{\tilde{q}_j \tilde{q}'_k \tilde{\chi}_i^\pm}|^2 + |R_{\tilde{q}_j \tilde{q}'_k \tilde{\chi}_i^\pm}|^2 \right) \right. \\ &\quad \left. + 4 m_{\tilde{\chi}_i^\pm} m_{\tilde{q}'_k} \operatorname{Re} \left[L_{\tilde{q}_j \tilde{q}'_k \tilde{\chi}_i^\pm} R_{\tilde{q}_j \tilde{q}'_k \tilde{\chi}_i^\pm}^* \right] \right) \lambda^{1/2}(m_{\tilde{\chi}_i^\pm}^2, m_{\tilde{q}_j}^2, m_{\tilde{q}'_k}^2) \end{aligned} \quad (51)$$

and

$$\begin{aligned} \Gamma_{\tilde{\chi}_i^\pm \rightarrow \tilde{\chi}_j^0 W^\pm} &= \frac{\alpha}{8 m_{\tilde{\chi}_i^\pm}^3 m_W^2 x_W} \left(\left(m_{\tilde{\chi}_i^\pm}^4 + m_{\tilde{\chi}_j^0}^4 - 2 m_W^4 + m_{\tilde{\chi}_i^\pm}^2 m_W^2 + m_{\tilde{\chi}_j^0}^2 m_W^2 - 2 m_{\tilde{\chi}_i^\pm}^2 m_{\tilde{\chi}_j^0}^2 \right) \right. \\ &\quad \left. \times \left(|O_{ij}^L|^2 + |O_{ij}^R|^2 \right) - 12 m_{\tilde{\chi}_i^\pm} m_W^2 m_{\tilde{\chi}_j^0} \operatorname{Re} \left[O_{ij}^L O_{ij}^{R*} \right] \right) \lambda^{1/2}(m_{\tilde{\chi}_i^\pm}^2, m_{\tilde{\chi}_j^0}^2, m_W^2), \end{aligned} \quad (52)$$

$$\begin{aligned} \Gamma_{\tilde{\chi}_i^\pm \rightarrow \tilde{\chi}_j^\pm Z} &= \frac{\alpha}{8 m_{\tilde{\chi}_i^\pm}^3 m_Z^2 x_W (1 - x_W)} \left(\left(m_{\tilde{\chi}_i^\pm}^4 + m_{\tilde{\chi}_j^\pm}^4 - 2 m_Z^4 + m_{\tilde{\chi}_i^\pm}^2 m_Z^2 + m_{\tilde{\chi}_j^\pm}^2 m_Z^2 - 2 m_{\tilde{\chi}_i^\pm}^2 m_{\tilde{\chi}_j^\pm}^2 \right) \right. \\ &\quad \left. \times \left(|O'_{ij}{}^L|^2 + |O'_{ij}{}^R|^2 \right) - 12 m_{\tilde{\chi}_i^\pm} m_Z^2 m_{\tilde{\chi}_j^\pm} \operatorname{Re} \left[O'_{ij}{}^L O'_{ij}{}^{R*} \right] \right) \lambda^{1/2}(m_{\tilde{\chi}_i^\pm}^2, m_{\tilde{\chi}_j^\pm}^2, m_Z^2) \end{aligned} \quad (53)$$

for charginos and

$$\begin{aligned} \Gamma_{\tilde{\chi}_i^0 \rightarrow \tilde{q}_j \tilde{q}_k} &= \frac{3\alpha}{4m_{\tilde{\chi}_i^0}^3 x_W (1-x_W)} \left(\left(m_{\tilde{\chi}_i^0}^2 - m_{\tilde{q}_j}^2 + m_{q_k}^2 \right) \left(|L_{\tilde{q}_j q_k \tilde{\chi}_i^0}|^2 + |R_{\tilde{q}_j q_k \tilde{\chi}_i^0}|^2 \right) \right. \\ &\quad \left. + 4m_{\tilde{\chi}_i^0} m_{q_k} \operatorname{Re} \left[L_{\tilde{q}_j q_k \tilde{\chi}_i^0} R_{\tilde{q}_j q_k \tilde{\chi}_i^0}^* \right] \right) \lambda^{1/2}(m_{\tilde{\chi}_i^0}^2, m_{\tilde{q}_j}^2, m_{q_k}^2) \end{aligned} \quad (54)$$

and

$$\begin{aligned} \Gamma_{\tilde{\chi}_i^0 \rightarrow \tilde{\chi}_j^\pm W^\mp} &= \frac{\alpha}{8m_{\tilde{\chi}_i^0}^3 m_W^2 x_W} \left(\left(m_{\tilde{\chi}_i^0}^4 + m_{\tilde{\chi}_j^\pm}^4 - 2m_W^4 + m_{\tilde{\chi}_i^0}^2 m_W^2 + m_{\tilde{\chi}_j^\pm}^2 m_W^2 - 2m_{\tilde{\chi}_i^0}^2 m_{\tilde{\chi}_j^\pm}^2 \right) \right. \\ &\quad \left. \times \left(|O_{ij}^L|^2 + |O_{ij}^R|^2 \right) - 12m_{\tilde{\chi}_i^0} m_W^2 m_{\tilde{\chi}_j^\pm} \operatorname{Re} \left[O_{ij}^L O_{ij}^{R*} \right] \right) \lambda^{1/2}(m_{\tilde{\chi}_i^0}^2, m_{\tilde{\chi}_j^\pm}^2, m_W^2), \end{aligned} \quad (55)$$

$$\begin{aligned} \Gamma_{\tilde{\chi}_i^0 \rightarrow \tilde{\chi}_j^0 Z} &= \frac{\alpha}{8m_{\tilde{\chi}_i^0}^3 m_Z^2 x_W (1-x_W)} \left(\left(m_{\tilde{\chi}_i^0}^4 + m_{\tilde{\chi}_j^0}^4 - 2m_Z^4 + m_{\tilde{\chi}_i^0}^2 m_Z^2 + m_{\tilde{\chi}_j^0}^2 m_Z^2 - 2m_{\tilde{\chi}_i^0}^2 m_{\tilde{\chi}_j^0}^2 \right) \right. \\ &\quad \left. \times \left(|O_{ij}^{\prime L}|^2 + |O_{ij}^{\prime R}|^2 \right) - 12m_{\tilde{\chi}_i^0} m_Z^2 m_{\tilde{\chi}_j^0} \operatorname{Re} \left[O_{ij}^{\prime L} O_{ij}^{\prime R*} \right] \right) \lambda^{1/2}(m_{\tilde{\chi}_i^0}^2, m_{\tilde{\chi}_j^0}^2, m_Z^2) \end{aligned} \quad (56)$$

for neutralinos, respectively. Chargino decays into a slepton and a neutrino (lepton and sneutrino) can be deduced from the previous equations by taking the proper limits, i.e. by removing colour factors and up-type masses in the coupling definitions. Our results agree then with those of Ref. [32] in the limit of non-mixing sneutrinos. Note that the same simplifications also permit a verification of our results for squark decays into a gaugino and a quark in Eqs. (44) and (45) when compared to their leptonic counterparts in Ref. [32].

IV. EXPERIMENTAL CONSTRAINTS, SCANS AND BENCHMARKS IN NMFV SUSY

In the absence of experimental evidence for supersymmetry, a large variety of data can be used to constrain the MSSM parameter space. For example, sparticle mass limits can be obtained from searches of charginos ($m_{\tilde{\chi}_1^\pm} \geq 85$ GeV for heavier sneutrinos at LEP2), neutralinos ($m_{\tilde{\chi}_1^0} \geq 59$ GeV in minimal supergravity (mSUGRA) from the combination of LEP2 results), gluinos ($m_{\tilde{g}} \geq 195$ GeV from CDF), stops ($m_{\tilde{t}_1} \geq 95 \dots 96$ GeV for neutral- or charged-current decays from the combination of LEP2 results), and other squarks ($m_{\tilde{q}} \geq 300$ GeV for gluinos of equal mass from CDF) at colliders [33]. Note that all of these limits have been obtained assuming minimal flavour violation. For non-minimal flavour violation, rather strong constraints can be obtained from low-energy, electroweak precision, and cosmological observables. These are discussed in the next subsection, followed by several scans for experimentally allowed/favoured regions of the constrained MSSM parameter space and the definition of four NMFV benchmark points/slopes. Finally, we exhibit the corresponding chirality and flavour decomposition of the various squark mass eigenstates.

A. Low-Energy, Electroweak Precision, and Cosmological Constraints

In a rather complete analysis of FCNC constraints more than ten years ago [18], upper limits from the neutral kaon sector (on Δm_K , ε , ε'/ε), on B - (Δm_B) and D -meson oscillations (Δm_D), various rare decays ($\operatorname{BR}(b \rightarrow s\gamma)$, $\operatorname{BR}(\mu \rightarrow e\gamma)$, $\operatorname{BR}(\tau \rightarrow e\gamma)$, and $\operatorname{BR}(\tau \rightarrow \mu\gamma)$), and electric dipole moments (d_n and d_e) were used to impose constraints on non-minimal flavour mixing in the squark and slepton sectors. The limit obtained for the absolute value in the left-handed, down-type squark sector was rather weak ($|\lambda_{LL}^{sb}| < 4.4 \dots 26$ for varying gluino-to-squark mass ratio), while the limits for the mixed/right-handed, imaginary or sleptonic parts were already several orders of magnitude smaller. In the meantime, many of the experimental bounds have been improved or absolute values for the observables have been determined, so that an updated analysis could be performed [34]. The results for the down-type squark sector are cited in Tab. I. As can be seen and as has already been hinted at in the introduction, only mixing between second- and third-generation squarks can be substantial, and this only in the left-left or right-right chiral sectors, the latter being disfavoured by its scaling with the soft SUSY-breaking mass. Independent analyses focusing

TABLE I: The 95% probability bounds on $|\lambda_{ij}^{d_k d_l}|$ obtained in Ref. [34].

$\frac{ij}{kl}$	LL	LR	RL	RR
12	1.4×10^{-2}	9.0×10^{-5}	9.0×10^{-5}	9.0×10^{-3}
13	9.0×10^{-2}	1.7×10^{-2}	1.7×10^{-2}	7.0×10^{-2}
23	1.6×10^{-1}	4.5×10^{-3}	6.0×10^{-3}	2.2×10^{-1}

on this particular sector, i.e. on $\text{BR}(b \rightarrow s\gamma)$, $\text{BR}(b \rightarrow s\mu\mu)$, and Δm_{B_s} , have been performed recently by two other groups [35, 36] with very similar results.

In our own analysis, we take implicitly into account all of the previously mentioned constraints by restricting ourselves to the case of only one real NMFV parameter, $\lambda \equiv \lambda_{LL}^{sb} = \lambda_{LL}^{ct}$. Allowed regions for this parameter are then obtained by imposing explicitly a number of low-energy, electroweak precision, and cosmological constraints. We start by imposing the theoretically robust inclusive branching ratio

$$\text{BR}(b \rightarrow s\gamma) = (3.55 \pm 0.26) \times 10^{-4}, \quad (57)$$

obtained from the combined measurements of BaBar, Belle, and CLEO [37], at the 2σ -level on the two-loop QCD/one-loop SUSY calculation [36, 38], which affects directly the allowed squark mixing between the second and third generation.

A second important consequence of NMFV in the MSSM is the generation of large splittings between squark-mass eigenvalues. The splitting within isospin doublets influences the Z - and W -boson self-energies at zero-momentum $\Sigma_{Z,W}(0)$ in the electroweak ρ -parameter

$$\Delta\rho = \Sigma_Z(0)/M_Z^2 - \Sigma_W(0)/M_W^2 \quad (58)$$

and consequently the W -boson mass M_W and the squared sine of the weak mixing angle $\sin^2 \theta_W$. The latest combined fits of the Z -boson mass, width, pole asymmetry, W -boson and top-quark mass constrain new physics contributions to $T = -0.13 \pm 0.11$ [33] or

$$\Delta\rho = -\alpha T = 0.00102 \pm 0.00086, \quad (59)$$

where we have used $\alpha(M_Z) = 1/127.918$. This value is then imposed at the 2σ -level on the one-loop NMFV and two-loop cMFV SUSY calculation [39].

A third observable sensitive to SUSY loop-contributions is the anomalous magnetic moment $a_\mu = (g_\mu - 2)/2$ of the muon, for which recent BNL data and the SM prediction disagree by [33]

$$\Delta a_\mu = (22 \pm 10) \times 10^{-10}. \quad (60)$$

In our calculation, we take into account the SM and MSSM contributions up to two loops [40, 41] and require them to agree with the region above within two standard deviations.

For cosmological reasons, i.e. in order to have a suitable candidate for non-baryonic cold dark matter [42], we require the lightest SUSY particle (LSP) to be stable, electrically neutral, and a colour singlet. The dark matter relic density is then calculated using a modified version of DarkSUSY 4.1 [43], that takes into account the six-dimensional squark helicity and flavour mixing, and constrained to the region

$$0.094 < \Omega_{CDM} h^2 < 0.136 \quad (61)$$

at 95% (2σ) confidence level. This limit has recently been obtained from the three-year data of the WMAP satellite, combined with the SDSS and SNLS survey and Baryon Acoustic Oscillation data and interpreted within an eleven-parameter inflationary model [44], which is more general than the usual six-parameter ‘‘vanilla’’ concordance model of cosmology. Note that this range is well compatible with the older, independently obtained range of $0.094 < \Omega_{CDM} h^2 < 0.129$ [45].

B. Scans of the Constrained NMFV MSSM Parameter Space

The above experimental limits are now imposed on the constrained MSSM (cMSSM), or minimal supergravity (mSUGRA), model with five free parameters m_0 , $m_{1/2}$, $\tan\beta$, A_0 , and $\text{sgn}(\mu)$ at the grand unification scale. Since

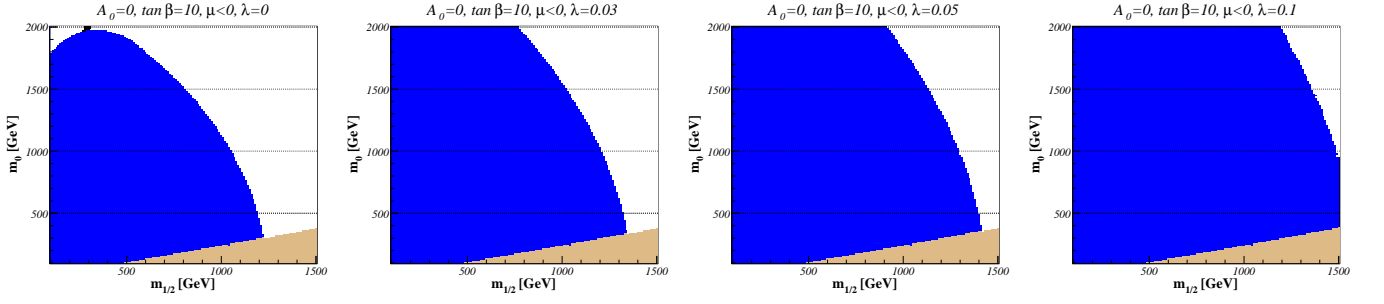


FIG. 10: The $(m_0, m_{1/2})$ -planes for $\tan\beta = 10$, $A_0 = 0$ GeV, $\mu < 0$, and $\lambda = 0, 0.03, 0.05$ and 0.1 . We show WMAP (black) favoured as well as $b \rightarrow s\gamma$ (blue) and charged LSP (beige) excluded regions of mSUGRA parameter space in minimal ($\lambda = 0$) and non-minimal ($\lambda > 0$) flavour violation.

our scans of the cMSSM parameter space in the common scalar mass m_0 and the common fermion mass $m_{1/2}$ depend very little on the trilinear coupling A_0 , we set it to zero in the following. Furthermore, we fix a small (10), intermediate (30), and large (50) value for the ratio of the Higgs vacuum expectation values $\tan\beta$. The impact of the sign of the off-diagonal Higgs mass parameter μ is investigated for $\tan\beta = 10$ only, before we set it to $\mu > 0$ for $\tan\beta = 30$ and 50 (see below).

With these boundary conditions at the grand unification scale, we solve the renormalization group equations numerically to two-loop order using the computer program SPheno 2.2.3 [46] and compute the soft SUSY-breaking masses at the electroweak scale with the complete one-loop formulas, supplemented by two-loop contributions in the case of the neutral Higgs bosons and the μ -parameter. At this point we generalize the squark mass matrices as described in Sec. II in order to account for flavour mixing in the left-chiral sector of the second- and third-generation squarks, diagonalize these mass matrices, and compute the low-energy, electroweak precision, and cosmological observables with the computer programs FeynHiggs 2.5.1 [47] and DarkSUSY 4.1 [43].

For the masses and widths of the electroweak gauge bosons and the mass of the top quark, we use the current values of $m_Z = 91.1876$ GeV, $m_W = 80.403$ GeV, $m_t = 174.2$ GeV, $\Gamma_Z = 2.4952$ GeV, and $\Gamma_W = 2.141$ GeV. The CKM-matrix elements are computed using the parameterization

$$V = \begin{pmatrix} c_{12}c_{13} & s_{12}c_{13} & s_{13}e^{-i\delta} \\ -s_{12}c_{23} - c_{12}s_{23}s_{13}e^{i\delta} & c_{12}c_{23} - s_{12}s_{23}s_{13}e^{i\delta} & s_{23}c_{13} \\ s_{12}s_{23} - c_{12}c_{23}s_{13}e^{i\delta} & -c_{12}s_{23} - s_{12}c_{23}s_{13}e^{i\delta} & c_{23}c_{13} \end{pmatrix}, \quad (62)$$

where $s_{ij} = \sin\theta_{ij}$ and $c_{ij} = \cos\theta_{ij}$ relate to the mixing of two specific generations i and j and δ is the SM CP -violating complex phase. The numerical values are given by

$$s_{12} = 0.2243, \quad s_{23} = 0.0413, \quad s_{13} = 0.0037, \quad \text{and } \delta = 1.05. \quad (63)$$

The squared sine of the electroweak mixing angle $\sin^2\theta_W = 1 - m_W^2/m_Z^2$ and the electromagnetic fine structure constant $\alpha = \sqrt{2}G_F m_W^2 \sin^2\theta_W/\pi$ are calculated in the improved Born approximation using the world average value of $G_F = 1.16637 \cdot 10^{-5}$ GeV⁻² for Fermi's coupling constant [33].

Typical scans of the cMSSM parameter space in m_0 and $m_{1/2}$ with a relatively small value of $\tan\beta = 10$ and $A_0 = 0$ are shown in Figs. 10 and 11 for $\mu < 0$ and $\mu > 0$, respectively. All experimental limits described in Sec. IV A are imposed at the 2σ -level. The $b \rightarrow s\gamma$ excluded region depends strongly on flavour mixing, while the regions favoured by $g_\mu - 2$ and the dark matter relic density are quite insensitive to variations of the λ -parameter. $\Delta\rho$ constrains the parameter space only for heavy scalar masses $m_0 > 2000$ GeV and heavy gaugino masses $m_{1/2} > 1500$ GeV, so that the corresponding excluded regions are not shown here.

The dominant SUSY effects in the calculation of the anomalous magnetic moment of the muon come from induced quantum loops of a gaugino and a slepton. Squarks contribute only at the two-loop level. This reduces the dependence on flavour violation in the squark sector considerably. Furthermore, the region $\mu < 0$ is disfavoured in all SUSY models, since the one-loop SUSY contributions are approximatively given by [48]

$$a_\mu^{\text{SUSY}, 1\text{-loop}} \simeq 13 \times 10^{-10} \left(\frac{100 \text{ GeV}}{M_{\text{SUSY}}} \right)^2 \tan\beta \text{sgn}(\mu), \quad (64)$$

if all SUSY particles (the relevant ones are the smuon, sneutralino, chargino, and neutralino) have a common mass M_{SUSY} . Negative values of μ would then increase, not decrease, the disagreement between the experimental measurements and the theoretical SM value of a_μ . Furthermore, the measured $b \rightarrow s\gamma$ branching ratio excludes virtually all

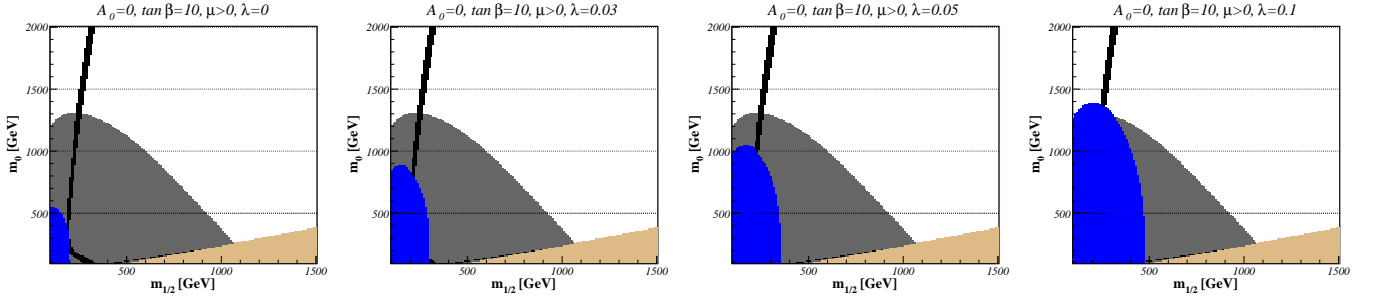


FIG. 11: The $(m_0, m_{1/2})$ -planes for $\tan \beta = 10$, $A_0 = 0$ GeV, $\mu > 0$, and $\lambda = 0, 0.03, 0.05$ and 0.1 . We show α_μ (grey) and WMAP (black) favoured as well as $b \rightarrow s\gamma$ (blue) and charged LSP (beige) excluded regions of mSUGRA parameter space in minimal ($\lambda = 0$) and non-minimal ($\lambda > 0$) flavour violation.

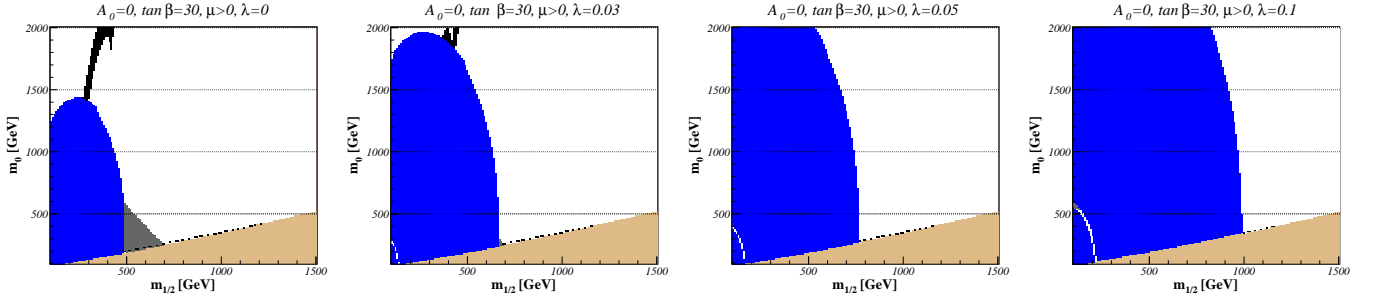


FIG. 12: The $(m_0, m_{1/2})$ planes for $\tan \beta = 30$, $A_0 = 0$ GeV, $\mu > 0$, and $\lambda = 0, 0.03, 0.05$ and 0.1 . We show α_μ (grey) and WMAP (black) favoured as well as $b \rightarrow s\gamma$ (blue) and charged LSP (beige) excluded regions of mSUGRA parameter space in minimal ($\lambda = 0$) and non-minimal ($\lambda > 0$) flavour violation.

of the region favoured by the dark matter relic density, except for very high scalar SUSY masses. We therefore do not consider negative values of μ in the rest of this work. As stated above, we have also checked that the shape of the different regions depends extremely weakly on the trilinear coupling A_0 .

In Figs. 12 and 13, we show the $(m_0, m_{1/2})$ -planes for larger $\tan \beta$, namely $\tan \beta = 30$ and $\tan \beta = 50$, and for $\mu > 0$. The regions which are favoured both by the anomalous magnetic moment of the muon and by the cold dark matter relic density, and which are not excluded by the $b \rightarrow s\gamma$ measurements, are stringently constrained and do not allow for large flavour violation.

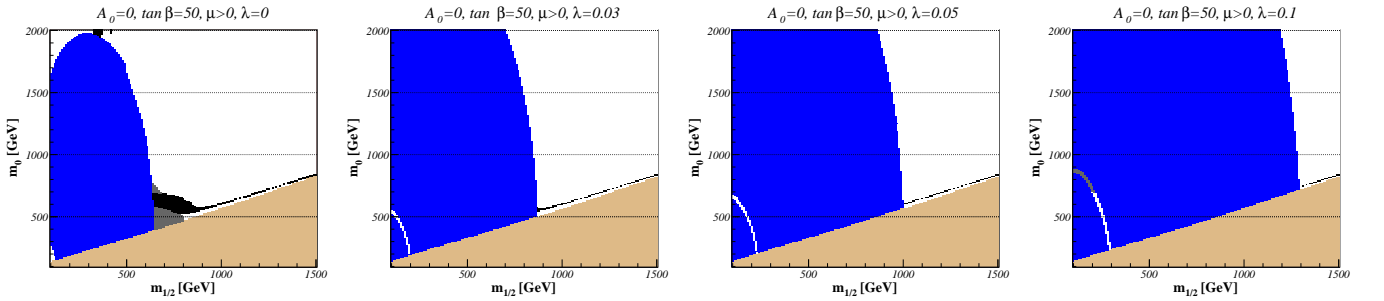


FIG. 13: The $(m_0, m_{1/2})$ planes for $\tan \beta = 50$, $A_0 = 0$ GeV, $\mu > 0$, and $\lambda = 0, 0.03, 0.05$ and 0.1 . We show α_μ (grey) and WMAP (black) favoured as well as $b \rightarrow s\gamma$ (blue) and charged LSP (beige) excluded regions of mSUGRA parameter space in minimal ($\lambda = 0$) and non-minimal ($\lambda > 0$) flavour violation.

TABLE II: Benchmark points allowing for flavour violation among the second and third generations for $A_0 = 0$, $\mu > 0$, and three different values of $\tan\beta$. For comparison we also show the nearest pre-WMAP SPS [49, 50] and post-WMAP BDEGOP [51] benchmark points and indicate the relevant cosmological regions.

	m_0 [GeV]	$m_{1/2}$ [GeV]	A_0 [GeV]	$\tan\beta$	$\text{sgn}(\mu)$	SPS	BDEGOP	Cosmol. Region
A	700	200	0	10	1	2	E'	Focus Point
B	100	400	0	10	1	3	C'	Co-Annihilation
C	230	590	0	30	1	1b	I'	Co-Annihilation
D	600	700	0	50	1	4	L'	Bulk/Higgs-funnel

C. (c)MFV and NMFV Benchmark Points and Slopes

Restricting ourselves to non-negative values of μ , we now inspect the $(m_0, m_{1/2})$ -planes in Figs. 11-13 for cMSSM scenarios that

- are allowed/favoured by low-energy, electroweak precision, and cosmological constraints,
- permit non-minimal flavour violation among left-chiral squarks of the second and third generation up to $\lambda \leq 0.1$,
- and are at the same time collider-friendly, i.e. have relatively low values of m_0 and $m_{1/2}$.

Our choices are presented in Tab. II, together with the nearest pre-WMAP Snowmass Points (and Slopes, SPS) [49, 50] and the nearest post-WMAP scenarios proposed in Ref. [51]. We also indicate the relevant cosmological region for each point and attach a model line (slope) to it, given by

$$\begin{aligned}
 \text{A: } & 180 \text{ GeV} \leq m_{1/2} \leq 250 \text{ GeV}, \quad m_0 = -1936 \text{ GeV} + 12.9 m_{1/2}, \\
 \text{B: } & 400 \text{ GeV} \leq m_{1/2} \leq 900 \text{ GeV}, \quad m_0 = 4.93 \text{ GeV} + 0.229 m_{1/2}, \\
 \text{C: } & 500 \text{ GeV} \leq m_{1/2} \leq 700 \text{ GeV}, \quad m_0 = 54 \text{ GeV} + 0.297 m_{1/2}, \\
 \text{D: } & 575 \text{ GeV} \leq m_{1/2} \leq 725 \text{ GeV}, \quad m_0 = 600 \text{ GeV}.
 \end{aligned} \tag{65}$$

These slopes trace the allowed/favoured regions from lower to higher masses and can, of course, also be used in cMFV scenarios with $\lambda = 0$. We have verified that in the case of MFV [7] the hierarchy $\Delta_{LL}^{qq'} \gg \Delta_{LR,RL}^{qq'} \gg \Delta_{RR}^{qq'}$ and the equality of $\lambda_{LL}^{sb} = \lambda_{LL}^{ct}$ are still reasonably well fulfilled numerically with the values of $\lambda_{LL}^{sb} \approx \lambda_{LL}^{ct}$ ranging from zero to $5 \times 10^{-3} \dots 1 \times 10^{-2}$ for our four typical benchmark points.

Starting with Fig. 11 and $\tan\beta = 10$, the bulk region of equally low scalar and fermion masses is all but excluded by the $b \rightarrow s\gamma$ branching ratio. This leaves as a favoured region first the so-called focus point region of low fermion masses $m_{1/2}$, where the lightest neutralinos are relatively heavy, have a significant Higgsino component, and annihilate dominantly into pairs of electroweak gauge bosons. Our benchmark point A lies in this region, albeit at smaller masses than SPS 2 ($m_0 = 1450 \text{ GeV}$, $m_{1/2} = 300 \text{ GeV}$) and BDEGOP E' ($m_0 = 1530 \text{ GeV}$, $m_{1/2} = 300 \text{ GeV}$), which lie outside the region favoured by a_μ (grey-shaded) and lead to collider-unfriendly squark and gaugino masses.

The second favoured region for small $\tan\beta$ is the co-annihilation branch of low scalar masses m_0 , where the lighter tau-slepton mass eigenstate is not much heavier than the lightest neutralino and the two have a considerable co-annihilation cross section. This is where we have chosen our benchmark point B, which differs from the points SPS 3 ($m_0 = 90 \text{ GeV}$, $m_{1/2} = 400 \text{ GeV}$) and BDEGOP C' ($m_0 = 85 \text{ GeV}$, $m_{1/2} = 400 \text{ GeV}$) only very little in the scalar mass. This minor difference may be traced to the fact that we use DarkSUSY 4.1 [43] instead of the private dark matter program SSARD of Ref. [51].

At the larger value of $\tan\beta = 30$ in Fig. 12, only the co-annihilation region survives the constraints coming from $b \rightarrow s\gamma$ decays. Here we choose our point C, which has slightly higher masses than both SPS 1b ($m_0 = 200 \text{ GeV}$, $m_{1/2} = 400 \text{ GeV}$) and BDEGOP I' ($m_0 = 175 \text{ GeV}$, $m_{1/2} = 350 \text{ GeV}$), due to the ever more stringent constraints from the above-mentioned rare B -decay.

For the very large value of $\tan\beta = 50$ in Fig. 13, the bulk region reappears at relatively heavy scalar and fermion masses. Here, the couplings of the heavier scalar and pseudo-scalar Higgses H^0 and A^0 to bottom quarks and tau-leptons and the charged-Higgs coupling to top-bottom pairs are significantly enhanced, resulting e.g. in increased dark matter annihilation cross sections through s -channel Higgs-exchange into bottom-quark final states. So as $\tan\beta$ increases further, the so-called Higgs-funnel region eventually makes its appearance on the diagonal of large scalar and fermion masses. We choose our point D in the concentrated (bulky) region favoured by cosmology and a_μ at masses, that are slightly higher than those of SPS 4 ($m_0 = 400 \text{ GeV}$, $m_{1/2} = 300 \text{ GeV}$) and BDEGOP L' ($m_0 = 300 \text{ GeV}$, $m_{1/2} = 450 \text{ GeV}$). We do so in order to escape again from the constraints of the $b \rightarrow s\gamma$ decay, which are stronger today than they were a few years ago. In this scenario, squarks and gluinos are very heavy with masses above 1 TeV.

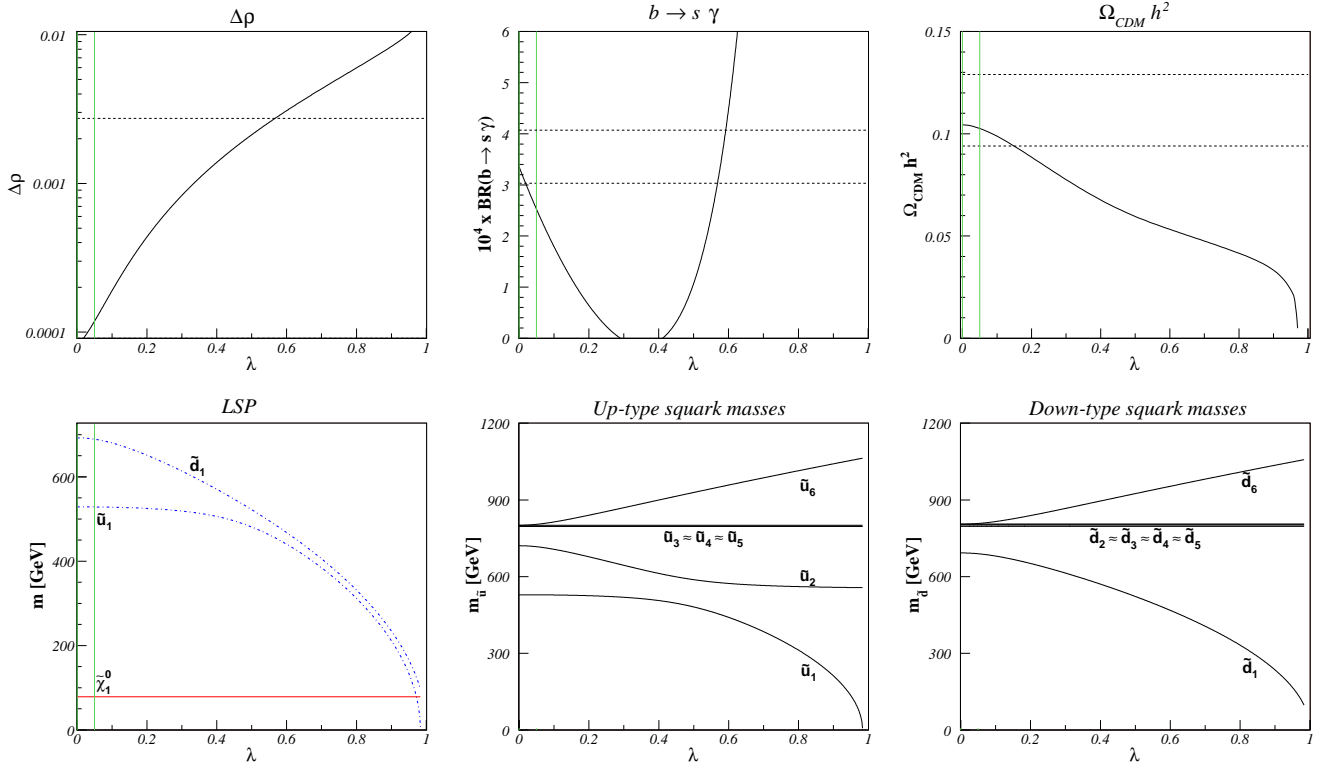


FIG. 14: Dependence of the precision variables $\text{BR}(b \rightarrow s\gamma)$, $\Delta\rho$, and the cold dark matter relic density $\Omega_{CDM}h^2$ (top) as well as of the lightest SUSY particle, up- and down-type squark masses (bottom) on the NMFV parameter λ in our benchmark scenario A. The experimentally allowed ranges (within 2σ) are indicated by horizontal dashed lines.

D. Dependence of Precision Observables and Squark-Mass Eigenvalues on Flavour Violation

Let us now turn to the dependence of the precision variables discussed in Sec. IV A on the flavour violating parameter λ in the four benchmark scenarios defined in Sec. IV C. As already mentioned, we expect the leptonic observable a_μ to depend weakly (at two loops only) on the squark sector, and this is confirmed by our numerical analysis. We find constant values of 6, 14, 16, and 13×10^{-10} for the benchmarks A, B, C, and D, all of which lie well within 2σ (the latter three even within 1σ) of the experimentally favoured range $(22 \pm 10) \times 10^{-10}$.

The electroweak precision observable $\Delta\rho$ is shown first in Figs. 14-17 for the four benchmark scenarios A, B, C, and D. On our logarithmic scale, only the experimental upper bound of the 2σ -range is visible as a dashed line. While the self-energy diagrams of the electroweak gauge bosons depend obviously strongly on the helicities, flavours, and mass eigenvalues of the squarks in the loop, the SUSY masses in our scenarios are sufficiently small and the experimental error is still sufficiently large to allow for relatively large values of $\lambda \leq 0.57$, 0.52 , 0.38 , and 0.32 for the benchmark points A, B, C, and D, respectively. As mentioned above, $\Delta\rho$ conversely constrains SUSY models in cMFV only for masses above 2000 GeV for m_0 and 1500 GeV for $m_{1/2}$.

The next diagram in Figs. 14-17 shows the dependence of the most stringent low-energy constraint, coming from the good agreement between the measured $b \rightarrow s\gamma$ branching ratio and the two-loop SM prediction, on the NMFV parameter λ . The dashed lines of the 2σ -bands exhibit two allowed regions, one close to $\lambda = 0$ (vertical green line) and a second one around $\lambda \simeq 0.57$, 0.75 , 0.62 , and 0.57 , respectively. As is well-known, the latter are, however, disfavoured by $b \rightarrow s\mu^+\mu^-$ data constraining the sign of the $b \rightarrow s\gamma$ amplitude to be the same as in the SM [52]. We will therefore limit ourselves later to the regions $\lambda \leq 0.05$ (points A, C, and D) and $\lambda \leq 0.1$ (point B) in the vicinity of (c)MFV (see also Tab. I).

The 95% confidence-level (or 2σ) region for the cold dark matter density was given in absolute values in Ref. [44] and is shown as a dashed band in the upper right part of Figs. 14-17. However, only the lower bound (0.094) is of relevance, as the relic density falls with increasing λ . This is not so pronounced in our model B as in our model A, where squark masses are light and the lightest neutralino has a sizable Higgsino-component, so that squark exchanges contribute significantly to the annihilation cross sections. For models C and D there is little sensitivity of $\Omega_{CDM}h^2$ (except at very large $\lambda \leq 1$), as the squark masses are generally larger.

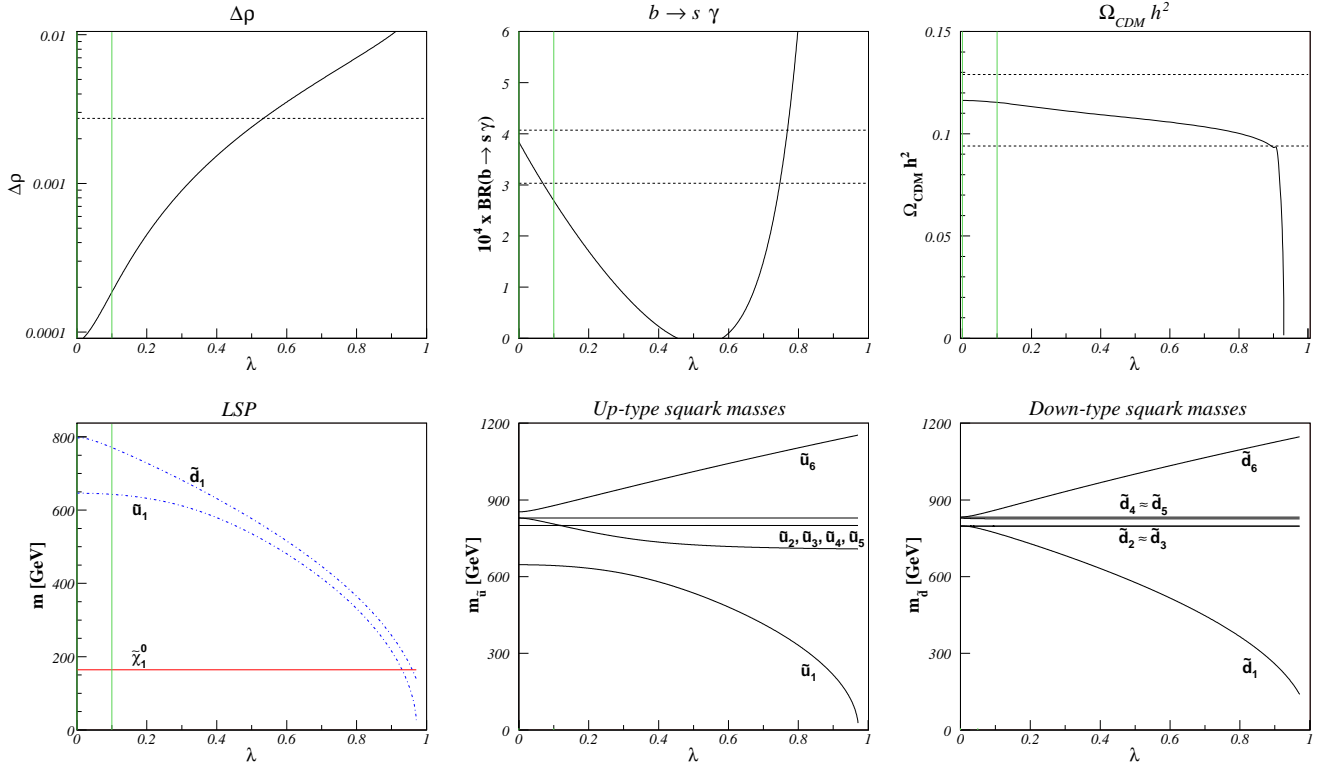


FIG. 15: Same as Fig. 14 for our benchmark scenario B.

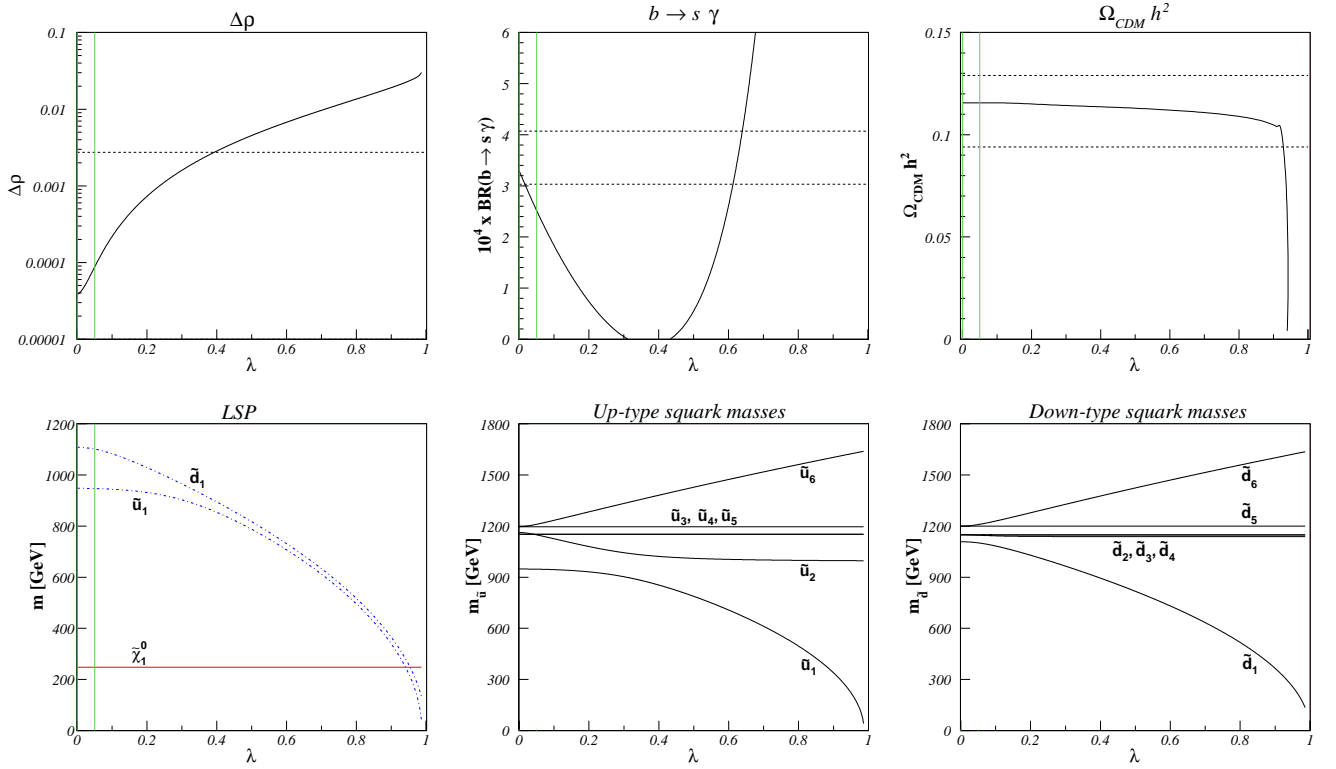


FIG. 16: Same as Fig. 14 for our benchmark scenario C.

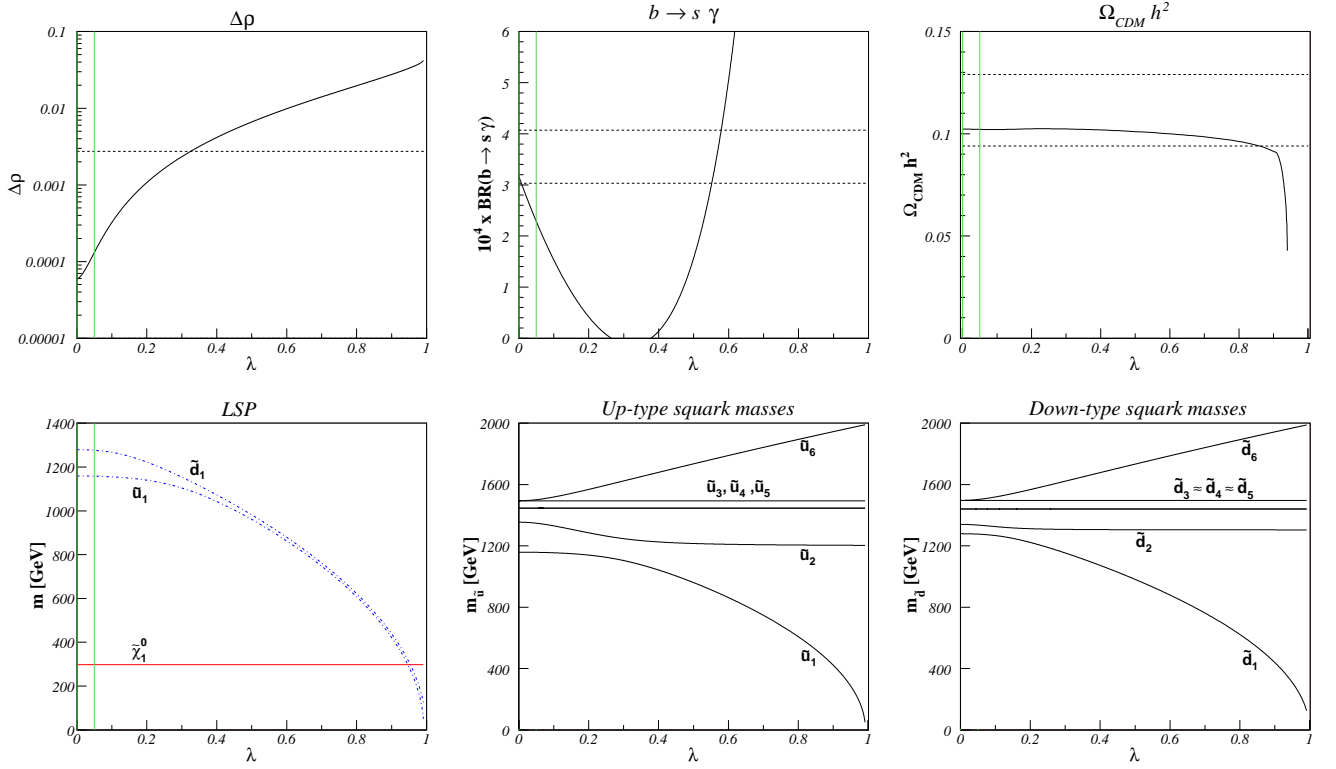


FIG. 17: Same as Fig. 14 for our benchmark scenario D.

The rapid fall-off of the relic density for very large $\lambda \leq 1$ can be understood by looking at the resulting lightest up- and down-type squark mass eigenvalues in the lower left part of Figs. 14-17. For maximal flavour violation, the off-diagonal squark mass matrix elements are of similar size as the diagonal ones, leading to one squark mass eigenvalue that approaches and finally falls below the lightest neutralino (dark matter) mass. Light squark propagators and co-annihilation processes thus lead to a rapidly falling dark matter relic density and finally to cosmologically excluded NMFV SUSY models, since the LSP must be electrically neutral and a colour singlet.

An interesting phenomenon of level reordering between neighbouring states can be observed in the lower central diagrams of Figs. 14-17 for the two lowest mass eigenvalues of up-type squarks. The squark mass eigenstates are, by definition, labeled in ascending order with the mass eigenvalues, so that \tilde{u}_1 represents the lightest, \tilde{u}_2 the second-lightest, and \tilde{u}_6 the heaviest up-type squark. As λ and the off-diagonal entries in the mass matrix increase, the splitting between the lightest and highest mass eigenvalues naturally increases, whereas the intermediate squark masses (of $\tilde{u}_{3,4,5}$) are practically degenerate and insensitive to λ . These remarks also hold for the down-type squark masses shown in the lower right diagrams of Figs. 14-17. However, for up-type squarks it is first the second-lowest mass that decreases up to intermediate values of $\lambda = 0.2 \dots 0.5$, whereas the lowest mass is constant, and only at this point the second-lowest mass becomes constant and takes approximately the value of the until here lowest squark mass, whereas the lowest squark mass starts to decrease further with λ . These ‘‘avoided crossings’’ are a common phenomenon for Hermitian matrices and reminiscent of meta-stable systems in quantum mechanics. At the point where the two levels should cross, the corresponding squark eigenstates mix and change character, as will be explained in the next subsection. For scenario C (Fig. 16), the phenomenon occurs even a second time with an additional avoided crossing between the states \tilde{u}_2 and \tilde{u}_3 at $\lambda \simeq 0.05$. For scenario B (Fig. 15), this takes place at $\lambda \simeq 0.1$, and there is even another crossing at $\lambda \simeq 0.02$. For down-type squarks, the level-reordering phenomenon is not so pronounced.

E. Chirality and Flavour Decomposition of Squark Mass Eigenstates

In NMFV, squarks will not only exhibit the traditional mixing of left- and right-handed helicities of third-generation flavour eigenstates, but will in addition exhibit generational mixing. As discussed before, we restrict ourselves here to the simultaneous mixing of left-handed second- and third-generation up- and down-type squarks. For our benchmark scenario A, the helicity and flavour decomposition of the six up-type (left) and down-type (right) squark mass eigen-

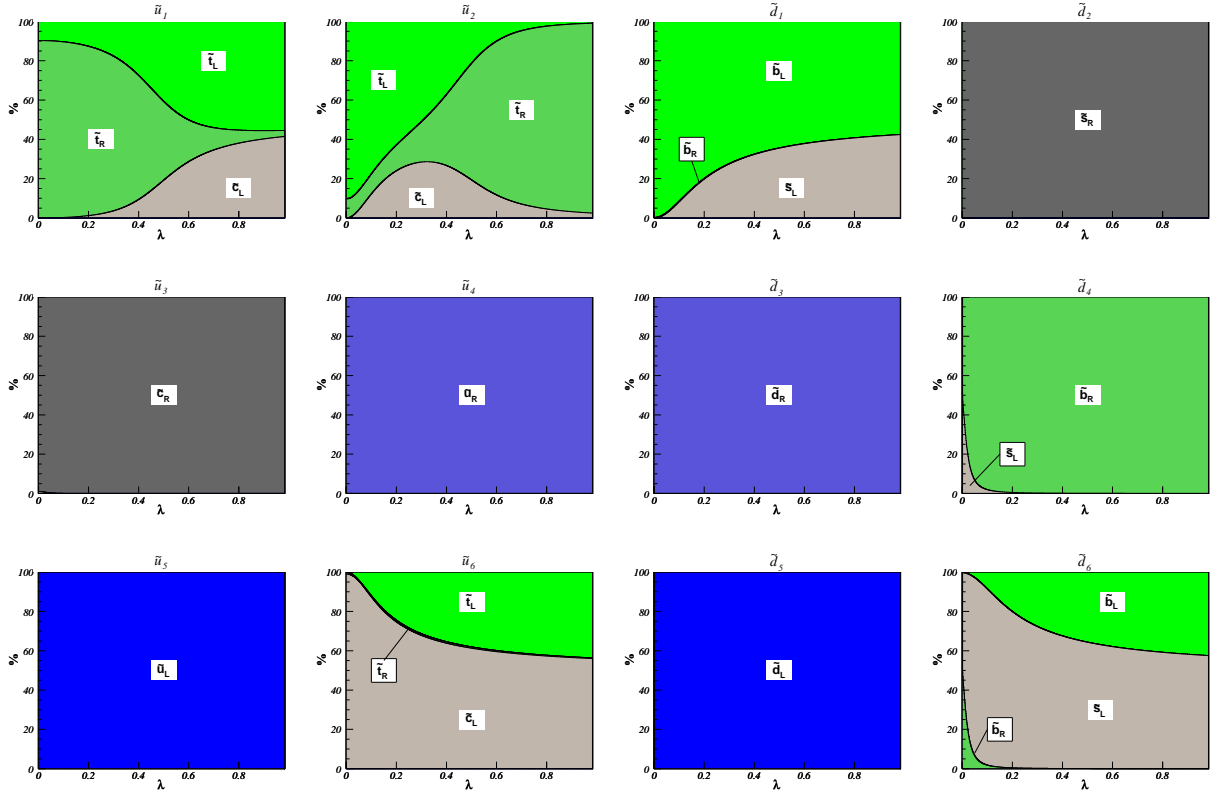


FIG. 18: Dependence of the chirality (L, R) and flavour (u , c , t ; d , s , and b) content of up- (\tilde{u}_i) and down-type (\tilde{d}_i) squark mass eigenstates on the NMFV parameter $\lambda \in [0; 1]$ for benchmark point A.

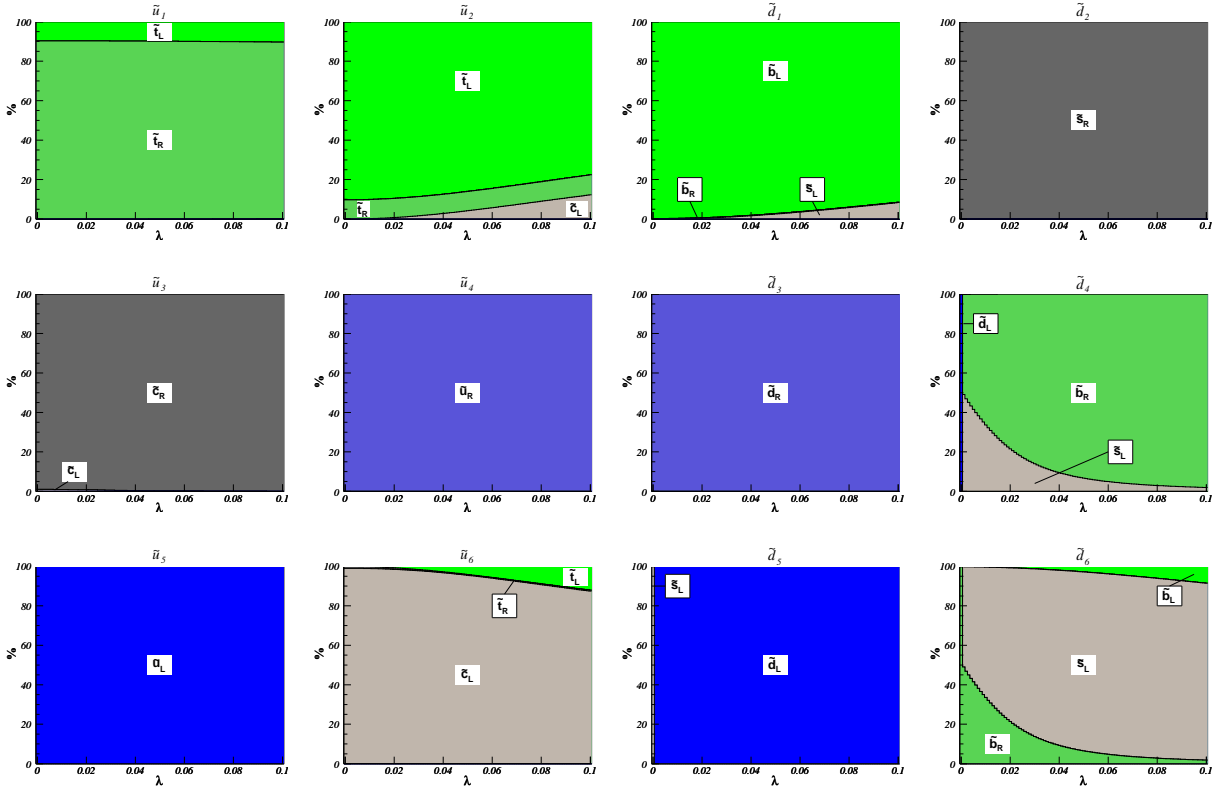


FIG. 19: Same as Fig. 18 for $\lambda \in [0; 0.1]$.

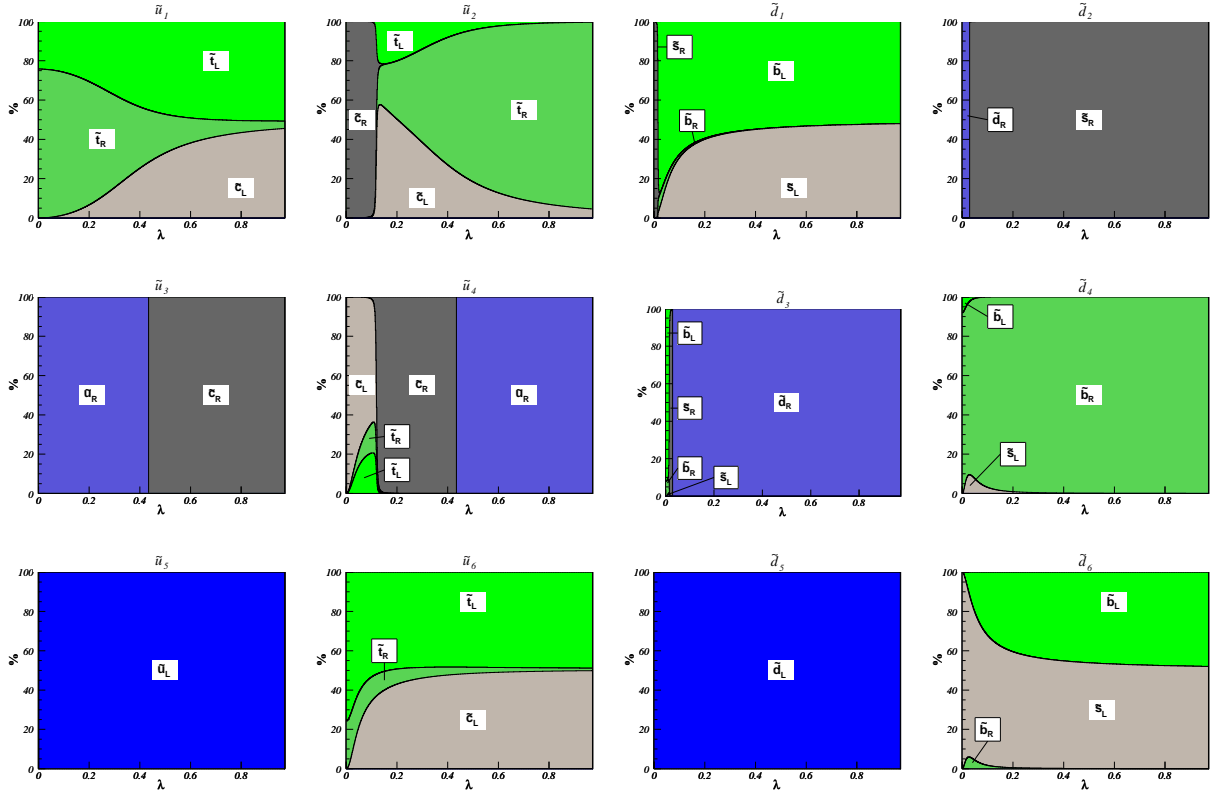
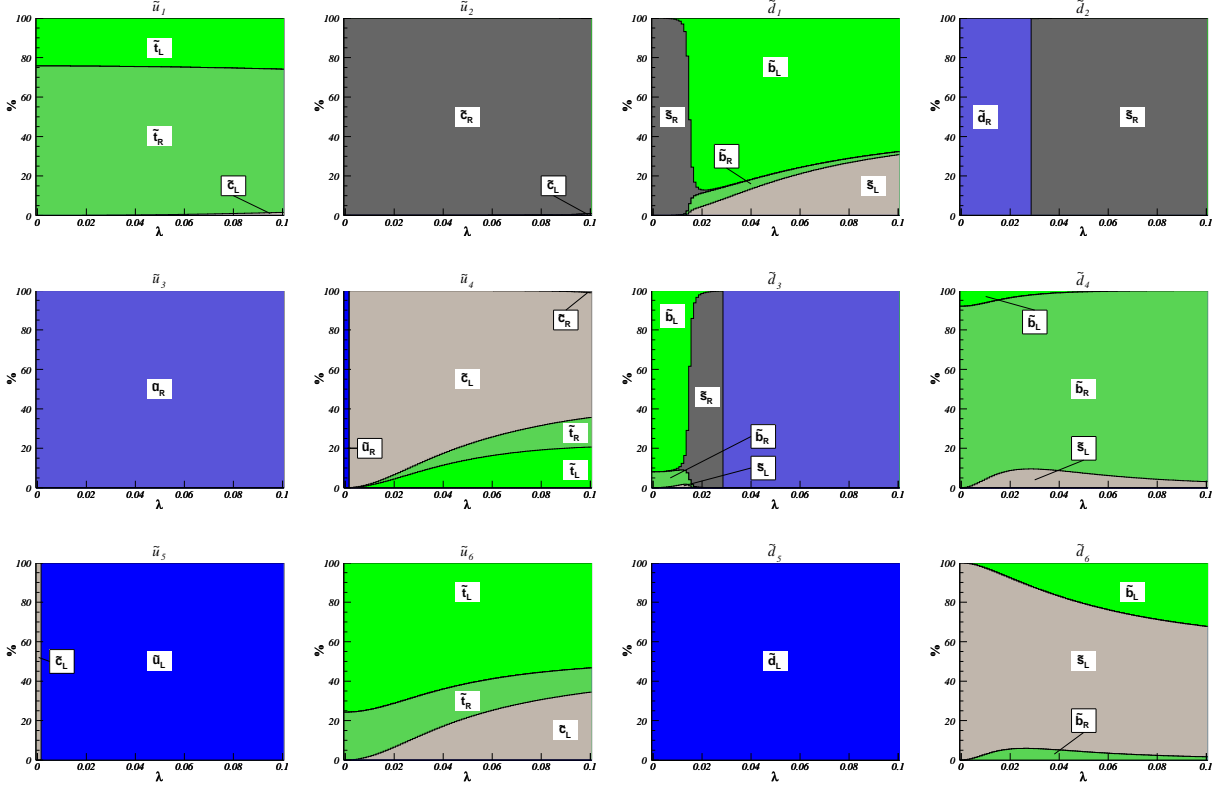


FIG. 20: Same as Fig. 18 for benchmark point B.

FIG. 21: Same as Fig. 20 for $\lambda \in [0, 0.1]$.

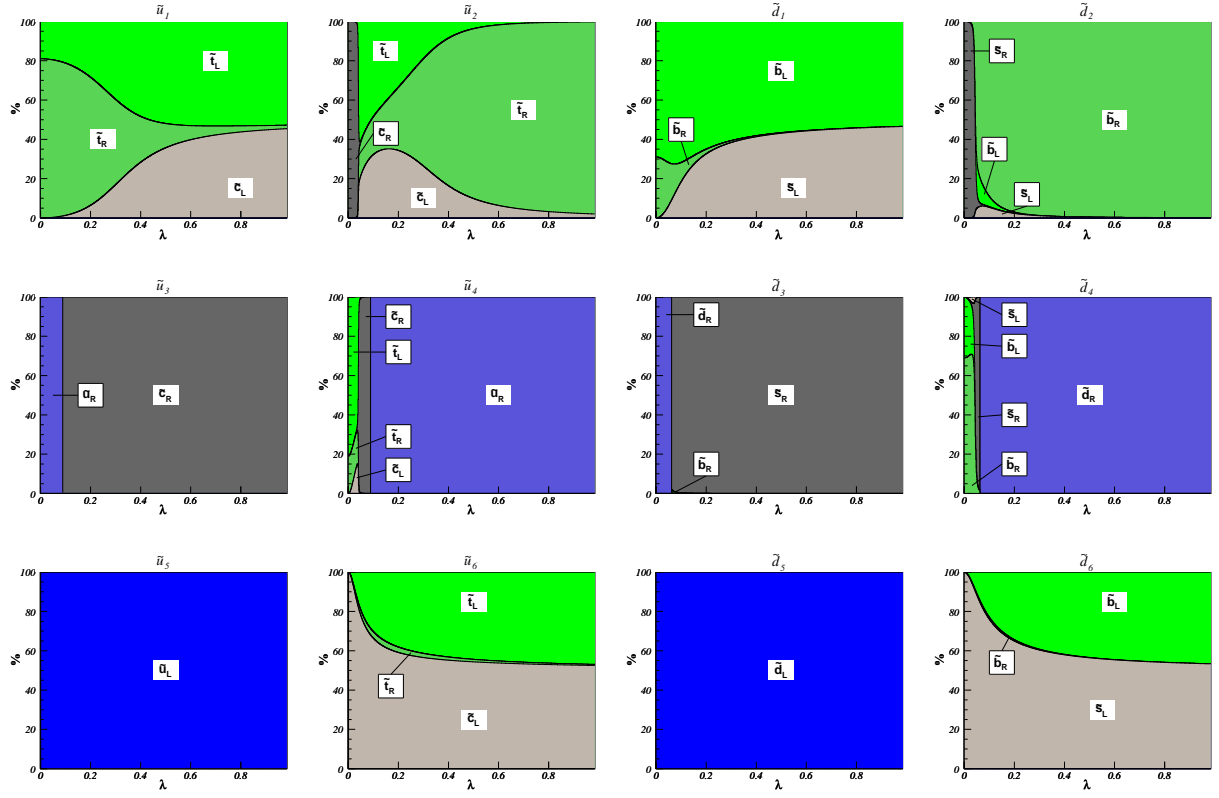
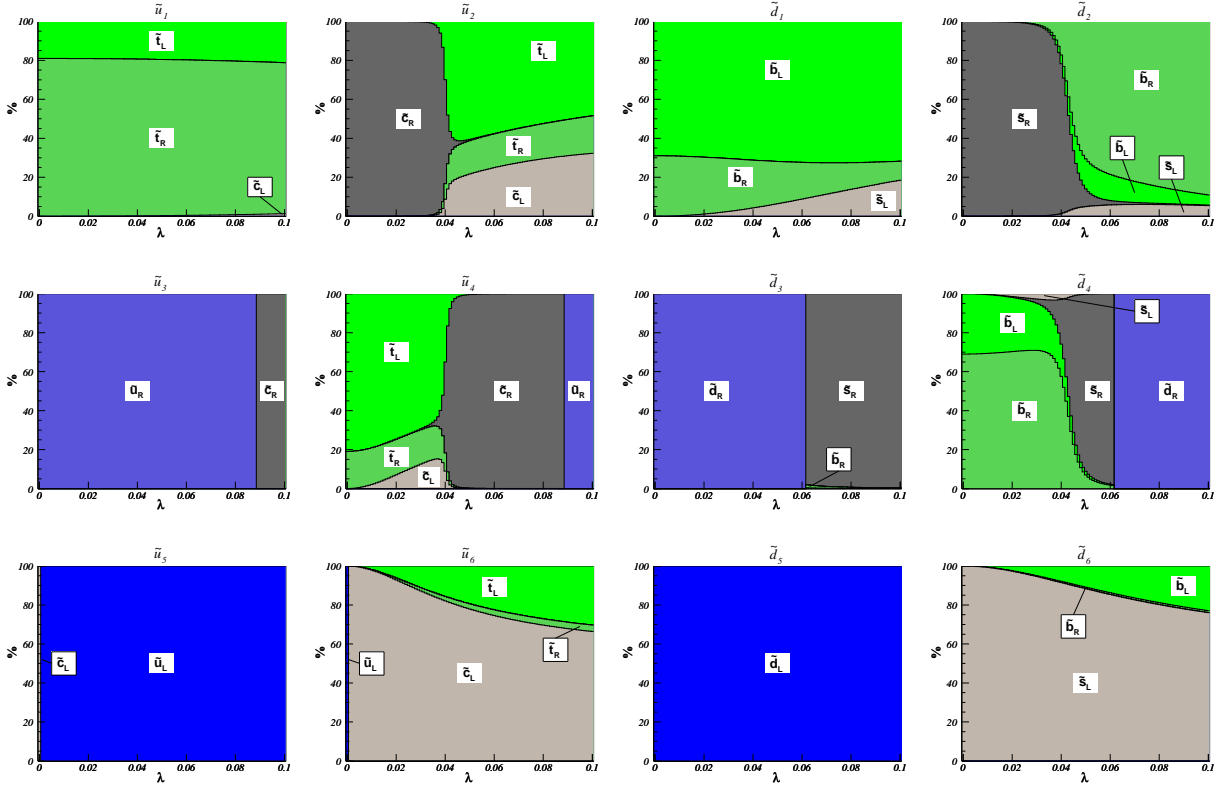


FIG. 22: Same as Fig. 18 for benchmark point C.

FIG. 23: Same as Fig. 22 for $\lambda \in [0, 0.1]$.

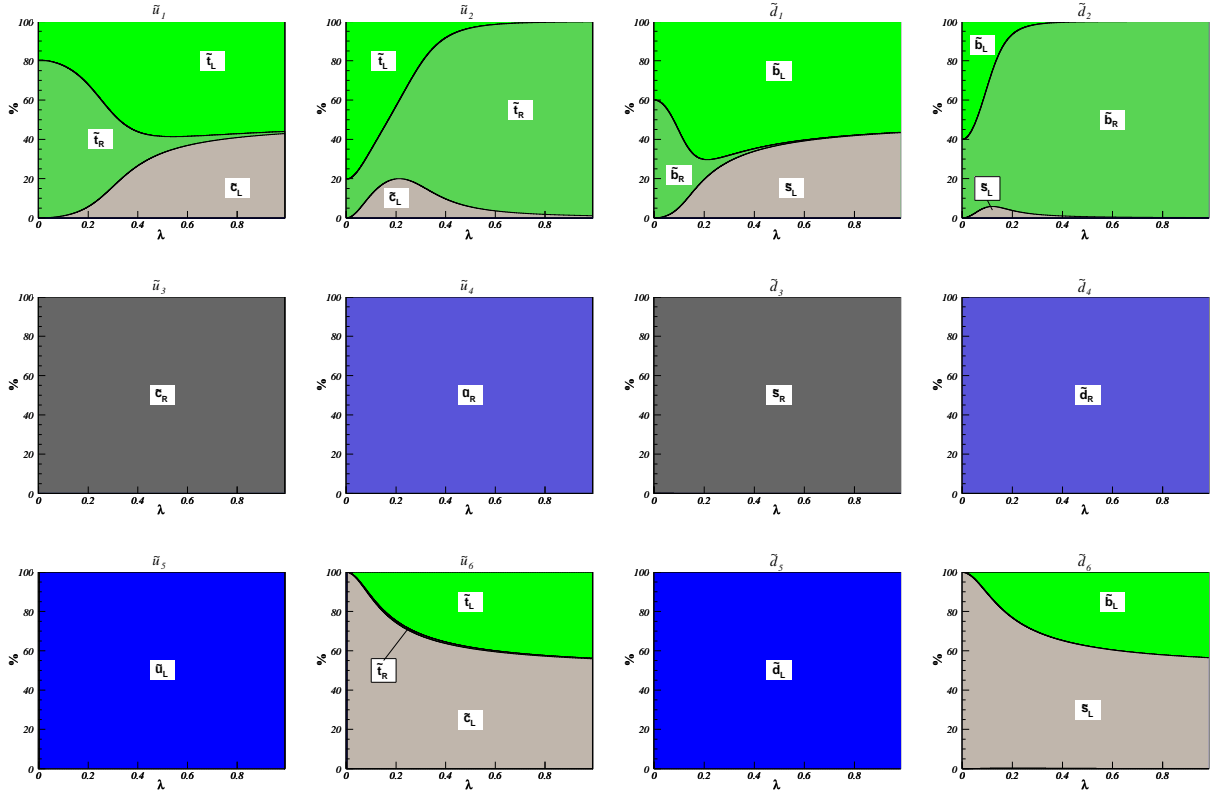
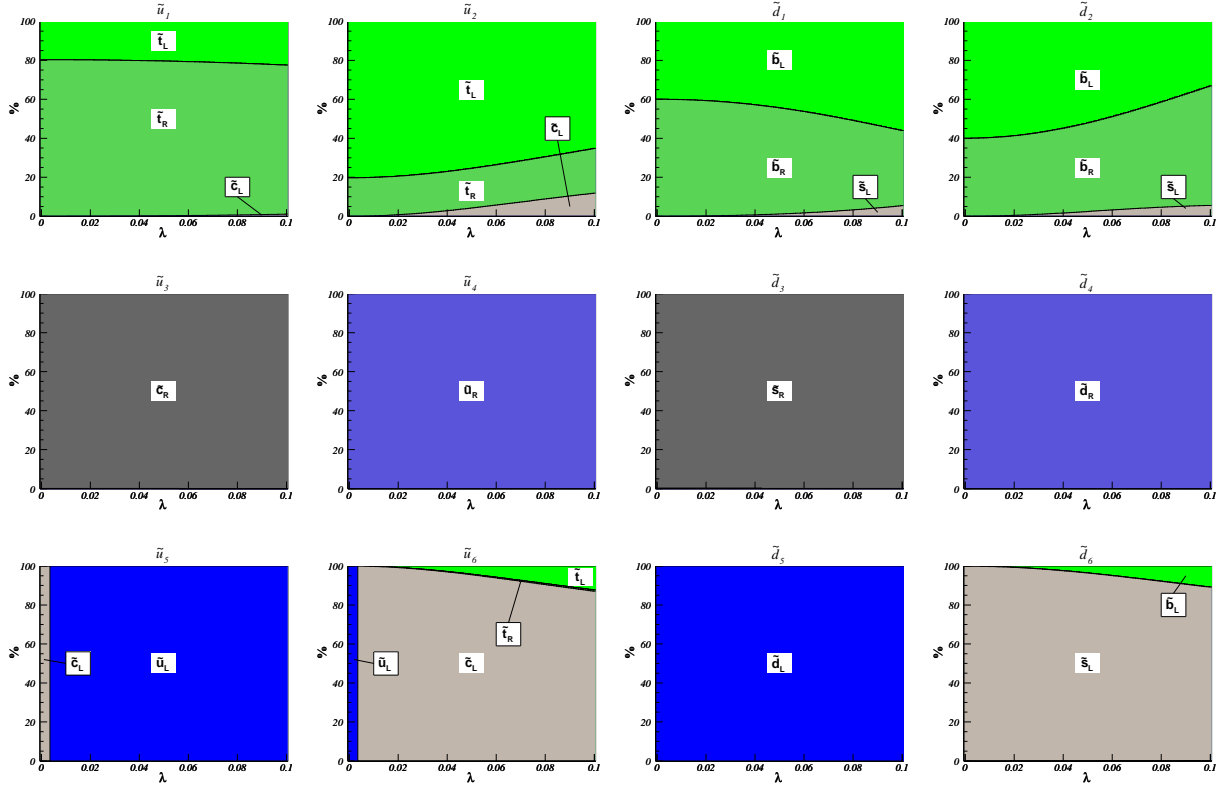


FIG. 24: Same as Fig. 18 for benchmark point D.

FIG. 25: Same as Fig. 24 for $\lambda \in [0, 0.1]$.

states is shown in Fig. 18 for the full range of the parameter $\lambda \in [0; 1]$ and in Fig. 19 for the experimentally favoured range in the vicinity of (c)MFV, $\lambda \in [0; 0.1]$. First-generation and right-handed second-generation squarks remain, of course, helicity- and flavour-diagonal,

$$\begin{aligned}\tilde{u}_3 &= \tilde{c}_R, & \tilde{d}_2 &= \tilde{s}_R, \\ \tilde{u}_4 &= \tilde{u}_R, & \tilde{d}_3 &= \tilde{d}_R, \\ \tilde{u}_5 &= \tilde{u}_L, & \tilde{d}_5 &= \tilde{d}_L,\end{aligned}\tag{66}$$

with the left-handed and first-generation squarks being slightly heavier due their weak isospin coupling (see Eqs. (5)-(7)) and different renormalization-group running effects. Production of these states will benefit from t - and u -channel contributions of first- and second-generation quarks with enhanced parton densities in the external hadrons, but they will not be identified easily with heavy-flavour tagging and are of little interest for our study of flavour violation. The lightest up-type squark \tilde{u}_1 remains the traditional mixture of left- and right-handed stops over a large region of $\lambda \leq 0.4$, but it shows at this point an interesting flavour transition, which is in fact expected from the level reordering phenomenon discussed in the lower central plot of Fig. 14. The transition happens, however, above the experimental limit of $\lambda \leq 0.1$. Below this limit, it is the states $\tilde{u}_2, \tilde{u}_6, \tilde{d}_1$, and in particular \tilde{d}_4 and \tilde{d}_6 that show, in addition to helicity mixing, the most interesting and smooth variation of second- and third-generation flavour content (see Fig. 19). Note that at very low $\lambda \simeq 0.002$ the states \tilde{d}_L and \tilde{s}_L rapidly switch levels. This numerically small change was not visible on the linear scale in Fig. 14.

For the benchmark point B, whose helicity and flavour decomposition is shown in Fig. 20, level reordering occurs at $\lambda \simeq 0.4$ for the intermediate-mass up-type squarks,

$$\begin{aligned}\tilde{u}_{3,4} &= \tilde{c}_R, & \tilde{d}_2 &= \tilde{s}_R, \\ \tilde{u}_{4,3} &= \tilde{u}_R, & \tilde{d}_3 &= \tilde{d}_R, \\ \tilde{u}_5 &= \tilde{u}_L, & \tilde{d}_5 &= \tilde{d}_L\end{aligned}\tag{67}$$

whereas the ordering of down-type squarks is very similar to scenario A. Close inspection of Fig. 21 shows, however, that also \tilde{d}_R and \tilde{s}_R switch levels at low values of $\lambda \simeq 0.02$. At $\lambda \simeq 0.01$, in addition \tilde{s}_R and \tilde{b}_L switch levels, and at $\lambda \simeq 0.002$ it is the states \tilde{u}_L and \tilde{c}_L . The lightest up-type squark is again nothing but a mix of left- and right-handed stops up to $\lambda \leq 0.4$. Phenomenologically smooth transitions below $\lambda \leq 0.1$ involving taggable third-generation squarks are observed for $\tilde{u}_4, \tilde{u}_6, \tilde{d}_1$, and \tilde{d}_6 .

The helicity and flavour decomposition for our scenario D, shown in Fig. 24, is rather similar to the one in scenario A, i.e.

$$\begin{aligned}\tilde{u}_3 &= \tilde{c}_R, & \tilde{d}_3 &= \tilde{s}_R, \\ \tilde{u}_4 &= \tilde{u}_R, & \tilde{d}_4 &= \tilde{d}_R, \\ \tilde{u}_5 &= \tilde{u}_L, & \tilde{d}_5 &= \tilde{d}_L\end{aligned}\tag{68}$$

are exactly the same in the up-squark sector, and only the mixed down-type state \tilde{d}_4 is now lighter and becomes \tilde{d}_2 . The lightest up-type squark, \tilde{u}_1 , is again mostly a mix of left- and right-handed top squarks up to $\lambda \simeq 0.4$, where the level reordering and generation mixing occurs (see lower central part of Fig. 17). At the experimentally favoured lower values of $\lambda \leq 0.1$, the states $\tilde{u}_2, \tilde{u}_6, \tilde{d}_1, \tilde{d}_2$, and \tilde{d}_6 exhibit some smooth variations, shown in detail in Fig. 25, albeit to a lesser extent than in scenario A. At very low $\lambda \simeq 0.004$, it is now the up-type squarks \tilde{u}_L and \tilde{c}_L that rapidly switch levels. This numerically small change was again not visible on a linear scale (see Fig. 17).

For our scenario C, shown in Fig. 22, the assignment of the intermediate states

$$\begin{aligned}\tilde{u}_3 &= \tilde{c}_R, & \tilde{d}_3 &= \tilde{s}_R, \\ \tilde{u}_4 &= \tilde{u}_R, & \tilde{d}_4 &= \tilde{d}_R, \\ \tilde{u}_5 &= \tilde{u}_L, & \tilde{d}_5 &= \tilde{d}_L\end{aligned}\tag{69}$$

is the same as for scenario D above $\lambda \geq 0.1$. Just below, \tilde{u}_R and \tilde{c}_R as well as \tilde{d}_R and \tilde{s}_R rapidly switch levels, whereas \tilde{u}_L and \tilde{c}_L switch levels at very low $\lambda \simeq 0.002$. These changes were already visible upon close inspection of the lower central and right plots in Fig. 16. On the other hand, the lightest squarks \tilde{u}_1 and \tilde{d}_1 only acquire significant flavour admixtures at relatively large $\lambda \simeq 0.2\dots 0.4$, whereas they are mostly superpositions of left- and right-handed stops and sbottoms in the experimentally favourable range of $\lambda \leq 0.1$ shown in Fig. 23. Here, the heaviest states \tilde{u}_6 and \tilde{d}_6 show already smooth admixtures of third-generation squarks as it was the case for the scenarios A and D discussed above. The most interesting states are, however, $\tilde{u}_2, \tilde{u}_4, \tilde{d}_2$, and \tilde{d}_4 , respectively, since they represent combinations of up to four different helicity and flavour states and have a significant, taggable third-generation flavour content.

V. NUMERICAL PREDICTIONS FOR NMFV SUSY PARTICLE PRODUCTION AT THE LHC

In this section, we present numerical predictions for the production cross sections of squark-antisquark pairs, squark pairs, the associated production of squarks and gauginos, and gaugino pairs in NMFV SUSY at the CERN LHC, i.e. for pp -collisions at $\sqrt{S} = 14$ TeV centre-of-mass energy. Thanks to the QCD factorization theorem, total unpolarized hadronic cross sections

$$\sigma = \int_{4m^2/S}^1 d\tau \int_{-1/2 \ln \tau}^{1/2 \ln \tau} dy \int_{t_{\min}}^{t_{\max}} dt f_{a/A}(x_a, M_a^2) f_{b/B}(x_b, M_b^2) \frac{d\hat{\sigma}}{dt} \quad (70)$$

can be calculated by convolving the relevant partonic cross sections $d\hat{\sigma}/dt$, computed in Sec. III, with universal parton densities $f_{a/A}$ and $f_{b/B}$ of partons a, b in the hadrons A, B , which depend on the longitudinal momentum fractions of the two partons $x_{a,b} = \sqrt{\tau} e^{\pm y}$ and on the unphysical factorization scales $M_{a,b}$. For consistency with our leading order (LO) QCD calculation in the collinear approximation, where all squared quark masses (except for the top-quark mass) $m_q^2 \ll s$, we employ the LO set of the latest CTEQ6 global parton density fit [53], which includes $n_f = 5$ “light” (including the bottom) quark flavours and the gluon, but no top-quark density. Whenever it occurs, i.e. for gluon initial states and gluon or gluino exchanges, the strong coupling constant $\alpha_s(\mu_R)$ is calculated with the corresponding LO value of $\Lambda_{\text{LO}}^{n_f=5} = 165$ MeV. We identify the renormalization scale μ_R with the factorization scales $M_a = M_b$ and set the scales to the average mass of the final state SUSY particles i and j , $m = (m_i + m_j)/2$.

The numerical cross sections for charged squark-antisquark and squark-squark production, neutral up- and down-type squark-antisquark and squark-squark pair production, associated production of squarks with charginos and neutralinos, and gaugino pair production are shown in Fig. 26 for our benchmark scenario A, in Fig. 27 for scenario B, in Fig. 28 for scenario C, and in Fig. 29 for scenario D. The magnitudes of the cross sections vary from the barely visible level of 10^{-2} fb for weak production of heavy final states over the semi-strong production of average squarks and gauginos and quark-gluon initial states to large cross sections of 10^2 to 10^3 fb for the strong production of diagonal squark-(anti)squark pairs or weak production of very light gaugino pairs. Unfortunately, these processes, whose cross sections are largest (top right, center left, and lower right parts of Figs. 26-29), are practically insensitive to the flavour violation parameter λ , as the strong gauge interaction is insensitive to quark flavours and gaugino pair production cross sections are summed over exchanged squark flavours.

Some of the subleading, non-diagonal cross sections show, however, sharp transitions, in particular down-type squark-antisquark production at the benchmark point B (centre-left part of Fig. 27), but also the other squark-antisquark and squark-squark production processes. At $\lambda = 0.02$, the cross sections for $\tilde{d}_1 \tilde{d}_6^*$ and $\tilde{d}_3 \tilde{d}_6^*$ switch places. Since the concerned strange and sbottom mass differences are rather small, this is mainly due to the different strange and bottom quark densities in the proton. The cross section is mainly due to the exchange of strongly coupled gluinos despite their larger mass. At $\lambda = 0.035$ the cross sections for $\tilde{d}_3 \tilde{d}_6^*$ and $\tilde{d}_1 \tilde{d}_3^*$ increase sharply, since $\tilde{d}_3 = \tilde{d}_R$ can then be produced from down-type valence quarks. The cross section of the latter process increases with the strange squark content of \tilde{d}_1 .

At the benchmark point C (Fig. 28), sharp transitions occur between the \tilde{u}_2/\tilde{u}_4 and \tilde{d}_2/\tilde{d}_4 states, which are pure charm/strange squarks below/above $\lambda = 0.035$, for all types of charged and neutral squark-antisquark and squark-squark production and also squark-gaugino associated production. As a side-remark we note that an interesting perspective might be the exploitation of these t -channel contributions to second- and third-generation squark production for the determination of heavy-quark densities in the proton. This requires, of course, efficient experimental techniques for heavy-flavour tagging.

Smooth transitions and semi-strong cross sections of about 1 fb are observed for the associated production of third-generation squarks with charginos (lower left diagrams) and neutralinos (lower centre diagrams) and in particular for the scenarios A and B. For benchmark point A (Fig. 26), the cross section for \tilde{d}_4 production decreases with its strange squark content, while the bottom squark content increases at the same time. For benchmark point B (Fig. 27), the same (opposite) happens for \tilde{d}_6 (\tilde{d}_1), while the cross sections for \tilde{u}_6 increase/decrease with its charm/top squark content. Even in minimal flavour violation, the associated production of stops and charginos is a particularly useful channel for SUSY particle spectroscopy, as can be seen from the fact that cross sections vary over several orders of magnitude among our four benchmark points (see also Ref. [54]).

An illustrative summary of flavour violating hadroproduction cross section contributions for third-generation squarks and/or gauginos is presented in Tab. III, together with the competing flavour-diagonal contributions.

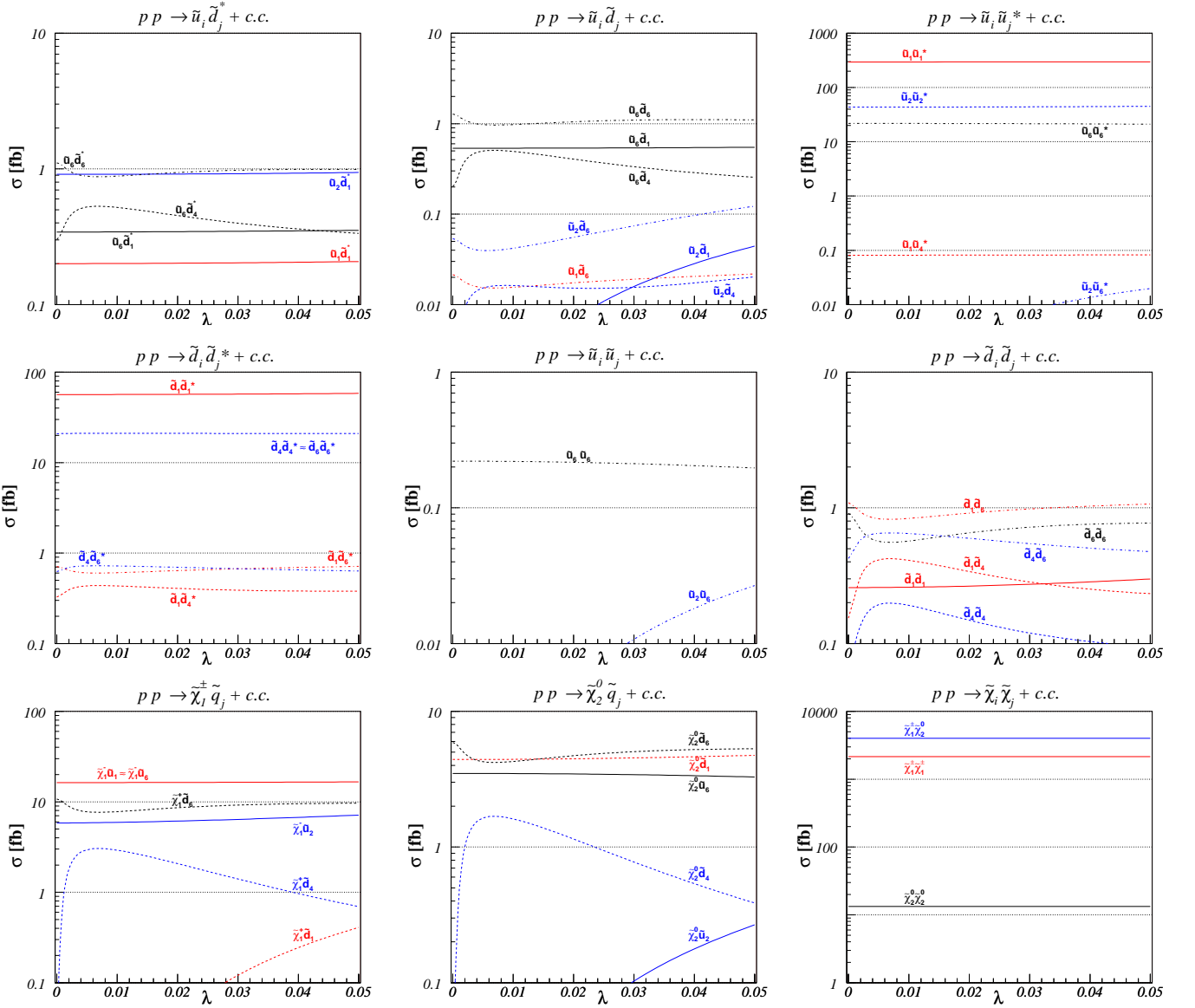


FIG. 26: Cross sections for charged squark-antisquark (top left) and squark-squark (top centre) production, neutral up-type (top right) and down-type (centre left) squark-antisquark and squark-squark pair (centre and centre right) production, associated production of squarks with charginos (bottom left) and neutralinos (bottom centre), and gaugino pair production (bottom right) at the LHC in our benchmark scenario A.

VI. CONCLUSIONS

In conclusion, we have performed an extensive analysis of squark and gaugino hadroproduction and decays in non-minimal flavour violating supersymmetry. Within the super-CKM basis, we have taken into account the possible misalignment of quark and squark rotations and computed all squared helicity amplitudes for the production and the decay widths of squarks and gauginos in compact analytic form, verifying that our results agree with the literature in the case of non-mixing squarks whenever possible. Flavour violating effects have also been included in our analysis of dark matter (co-)annihilation processes. We have then analyzed the NMFV SUSY parameter space for regions allowed by low-energy, electroweak precision, and cosmological data and defined four new post-WMAP benchmark points and slopes equally valid in minimal and non-minimal flavour violating SUSY. We found that left-chiral mixing of second- and third-generation squarks is slightly stronger constrained than previously believed, mostly due to smaller experimental errors on the $b \rightarrow s\gamma$ branching ratio and the cold dark matter relic density. For our four benchmark points, we have presented the dependence of squark mass eigenvalues and the flavour and helicity decomposition of

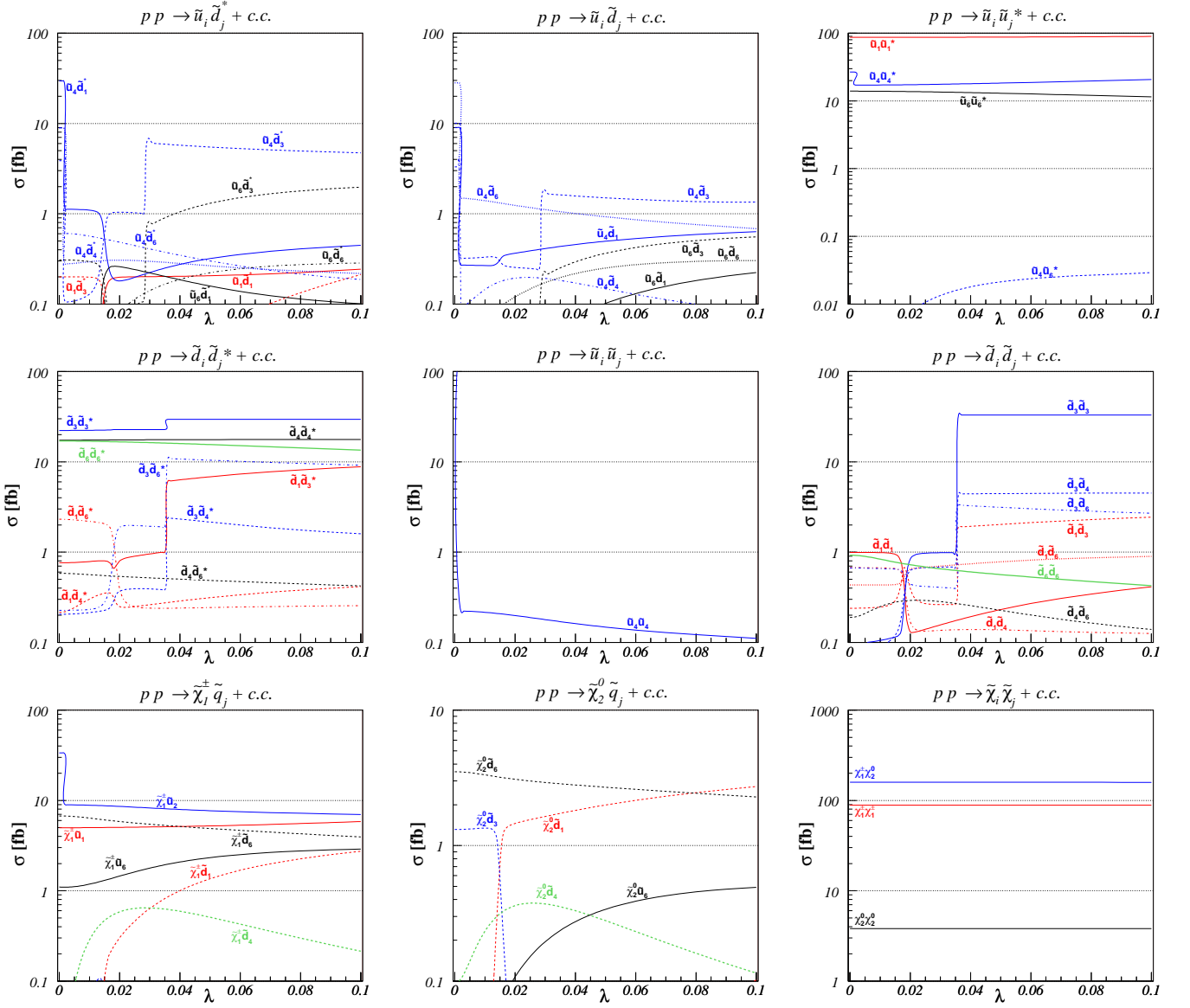


FIG. 27: Same as Fig. 26 for our benchmark scenario B.

TABLE III: Dominant s -, t -, and u -channel contributions to the flavour violating hadroproduction of third-generation squarks and/or gauginos and the competing dominant flavour-diagonal contributions.

Exchange Final State	s	t	u
$\tilde{t}\tilde{b}^*$	W	NMFV- \tilde{g}	-
$\tilde{b}\tilde{s}^*$	NMFV- Z	NMFV- \tilde{g}	-
$\tilde{t}\tilde{c}^*$	NMFV- Z	NMFV- \tilde{g}	-
$\tilde{t}\tilde{b}$	-	-	NMFV- \tilde{g}
$\tilde{b}\tilde{b}$	-	\tilde{g}	\tilde{g}
$\tilde{t}\tilde{t}$	-	NMFV- \tilde{g}	NMFV- \tilde{g}
$\tilde{\chi}^0\tilde{b}$	b	b	-
$\tilde{\chi}^\pm\tilde{b}$	NMFV- c	NMFV- \tilde{b}	-
$\tilde{\chi}^0\tilde{t}$	NMFV- c	NMFV- \tilde{t}	-
$\tilde{\chi}^\pm\tilde{t}$	b	\tilde{t}	-
$\tilde{\chi}\tilde{\chi}$	γ, Z, W	\tilde{q}	\tilde{q}

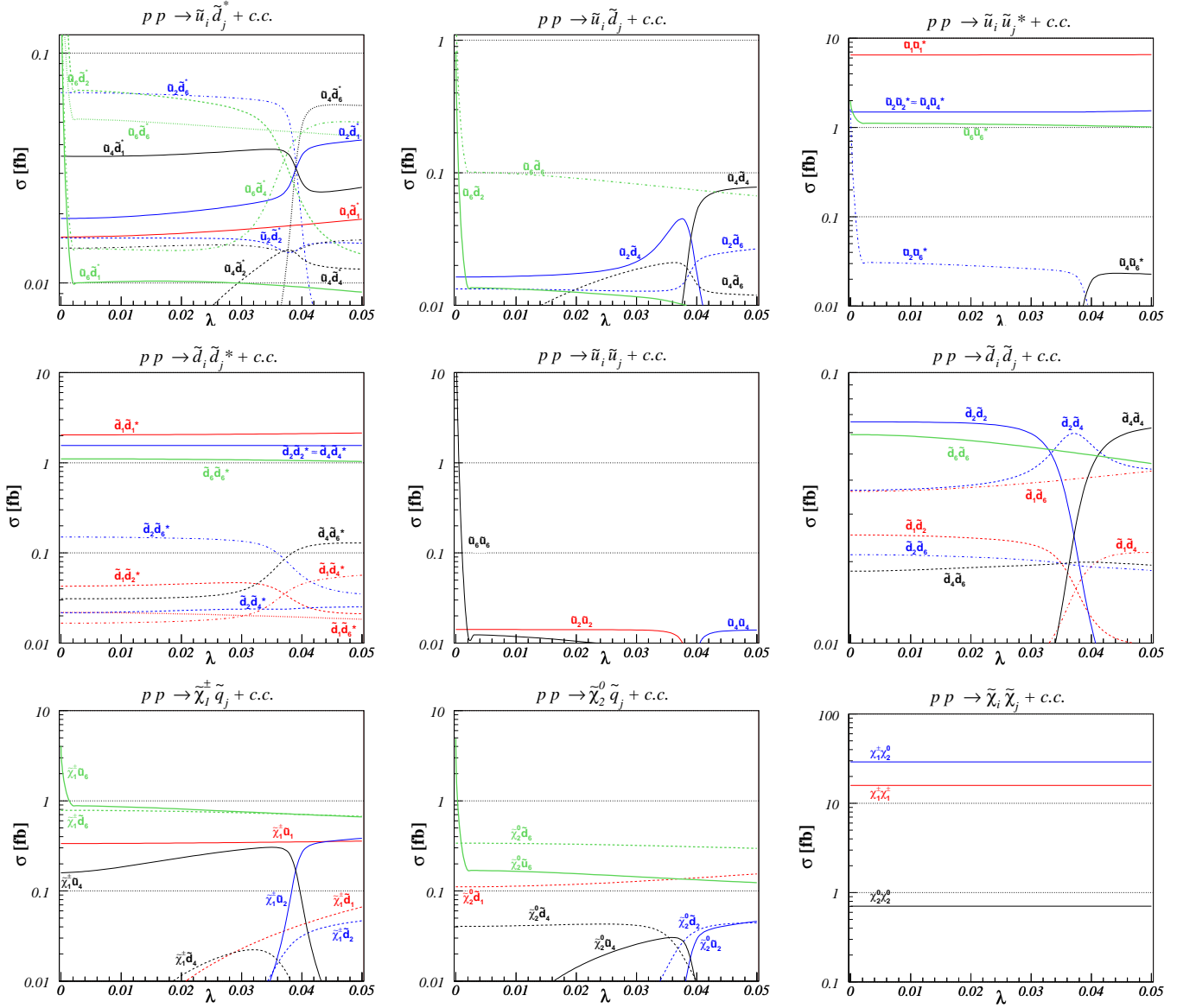


FIG. 28: Same as Fig. 26 for our benchmark scenario C.

the squark mass eigenstates on the flavour violating parameter λ . We have computed numerically all production cross sections for the LHC and discussed in detail their dependence on flavour violation. A full experimental study including heavy-flavour tagging efficiencies, detector resolutions, and background processes would, of course, be very interesting in order to establish the experimental significance of NMFV. While the implementation of our analytical results in a general-purpose Monte Carlo generator should now be straight-forward, such a detailed experimental study represents a research project of its own [55] and is beyond the scope of the work presented here.

Acknowledgments

A large part of this work has been performed in the context of the CERN 2006/2007 workshop on “Flavour in the Era of the LHC”. The authors also acknowledge interesting discussions with J. Debove, A. Djouadi, W. Porod, J.M. Richard, and P. Skands. This work was supported by two Ph.D. fellowships of the French ministry for education and research.

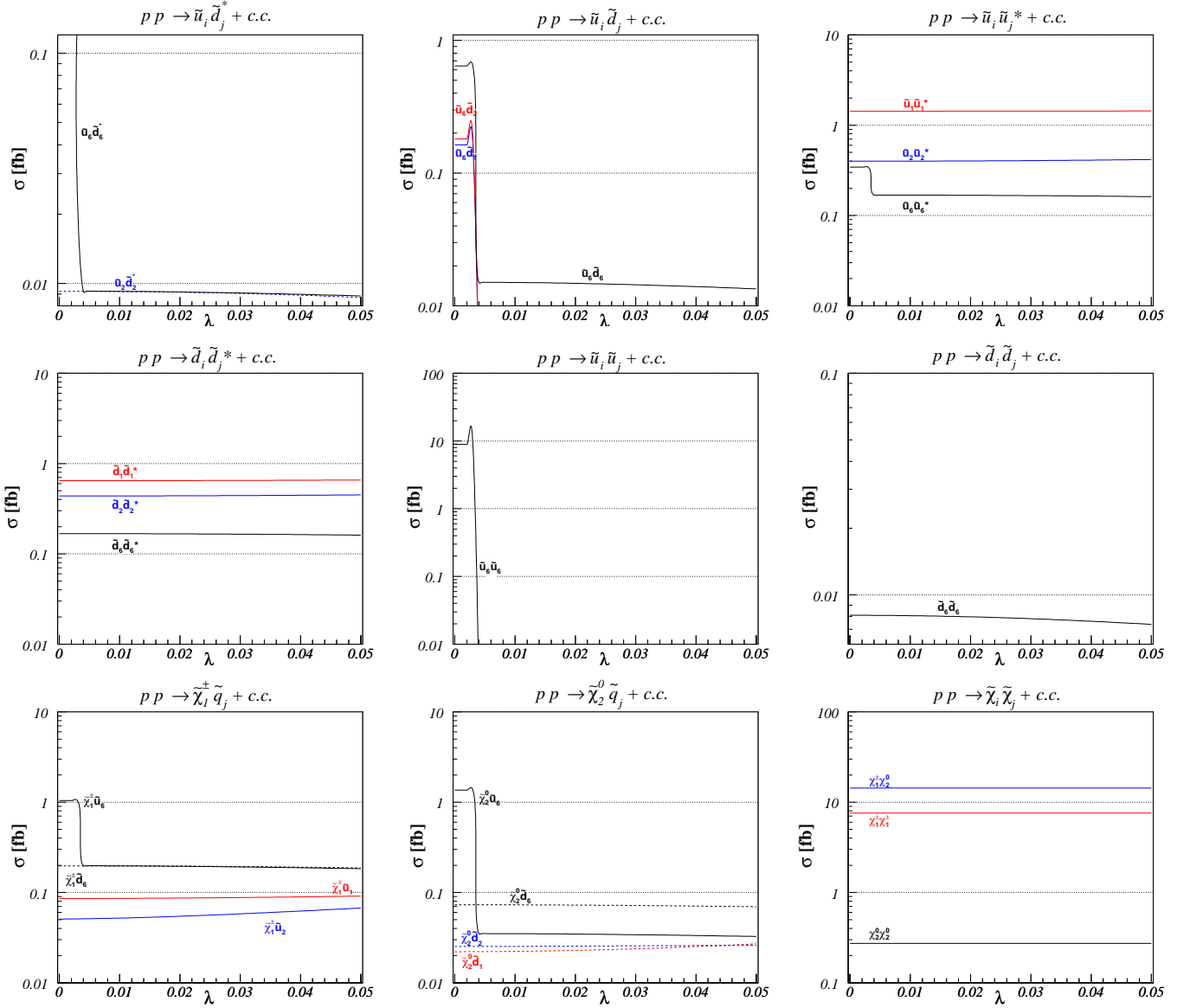


FIG. 29: Same as Fig. 26 for our benchmark scenario D.

APPENDIX A: GAUGINO AND HIGGSINO MIXING

The soft SUSY-breaking terms in the minimally supersymmetric Lagrangian include a term

$$\mathcal{L} \supset -\frac{1}{2}(\psi^0)^T Y \psi^0 + \text{h.c.}, \quad (\text{A1})$$

which is bilinear in the (2-component) fermionic partners

$$\psi_j^0 = (-i\tilde{B}, -i\tilde{W}^3, \tilde{H}_1^0, \tilde{H}_2^0)^T \quad (\text{A2})$$

of the neutral electroweak gauge and Higgs bosons and proportional to the, generally complex and symmetric, neutralino mass matrix

$$Y = \begin{pmatrix} M_1 & 0 & -m_Z s_W c_\beta & m_Z s_W s_\beta \\ 0 & M_2 & m_Z c_W c_\beta & -m_Z c_W s_\beta \\ -m_Z s_W c_\beta & m_Z c_W c_\beta & 0 & -\mu \\ m_Z s_W s_\beta & -m_Z c_W s_\beta & -\mu & 0 \end{pmatrix}. \quad (\text{A3})$$

Here, M_1 , M_2 , and μ are the SUSY-breaking bino, wino, and off-diagonal higgsino mass parameters with $\tan\beta = s_\beta/c_\beta = v_u/v_d$ being the ratio of the vacuum expectation values $v_{u,d}$ of the two Higgs doublets, while m_Z is the SM Z -boson mass and s_W (c_W) is the sine (co-sine) of the electroweak mixing angle θ_W . After electroweak gauge-symmetry breaking and diagonalization of the mass matrix Y , one obtains the neutralino mass eigenstates

$$\chi_i^0 = N_{ij} \psi_j^0, \quad i, j = 1, \dots, 4, \quad (\text{A4})$$

where N is a unitary matrix satisfying the relation

$$N^* Y N^{-1} = \text{diag}(m_{\tilde{\chi}_1^0}, m_{\tilde{\chi}_2^0}, m_{\tilde{\chi}_3^0}, m_{\tilde{\chi}_4^0}). \quad (\text{A5})$$

In 4-component notation, the Majorana-fermionic neutralino mass eigenstates can be written as

$$\tilde{\chi}_i^0 = \begin{pmatrix} \chi_i^0 \\ \bar{\chi}_i^0 \end{pmatrix}, \quad i = 1, \dots, 4. \quad (\text{A6})$$

Their mass eigenvalues $m_{\tilde{\chi}_i^0}$ can, e.g., be found in analytic form in [56] and can be chosen to be real and non-negative.

The chargino mass term in the SUSY Lagrangian

$$\mathcal{L} \supset -\frac{1}{2}(\psi^+ \psi^-) \begin{pmatrix} 0 & X^T \\ X & 0 \end{pmatrix} \begin{pmatrix} \psi^+ \\ \psi^- \end{pmatrix} + \text{h.c.} \quad (\text{A7})$$

is bilinear in the (2-component) fermionic partners

$$\psi_j^\pm = (-i\tilde{W}^\pm, \tilde{H}_{2,1}^\pm)^T \quad (\text{A8})$$

of the charged electroweak gauge and Higgs bosons and proportional to the, generally complex, chargino mass matrix

$$X = \begin{pmatrix} M_2 & m_W \sqrt{2} s_\beta \\ m_W \sqrt{2} c_\beta & \mu \end{pmatrix}, \quad (\text{A9})$$

where m_W is the mass of the SM W -boson. Its diagonalization leads to the chargino mass eigenstates

$$\begin{aligned} \chi_i^+ &= V_{ij} \psi_j^+ \\ \chi_i^- &= U_{ij} \psi_j^- \end{aligned}, \quad i, j = 1, 2, \quad (\text{A10})$$

where the matrices U and V satisfy the relation

$$U^* X V^{-1} = \text{diag}(m_{\tilde{\chi}_1^\pm}, m_{\tilde{\chi}_2^\pm}). \quad (\text{A11})$$

In 4-component notation, the Dirac-fermionic chargino mass eigenstates can be written as

$$\tilde{\chi}_i^\pm = \begin{pmatrix} \chi_i^\pm \\ \bar{\chi}_i^\pm \end{pmatrix}. \quad (\text{A12})$$

The mass eigenvalues can be chosen to be real and non-negative and are given by [2]

$$m_{\tilde{\chi}_{1,2}^\pm}^2 = \frac{1}{2} \left\{ M_2^2 + \mu^2 + 2m_W^2 \mp \left[(M_2^2 - \mu^2)^2 + 4m_W^4 c_{2\beta}^2 + 4m_W^2 (M_2^2 + \mu^2 + 2M_2 \mu s_{2\beta}) \right]^{1/2} \right\}, \quad (\text{A13})$$

while the matrices

$$U = \mathcal{O}_- \quad \text{and} \quad V = \begin{cases} \mathcal{O}_+ & , \text{ if } \det X \geq 0 \\ \sigma_3 \mathcal{O}_+ & , \text{ if } \det X < 0 \end{cases} \quad \text{with} \quad \mathcal{O}_\pm = \begin{pmatrix} \cos \theta_\pm & \sin \theta_\pm \\ -\sin \theta_\pm & \cos \theta_\pm \end{pmatrix} \quad (\text{A14})$$

are determined by the mixing angles θ_\pm with $0 \leq \theta_\pm \leq \pi/2$ and

$$\tan 2\theta_+ = \frac{2\sqrt{2}m_W (M_2 \sin \beta + \mu \cos \beta)}{M_2^2 - \mu^2 + 2m_W^2 \cos 2\beta} \quad \text{and} \quad \tan 2\theta_- = \frac{2\sqrt{2}m_W (M_2 \cos \beta + \mu \sin \beta)}{M_2^2 - \mu^2 - 2m_W^2 \cos 2\beta}. \quad (\text{A15})$$

[1] H. P. Nilles, Phys. Rept. **110** (1984) 1.

- [2] H. E. Haber and G. L. Kane, Phys. Rept. **117** (1985) 75.
- [3] M. Ciuchini, G. Degrassi, P. Gambino and G. F. Giudice, Nucl. Phys. B **534** (1998) 3.
- [4] A. J. Buras, P. Gambino, M. Gorbahn, S. Jäger and L. Silvestrini, Phys. Lett. B **500** (2001) 161.
- [5] L. J. Hall and L. Randall, Phys. Rev. Lett. **65** (1990) 2939.
- [6] G. D'Ambrosio, G. F. Giudice, G. Isidori and A. Strumia, Nucl. Phys. B **645** (2002) 155.
- [7] W. Altmannshofer, A. J. Buras and D. Guadagnoli, arXiv:hep-ph/0703200.
- [8] N. Cabibbo, Phys. Rev. Lett. **10** (1963) 531.
- [9] M. Kobayashi and T. Maskawa, Prog. Theor. Phys. **49** (1973) 652.
- [10] L. J. Hall, V. A. Kostelecky and S. Raby, Nucl. Phys. B **267** (1986) 415.
- [11] J. F. Donoghue, H. P. Nilles and D. Wyler, Phys. Lett. B **128** (1983) 55.
- [12] M. J. Duncan, Nucl. Phys. B **221** (1983) 285.
- [13] A. Bouquet, J. Kaplan and C. A. Savoy, Phys. Lett. B **148** (1984) 69.
- [14] F. Borzumati and A. Masiero, Phys. Rev. Lett. **57** (1986) 961.
- [15] F. Gabbiani and A. Masiero, Nucl. Phys. B **322** (1989) 235.
- [16] P. Brax and C. A. Savoy, Nucl. Phys. B **447** (1995) 227.
- [17] J. S. Hagelin, S. Kelley and T. Tanaka, Nucl. Phys. B **415** (1994) 293.
- [18] F. Gabbiani, E. Gabrielli, A. Masiero and L. Silvestrini, Nucl. Phys. B **477** (1996) 321.
- [19] M. Ciuchini, E. Franco, D. Guadagnoli, V. Lubicz, M. Pierini, V. Porretti and L. Silvestrini, hep-ph/0703204.
- [20] W. Beenakker, R. Höpker, M. Spira and P. M. Zerwas, Nucl. Phys. B **492** (1997) 51;
E. L. Berger, M. Klasen and T. Tait, Phys. Rev. D **59** (1999) 074024.
- [21] H. Baer, B. W. Harris and M. H. Reno, Phys. Rev. D **57** (1998) 5871.
- [22] W. Beenakker, M. Klasen, M. Krämer, T. Plehn, M. Spira and P. M. Zerwas, Phys. Rev. Lett. **83** (1999) 3780.
- [23] E. L. Berger, M. Klasen and T. Tait, Phys. Lett. B **459** (1999) 165;
E. L. Berger, M. Klasen and T. M. P. Tait, Phys. Rev. D **62** (2000) 095014 [Erratum-ibid. D **67** (2003) 099901].
- [24] W. Beenakker, M. Krämer, T. Plehn, M. Spira and P. M. Zerwas, Nucl. Phys. B **515** (1998) 3
- [25] E. L. Berger, B. W. Harris, D. E. Kaplan, Z. Sullivan, T. M. P. Tait and C. E. M. Wagner, Phys. Rev. Lett. **86** (2001) 4231.
- [26] G. Bozzi, B. Fuks and M. Klasen, Phys. Rev. D **72** (2005) 035016.
- [27] S. Dawson, E. Eichten and C. Quigg, Phys. Rev. D **31** (1985) 1581.
- [28] S. Y. Choi, A. Djouadi, H. S. Song and P. M. Zerwas, Eur. Phys. J. C **8** (1999) 669.
- [29] M. Spira, Nucl. Phys. Proc. Suppl. **89** (2000) 222.
- [30] G. J. Gounaris, J. Layssac, P. I. Porfyriadis and F. M. Renard, Phys. Rev. D **70** (2004) 033011.
- [31] A. Bartl, W. Majerotto and W. Porod, Z. Phys. C **64** (1994) 499 [Erratum-ibid. C **68** (1995) 518].
- [32] M. Obara and N. Oshimo, JHEP **0608** (2006) 054.
- [33] W. M. Yao *et al.* [Particle Data Group], J. Phys. G **33** (2006) 1.
- [34] M. Ciuchini, A. Masiero, P. Paradisi, L. Silvestrini, S. K. Vempati and O. Vives, hep-ph/0702144.
- [35] J. Foster, K. I. Okumura and L. Roszkowski, Phys. Lett. B **641** (2006) 452.
- [36] T. Hahn, W. Hollik, J. I. Illana and S. Penaranda, hep-ph/0512315.
- [37] E. Barberio *et al.* [Heavy Flavor Averaging Group (HFAG)], hep-ex/0603003.
- [38] A. L. Kagan and M. Neubert, Phys. Rev. D **58** (1998) 094012.
- [39] S. Heinemeyer, W. Hollik, F. Merz and S. Penaranda, Eur. Phys. J. C **37** (2004) 481.
- [40] S. Heinemeyer, D. Stöckinger and G. Weiglein, Nucl. Phys. B **690** (2004) 62.
- [41] S. Heinemeyer, D. Stöckinger and G. Weiglein, Nucl. Phys. B **699** (2004) 103.
- [42] J. R. Ellis, J. S. Hagelin, D. V. Nanopoulos, K. A. Olive and M. Srednicki, Nucl. Phys. B **238** (1984) 453.
- [43] P. Gondolo, J. Edsjo, P. Ullio, L. Bergstrom, M. Schelke and E. A. Baltz, JCAP **0407** (2004) 008.
- [44] J. Hamann, S. Hannestad, M. S. Sloth and Y. Y. Y. Wong, Phys. Rev. D **75** (2007) 023522.
- [45] J. R. Ellis, K. A. Olive, Y. Santoso and V. C. Spanos, Phys. Lett. B **565** (2003) 176.
- [46] W. Porod, Comput. Phys. Commun. **153** (2003) 275.
- [47] S. Heinemeyer, W. Hollik and G. Weiglein, Comput. Phys. Commun. **124** (2000) 76.
- [48] T. Moroi, Phys. Rev. D **53** (1996) 6565 [Erratum-ibid. D **56** (1997) 4424].
- [49] B. C. Allanach *et al.*, Eur. Phys. J. C **25** (2002) 113.
- [50] J. A. Aguilar-Saavedra *et al.*, Eur. Phys. J. C **46** (2006) 43.
- [51] M. Battaglia, A. De Roeck, J. R. Ellis, F. Gianotti, K. A. Olive and L. Pape, Eur. Phys. J. C **33** (2004) 273.
- [52] P. Gambino, U. Haisch and M. Misiak, Phys. Rev. Lett. **94** (2005) 061803.
- [53] J. Pumplin, D. R. Stump, J. Huston, H. L. Lai, P. Nadolsky and W. K. Tung, JHEP **0207** (2002) 012.
- [54] M. Beccaria, G. Macorini, L. Panizzi, F. M. Renard and C. Verzegnassi, Phys. Rev. D **74** (2006) 093009.
- [55] B. Fuks, M. Klasen and P. Skands, in preparation.
- [56] M. M. El Kheishen, A. A. Aboshousha and A. A. Shafik, Phys. Rev. D **45** (1992) 4345.